

Paths for Epidemics in Static and Temporal Networks

DISSERTATION

zur Erlangung des akademischen Grades

**doctor rerum naturalium
(Dr. rer. nat.)
im Fach Physik**

**eingereicht an der
Mathematisch-Wissenschaftlichen Fakultät I
Humboldt-Universität zu Berlin**

**von
Dipl.-Phys. Hartmut Lentz**

**Präsident der Humboldt-Universität zu Berlin:
Prof. Dr. Jan-Hendrik Olbertz**

**Dekan der Mathematisch-Wissenschaftlichen Fakultät I:
Prof. Stefan Hecht, PhD**

Gutachter:

1. Prof. Dr. I. M. Sokolov, Humboldt-Universität zu Berlin
2. Prof. Dr. Dr. J. Kurths, Potsdam-Institut für Klimafolgenforschung
3. Prof. Dr. B. Blasius, Carl von Ossietzky Universität, Oldenburg

Tag der mündlichen Prüfung: 06. November 2013

Abstract

The objective of this thesis is to examine the role of paths for the spread of infectious diseases on complex networks. We demonstrate the importance of paths in the context of epidemiology for the case of static and temporal networks. As a central result, we introduce the unfolding accessibility method, that allows for the analysis of the path structure of temporal networks.

In this thesis, we analyze the impact of two particular attributes of static networks on the properties of their path structure. As a case study, we analyze the properties of a livestock trade network in Germany. This network exhibits a giant component and a modular structure. The main findings here are that networks close to the percolation threshold are likely to show two disjoint risk classes for the nodes and, a modular structure causes a significant delay for disease outbreaks.

Furthermore, special emphasis should be placed on the methods introduced in this thesis for the analysis of temporal networks, i.e. systems where the occurrence of edges varies over time. In this work we introduce a novel method to obtain the causal accessibility graph of a temporal network. Moreover, we introduce unfolding accessibility as a novel formalism for the evaluation of shortest path durations in temporal networks. This approach is able to reveal characteristic timescales for the traversal of temporal networks. Knowledge of these timescales is of fundamental importance for the estimation of times needed for the spread of infectious diseases.

The accessibility graph of a temporal network can be compared to its aggregated counterpart. Hence we define the causal fidelity, which quantifies the goodness of the static approximation of a temporal network from the causal point of view.

Keywords: Complex Network, Epidemiology, Temporal Network, Statistical Physics

Zusammenfassung

Ziel dieser Arbeit ist es, die Rolle von Pfaden für die Ausbreitung von Infektionskrankheiten auf komplexen Netzwerken zu untersuchen. Wir zeigen die Relevanz von Pfaden im Kontext der Epidemiologie in statischen und zeitabhängigen Netzwerken. Ein zentrales Ergebnis ist hierbei die Erreichbarkeitsentwicklung, die eine Analyse der Pfadstruktur zeitabhängiger Netzwerke erlaubt.

In dieser Dissertation wird der Einfluss zweier bestimmter Merkmale statischer Netzwerke auf die Eigenschaften ihrer Pfadstruktur untersucht. Als Fallbeispiel analysieren wir hierfür ein Viehhandelsnetzwerk in Deutschland. Dieses Netzwerk besitzt eine Riesenkomponente und eine modulare Struktur. Die wichtigsten Ergebnisse sind hierbei, dass Netzwerke, die nahe an der Perkolationsschwelle liegen, mit großer Wahrscheinlichkeit zwei disjunkte Risikoklassen für Knoten aufweisen und, dass eine modulare Struktur eine signifikante Verzögerung von Krankheitsausbrüchen zur Folge hat.

Hervorzuheben sind außerdem die Methoden, die hier zur Analyse zeitabhängiger Netzwerke vorgestellt werden. Das sind Systeme, in denen das Auftreten von Kanten mit der Zeit variiert. In dieser Arbeit stellen wir eine neue Methode vor, mit der die kausale Erreichbarkeit eines zeitabhängigen Netzwerks berechnet werden kann.

Darüber hinaus stellen wir Erreichbarkeitsentwicklung als eine neue Methode zur Berechnung kürzester Pfaddauern in zeitabhängigen Netzwerken vor. Diese Herangehensweise ermöglicht es, charakteristische Zeitskalen für das Durchqueren von zeitabhängigen Netzwerken aufzuzeigen. Die Kenntnis solcher Zeitskalen ist von fundamentaler Wichtigkeit für die Abschätzung von Zeiten, die für die Verbreitung von Epidemien benötigt werden.

Die Erreichbarkeit eines zeitabhängigen Netzwerks kann mit ihrem aggregierten Gegenstück verglichen werden. Damit definieren wir die Kausalitätstreue, die die Güte einer statischen Approximation eines zeitabhängigen Netzwerks quantifiziert.

Schlagwörter: Komplexes Netzwerk, Epidemiologie, zeitabhängiges Netzwerk, Statistische Physik

Contents

1	Introduction	1
2	Theory	7
2.1	Models of infectious diseases	7
2.1.1	SI model	7
2.1.2	SIR model	8
2.1.3	Force of infection	11
2.2	Network theory	12
2.2.1	Matrix representations	13
2.2.2	Network measures	15
2.3	Network models and epidemiology	22
2.3.1	Lattice model	23
2.3.2	Erdős-Rényi model	23
2.3.3	Watts-Strogatz model	26
2.3.4	Barabási-Albert model	27
2.3.5	Resilience of different network types	29
2.3.6	Epidemics on networks	30
3	Static network analysis – Case study: Livestock trade network	37
3.1	Network analysis	38
3.1.1	Components and ranges	39
3.1.2	Modules	41
3.2	Range & modules: Spreading potential	44
3.2.1	Epidemic model	45
3.2.2	Computer-generated networks	47
3.2.3	Impact of directionality	49
3.2.4	Impact of modularity	51
3.2.5	Impact of reciprocity in modular networks	52
4	Temporal network analysis – Case study: Livestock trade network	55
4.1	Introduction	55
4.1.1	Formal definition	56
4.1.2	Viewpoints and implementation	57
4.1.3	Paths in temporal networks	58

4.1.4	Conceptional problems in temporal networks	59
4.2	Data-driven network analysis	60
4.2.1	Representative sample	60
4.2.2	Simulated disease outbreaks	61
4.2.3	Node rankings	65
4.2.4	Inaccurate infectious periods and the robustness of node rankings .	66
4.2.5	Temporal vs. static representation	68
4.3	Graph centric temporal network analysis	70
4.3.1	Accessibility of static networks	70
4.3.2	Unfolding Accessibility of temporal networks	75
4.3.3	Representative sample / characteristic time scale	79
4.3.4	Causal fidelity	80
4.3.5	Randomization techniques	82
4.3.6	Temporal and topological mixing patterns	85
4.3.7	Further case studies	86
5	Conclusion	91
A	Appendix	95
A.1	Network implementation	95
A.2	Degree vs. other centrality measures	98
A.3	Subgraphs and maximum modularity	99
A.3.1	Two modules	99
A.3.2	Arbitrary number of modules	100
Bibliography		107

List of abbreviations

Static networks.

G	Network/Graph. A tuple $G = (V, E)$ of a set of nodes V and a set of edges E .
N	Number of nodes of a network.
m	Number of edges of a network.
D	Network diameter.
\mathbf{A}	Adjacency matrix.
\mathbf{P}_{N-1}	Accessibility matrix.
G_n^*	Accessibility graph up to path length n . The transitive closure is given by $G_{N-1}^* \equiv G^*$.
$u \rightarrow v$	A path of arbitrary length exists between u and v .
k, k^+, k^-	Degree of a node, Out-degree, In-degree.
$G(S)CC$	Giant (strongly) connected component.
$GWCC$	Giant weakly connected component.
$L(S)CC$	Largest (strongly) connected component. Often used synonymous for G(S)CC.
Q	Modularity.

Epidemic models.

α	Infection rate.
γ	Recovery rate.
R_∞	Outbreak size in SIR model.

Temporal networks.

\mathcal{G}	Temporal network given by triple $\mathcal{G} = (V, \mathcal{E}, T)$.
---------------	--

Contents

\mathcal{A}	Sequence of adjacency matrices as a graph centric temporal network representation.
\mathcal{P}_n	Accessibility matrix of a temporal network over n time steps.
\mathcal{G}_n^*	Accessibility graph up to path <i>duration</i> n . The real fully unfolded accessibility graph is in general $\mathcal{G}^* \equiv \mathcal{G}_\infty^*$.
$u \rightsquigarrow v$	A time respecting (causal) path exists between u and v .
\mathcal{H}_v	Horizon of node v .
$\text{nnz}(\mathbf{X})$	Number of non zeros of a matrix \mathbf{X} .
$\rho(\mathbf{X})$	Density of a matrix \mathbf{X} , i.e. the number of occupied non zeros normalized by the number of all possible entries.
$R(Y)$	Node ranking according to some measure Y .
d	Infectious period.
$r(v, d, t_0)$	Range of a node for memory/infectious period d and starting time t_0 . Equivalent to outbreak size for simple compartment models.
\mathcal{S}	Set of outbreak scenarios containing elements of the form $(v, d, t_0, r(v, d, t_0))$.

Randomization models.

RE	Randomized edges model. Each \mathbf{A} in \mathcal{A} is randomized so that the degree of each nodes is preserved.
TR	Time reversal. All edges and the order of matrices in \mathcal{A} are reversed.
GST	Globally shuffled times. The sequence \mathcal{A} is rearranged in random order.
LST	Locally shuffled times. All edge occurrence times are placed randomly and the number of occurrences is preserved.
RT	Random times. Every snapshot of \mathcal{G} is taken as a random subset of the aggregated network.

1 Introduction

Models for epidemics. Epidemics have always been a serious issue for societies and therefore, the understanding and prediction of the spread of infectious diseases became an important area of research. Medieval disease outbreaks, such as the spread of black death in Europe, showed a traveling wave spreading pattern (Noble, 1974). Although the course of this particular outbreak was rather simple from a present-day perspective, modeling the dynamics of an infectious disease is in general a challenging endeavor. Early attempts go back to the 18th century; in his review about the mathematics of infectious diseases, Hethcote reports that a model for smallpox was formulated already in 1760 by D. Bernoulli (see Hethcote (2000) and references therein).

In the early 20th century, the foundations for modern mathematical models of epidemics were developed: a discrete time model in 1906 (Hamer, 1906) and a differential equation model in 1911 (Ross, 1911). Major contributions to the modern theoretical framework were provided by Kermack and McKendrick (1927), Bailey (1957), and Anderson and May (1991). In particular, Kermack and McKendrick found the existence of an epidemic threshold, i.e. a disease requires a critical infection rate in order to propagate (Kermack and McKendrick, 1927). Starting from Bailey's book (Bailey, 1957) in the 1950s, the modeling of infectious diseases became a major scientific research field. Modern models of infectious diseases increase in complexity: They include vaccination, demographic structure, disease vectors and quarantine (see references in (Hethcote, 2000)). In addition to that, the actual usage of vaccines in the population can be modeled in terms of game theory (Bauch and Earn, 2004). The availability of host contact data in recent years led to a strong impact of network analysis on epidemiology (Mossong et al., 2008). Well-known concepts of mathematics, such as graph theory (Bollobás, 1985), and social sciences, such as social network analysis (Wasserman and Faust, 1994), have been adopted to disease modeling, since the links between individuals are related to their epidemic spreading potential (Keeling and Eames, 2005).

Besides infectious diseases of humans, many methods from human epidemiology have also been adopted to animal diseases and livestock diseases in particular. Livestock epidemics are a major economic issue in agriculture. A prominent example is foot-and-mouth disease, which caused tremendous economic losses in the UK in 2001 (Kitching et al., 2005). Due to legislation introduced 2001 after the BSE crisis, large amounts of data on livestock movements have been collected in Europe. Network models reflecting livestock trade movements have gained particular attention in recent years (Christley et al., 2005; Green et al., 2006; Kao et al., 2007; Bigras-Poulin et al., 2007; Dubé et al.,

2009; Martínez-López et al., 2009; Lentz et al., 2011; Konschake et al., 2013; Fournié et al., 2013). Livestock trade network analysis provides support for the planning of surveillance and vaccination strategies in livestock disease management.

Epidemic models can be divided into two classes: *forecast* models and *conceptual* models. Forecast models incorporate as much information as necessary to predict the course of a disease. Conceptual models are used in the context of understanding the principles behind epidemic spreading processes, i.e. the way how a disease is transmitted through a population. They make use of simple assumptions for the local dynamics and focus on a macroscopic picture of the process. Conceptual models are very similar to models in theoretical physics, because they focus on the very essence of the problem. However, they have to neglect many details of the real problem – such as physiology, symptoms, individual behavior, infection pathways and many more! – in order to be mathematically feasible.

In this work, we use conceptual models in combination with different network topologies in order to gain insights into the impact of certain network properties on the course of a disease outbreak.

Complex networks as spreading substrates. Network analysis has become an essential element of epidemiology, where networks are used to model interactions between the individuals of a population. Besides epidemiological substrates, networks can be anything comprising actors (nodes) that are connected by links (edges). Modern network science is concerned in the broadest sense with the description and development of complex networks, regardless of what the network structure describes in particular. Reviews on network science are provided by Newman (2003) and Albert and Barabási (2002).

The mathematical roots of network science go back to *graph theory* developed by Euler in the 18th century. Euler solved the so-called seven bridges of Königsberg problem by showing that there is no closed path traversing all edges of a network exactly once, if more than two nodes have an odd number of adjacent links (Euler, 1736), say an odd degree. Since detailed information about most networks was not available until the end of the 20th century, early network science focused on the study of random networks. In 1959, Erdős and Rényi studied dense random networks and later analyzed the percolation properties of these systems (Erdős and Rényi, 1960, 1961).

Beyond the tools and methods of graph theory, the origins of modern network science also go back to *sociology*. More specifically, the complexity of human interactions was modeled in terms of social networks. The analysis of social networks raised a lot of questions about the roles of particular individuals in these systems. In fact, many of the measures used in modern network science have been defined in the sociological literature decades ago (Milgram, 1967; Merton, 1968; Granovetter, 1973; Zachary, 1977; Freeman, 1978; Wasserman and Faust, 1994).

In recent years, data of huge scale have emerged by the proliferation of computerized

data acquisition and storage volumes. These data can be used in order to gain a deeper insight into many networked systems such as the trade of livestock animals between farms (EUR-Lex, 2000) or the structure of the world-wide web (Albert et al., 1999; Barabási and Albert, 1999). Other prominent examples are food webs (Martinez, 1991), citation networks (Egghe and Rousseau, 1990), power grids (Watts and Strogatz, 1998), or mobile phone call networks (Schneider et al., 2013). As a particular case study, we analyze the network of livestock trade in Germany (EUR-Lex, 2000) in detail in this thesis.

The analysis of real-world networks lead to the formulation of network models which structurally deviate from random graphs. It was found that many real-world networks show a high degree of clustering, i.e. a relatively large number of closed triangles. This fact was first reported by Milgram (1967) and finally incorporated into the small-world model by Watts and Strogatz (1998). Additionally, observations of real-world network datasets showed that many networks are scale-free, i.e. their degree distribution can be approximated by power laws (Albert et al., 1999; Newman, 2003). The existence of these power laws can be explained using a preferential attachment model for the formation of the network (Barabási and Albert, 1999). It has been shown that scale-free networks are particularly vulnerable to targeted attacks (Albert et al., 2000) and the epidemic threshold vanishes in these systems (Pastor-Satorras and Vespignani, 2001).

The very essence of the investigation of spread of infectious diseases on networks is to determine the *paths* that a spreading process can unfold on. The path structure between the nodes of a network is closely related to its percolation properties, i.e. the existence of a giant connected component or percolating cluster. In fact, percolation is inherently related to the epidemic threshold (Sander et al., 2002, 2003). Furthermore, the structure of the percolating cluster is generally comprised of other complex substructures in directed networks (Dorogovtsev et al., 2001). As a concept similar to connected components, densely connected subgraphs – so called modules – were introduced by Newman (2006). Modules allow for a statistically small number of paths between each other. These structures have been observed in the livestock network analyzed in this thesis (see Section 3.1.2 and Lentz et al. (2011)) and in other networks (Clauset et al., 2004; Fortunato, 2010).

The impact of modular structure on disease spreading has been studied for social networks by Salathé and Jones (2010). However, livestock trade networks differ from social networks in the sense that in livestock trade networks, nodes are not individuals and edges appear as directed links. For the case livestock trade networks, the impact of a modular structure has not been analyzed systematically yet. Moreover, the directed nature of these systems requires investigation of the role of edge direction. The following unanswered questions remain:

- What role does the direction of edges play for the spread of infectious diseases?
- How does a modular structure affect epidemics in a livestock trade network?

We address these questions in Chapter 3, where we derive a model for infection dynamics on a network of metapopulations connected by directed edges.

Although network analysis in the sense above provides a powerful tool for the understanding and forecast of epidemics, it neglects the fact that most real world networks are not static systems. As a matter of fact, the edges of many networks show heavy fluctuations over time. Therefore, the analysis of *temporal networks* has attracted significant attention during the last years. Reviews about temporal networks are provided by Casteigts et al. (2012) and Holme and Saramäki (2012). In contrast to static network analysis, a number of problems arise from the significance of causality in temporal network analysis (Casteigts et al., 2012; Nicosia et al., 2012).

For this reason, the majority of contributions to temporal network analysis has made use of data-driven approaches. In the first instance, a quasi static treatment of temporal networks can be considered in order to examine the usability of static network analysis tools. Different time aggregation windows have been investigated in data-driven analyses of livestock trade networks of different European countries in (Vernon and Keeling, 2009; Bajardi et al., 2011). Vernon and Keeling (2009) and Bajardi et al. (2011) showed that time aggregated networks may fail to capture the epidemic behavior of the temporal system. The stability of node rankings in a temporal livestock trade network was analyzed by Konschake et al. (2013) for different infectious periods, where stability regions of node rankings have been found numerically.

Considering human mobility networks, temporal distances between nodes have been analyzed in an air transportation network, where systematical deviations between static shortest path distances and temporal shortest path durations were observed (Pan and Saramäki, 2011). On a more local mobility level, a network of bike sharing locations has been investigated by Vogel et al. (2011), where the authors found different node classes according to a similarity of temporal degree patterns. Temporal contact patterns in form of a growing network of sexual contacts were analyzed by Rocha et al. (2010, 2011). Rocha et al. found a preferential attachment rule for a growing web community.

Beyond data-driven approaches, there have been only a few approaches to provide a graph centric, formal view on temporal networks. This is attributed to the central role of causality in temporal networks. In fact, it has been shown that even the detection of connected components is an intractable problem in most temporal networks (Bhadra and Ferreira, 2003; Nicosia et al., 2012). Nevertheless, network snapshots can be used to generalize static centrality concepts. Grindrod et al. found a convenient way to quantify the ability of every node to receive and broadcast information (Grindrod et al., 2011). Network snapshots have also been used in order to generalize the concept of small-world networks in (Tang et al., 2010), where clustering is measured in terms of the persistence of links over time. Besides the temporal network model introduced by Tang et al. (2010), random walk models can be used in order to generate synthetic temporal networks reproducing the bursty behavior of real-world datasets (Barrat et al., 2013).

What is still missing is a closed mathematical formalism for temporal network analysis

preserving the causality of paths. As a fundamental element, this formalism must contain the mere topological path structure and the time-scales needed for path traversal. Central questions in this context are

- How can causal paths be computed using adjacency matrices?
- What is the distribution of shortest path durations?
- How can the causal goodness of the static approximation of a temporal network be quantified?

We address these questions in Chapter 4, where we introduce the novel method of *unfolding accessibility* for temporal networks. The method is capable of answering all questions above. We believe that providing the causal path structure of temporal networks contributes a key element for the construction of a variety of other temporal network analysis tools.

This work is structured as follows: We review some fundamental results of mathematical epidemiology and network science necessary for understanding the other chapters in **Chapter 2**. Classic models for the spread of infectious diseases are discussed in Section 2.1. In Section 2.2, we report basic concepts of network theory and discuss the relevance of different network types for epidemiological questions in Section 2.3. In **Chapter 3**, for the first time we systematically analyze the trade of livestock pigs in Germany as a static network. Hereby, we identify its path structure as a crucial epidemiological factor in Section 3.1. The spreading potential of the observed path structure is analyzed in Section 3.2. **Chapter 4** is devoted to the investigation of the full temporal information of the livestock trade network. After a general discussion of temporal networks in Section 4.1, we analyze the network data systematically in Section 4.2. Moreover, we introduce the unfolding accessibility method as a new approach to measure the causal path structure in temporal networks in Section 4.3. We use accessibility in order to quantify the goodness of an aggregated representation of a temporal network in Section 4.3.4. Finally, we demonstrate the capability of the introduced methods for additional datasets in Section 4.3.7.

2 Theory

In this chapter, we review the mathematical formalism that is used to model infectious diseases and networks. We define mathematical frameworks for the analysis of epidemics and networks in this chapter and summarize several relevant results of earlier research. The modeling of infectious diseases makes extensive use of compartment models. We address these models in sections 2.1.1 and 2.1.2. Section 2.2 gives an overview over several results of modern network theory. In addition, Appendix A.1 describes efficient computer implementations of networks.

2.1 Models of infectious diseases

Before we formulate models for the spread of epidemic diseases, we have to differentiate between *conceptual* models and *realistic* disease models. While the former class is used to provide conceptional results such as the computation of thresholds or testing theories (Hethcote, 2000), realistic disease models use as many aspects as possible to provide a forecast of a particular spreading process. Realistic disease models can be very complex and are beyond the scope of this work, hence we focus on the use of conceptional models. In the following section we briefly report some properties of basic epidemic models following the lecture notes of Chasnov (2010).

2.1.1 SI model

Let us consider a population of N individuals. In the simplest case, the infection status of each individual is either susceptible (S) or infected (I) and there are no births and deaths in the population. Susceptible individuals become infected, if they are in contact with an infected¹. In epidemiology, the classes susceptible and infected are called *compartments* and every new infection increases the population of the infected compartment following the local reaction scheme

$$S + I \rightarrow 2I.$$

¹There is a distinction between infected and infectious, in general. By definition, infected individuals are invaded by a pathogen and act as hosts for its multiplication. On the contrary, only *infectious* individuals have the ability to infect others and infected individuals are not necessarily infectious (Rolle and Mayr, 2006). Nevertheless, we consider infected equivalent infectious throughout this thesis.

This mimics the behavior of an infectious disease without immunization, i.e. infected individuals stay permanently infected.

Provided that α is the rate, under which new susceptible become infected, we obtain the corresponding differential equation model

$$\begin{aligned}\frac{dS}{dt} &= -\alpha SI \\ \frac{dI}{dt} &= \alpha SI,\end{aligned}\tag{2.1}$$

where S and I are the numbers of susceptible and infected individuals respectively. The model (2.1) is called SI-model. The total population is $N = S + I$. Thus, (2.1) can be rewritten as

$$\frac{dI}{dt} = \alpha(N - I)I,$$

i.e. a logistic differential equation. Hence, in the limit $t \rightarrow \infty$ the whole population is infected ($I(\infty) = N$).

2.1.2 SIR model

In contrast to the infection dynamics introduced in the previous section, many epidemics include an immunized state, where immunized individuals do not contribute to disease spread. Examples are measles or whooping cough (Anderson and May, 1991; Grenfell, 1992). In these cases, individuals recover from the disease after being infected for a certain time period. This behavior is modeled by the introduction of an additional compartment for the recovered population. The infection scheme is extended to susceptible-infected-recovered (SIR) as in the following infection model (Kermack and McKendrick, 1927):

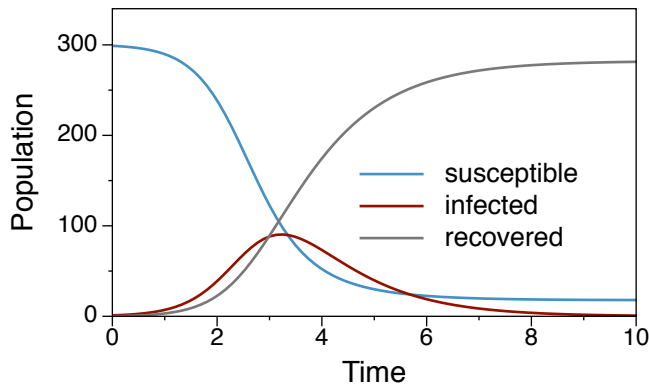
$$\begin{aligned}\frac{dS}{dt} &= -\alpha SI \\ \frac{dI}{dt} &= \alpha SI - \gamma I \\ \frac{dR}{dt} &= \gamma I,\end{aligned}\tag{2.2}$$

where α is the infection rate and γ is the immunization or recovery rate. A typical solution of (2.2) is shown in Figure 2.1. There is no analytic solution for the system (2.2), but some fundamental conclusions can be obtained analytically.

The SIR model shows more sophisticated features than the SI model (2.1). To begin with, we analyze the fixed points of the system, i.e. (S_*, I_*, R_*) where

$$\frac{dS_*}{dt} = -\alpha S_* I_* = 0, \quad \frac{dI_*}{dt} = \alpha S_* I_* - \gamma I_* = 0, \quad \frac{dR_*}{dt} = \gamma I_* = 0.\tag{2.3}$$

Figure 2.1. Solution of the susceptible-infected-recovered (SIR) model (2.2). The number of infected shows that the spreading process is a single event. Note that a fraction of the population is still susceptible at the end of the process. Parameters: $\alpha = 3$, $\gamma = 1$, $N = 300$, $S_0 = 1$.



It follows from the last equation that $I_* = 0$ at the fixed point, where S_* and R_* can be arbitrary as long as $S_* + R_* = N$. Hence, $(S_*, 0, R_*)$ is a fixed point.

Let us first analyze the stability of the fixed point in the early phase of an infection. Almost all individuals are susceptible and consequently $I_* = N - S_*$. An outbreak occurs, if and only if $dI/dt > 0$ in this phase, i.e.

$$\frac{dI}{dt} = \alpha S_*(N - S_*) - \gamma(N - S_*) = (N - S_*)(\alpha S_* - \gamma) > 0. \quad (2.4)$$

It follows from (2.4) that the number of infected grows, if

$$\alpha S_* / \gamma > 1. \quad (2.5)$$

Equation (2.5) is extremely important in epidemiology, because it defines a threshold for the unfolding of an infection spreading process. This fraction is called the *basic reproduction number* R_0 . Recall that $S_* \approx N$ in the fixed point. Thus, it follows that the outbreak condition is

$$R_0 = N \frac{\alpha}{\gamma} > 1. \quad (2.6)$$

The basic reproduction number describes the average number of follow-up infections by each infected individual. It is one of the main goals in epidemiology to bring down the basic reproduction number of a disease below the critical value $R_0 = 1$. As one can immediately see from Equation (2.6), this can be done by reducing the infection rate α or by increasing the immunization rate γ . This is the reason for the implementation of mass vaccination. Vaccination basically decreases the size of the initial susceptible population $S_0 = S_*$. A reduction of the infection rate can be achieved by increasing hygiene standards or appropriate behavior, say wearing warm clothes in winter time to avoid common cold. The immunization rate can be increased by drugs.

Let us now focus on the late phase of an SIR-infection. In contrast to the SI-model of

Section 2.1.1 an SIR like outbreak does not necessarily infect the whole population, even if $R_0 > 1$. The reason is that there has to be a critical mass of susceptible individuals in order to keep an infection alive (see Equation (2.5)). The total number of infected during an infection given by the number of recovered at the end of the infection, since every recovered has to be in the infected state in the first place. A central measure throughout this work is therefore the *outbreak size* R_∞ .

To compute the outbreak size, we consider the second fixed point of (2.2), i.e. the fixed point for $t \rightarrow \infty$. At this point there are no infected and a fraction of the population is recovered. Hence, the fixed point is $(N - R_\infty, 0, R_\infty)$. A simple way to obtain the outbreak size R_∞ is to use equations (2.2) and compute

$$\frac{dS}{dR} = -\frac{\alpha}{\gamma} S$$

and separate the variables (Chasnov, 2010). This yields

$$\int_{S_*}^{N-R_\infty} \frac{dS}{S} = -\frac{\alpha}{\gamma} \int_{R_*}^{R_\infty} dR.$$

We integrate from the initial condition at $t = 0$ to the final condition at $t \rightarrow \infty$, where $S_\infty = N - R_\infty$. Using that $R_* = 0$ at $t = 0$ gives

$$R_\infty = S_* - S_* e^{-\frac{\alpha}{\gamma} R_\infty}. \quad (2.7)$$

This transcendental equation can be solved numerically using a Newton-Raphson technique. The outbreak size R_∞ only takes finite values for $\alpha/\gamma > 1$. A solution of Equation (2.7) is shown in Figure 2.2

It should be noted that an SIR epidemic is a single event, i.e. it possesses a *characteristic time scale*. The analysis of the late phase of an epidemic also gives information about these time scales. Let us consider the second equation of (2.2).

$$\frac{dI}{dt} = \alpha SI - \gamma I \quad (2.8)$$

In the late phase of an SIR-type epidemic, the fraction of infected is small. Given sufficiently large values of R_0 , the fraction of susceptible is also small in this phase (see Figure 2.2). Thus, we neglect the quadratic term in (2.8). This gives $\frac{dI}{dt} = -\gamma I$, which has the solution

$$I(t) = I(0)e^{-\gamma t}. \quad (2.9)$$

Hence, the infection decays exponentially for large t and the inverse recovery rate $1/\gamma$ defines the characteristic time of the epidemic.

A similar concept to the SIR model is the SIS model, where infected individuals return

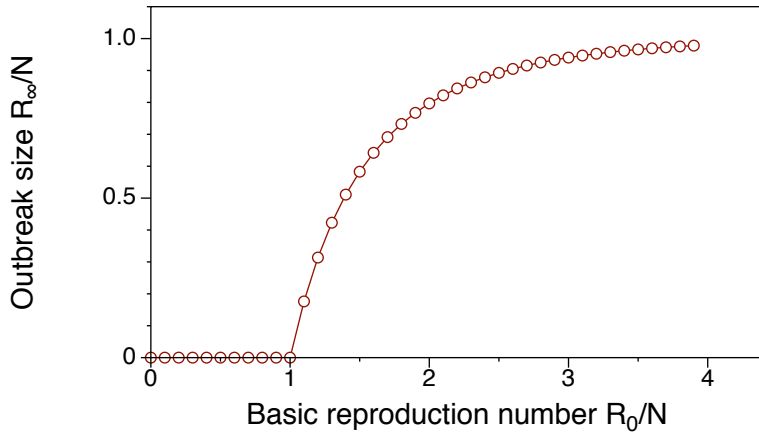


Figure 2.2. Relative outbreak size vs. basic reproduction number. The outbreak size takes finite values only for $R_0/N > 1$. Note that even for supercritical R_0 the outbreak size is in general smaller than the total population.

to the susceptible state after a certain period. Being a single-event model, the SIS model has many similarities to the SIR model. The most crucial difference is that SIS models show an endemic state for $t \rightarrow \infty$, i.e. both S and I take finite values in the long term so that fraction of infected remains in the system permanently.

2.1.3 Force of infection

The model presented in Section 2.1.2 describes only the very basic behavior of epidemic dynamics, and is therefore a conceptional model. However, it is one of the main objectives in epidemiology to have an understanding of the explicit *infection rates* in the process. Depending on their detailed structure, the infection rates themselves can cause complex infection dynamics.

The term αI used in αSI in the second equation of (2.2) is a special, very simple case of an infection rate. It corresponds to the case where every susceptible is in contact with every infected in the population. More generally, we have to replace αI by an abstract infection rate λ containing more information about the interaction between susceptible and infected individuals (Keeling and Eames, 2005). Thus, the equation for the infected becomes

$$\frac{dI}{dt} = -\lambda S - \gamma I.$$

The rate λ is called the *force of infection*. In principle, this parameter can be arbitrarily complex, because it contains detailed information about the mixing properties of the population. This information can be represented as contact networks, demographic

contact structures, etc.

In most cases, detailed information about mixing is not available. Instead, we assume *random mixing* of the population, i.e. every individual can be in contact with every other individual.

Considering a contact rate, where each individual has a small chance of being connected to any other individual in the population yields a transmission rate (Keeling and Eames, 2005)

$$\lambda = \tau n \frac{I}{N} \equiv \beta \frac{I}{N}, \quad (2.10)$$

where τ is the transmission rate, n is the effective contact rate and I/N is the fraction of infectious contacts. The factor $1/N$ can be interpreted as the “contact surface” between the susceptible and infected population. It is reasonable to replace the infection term α in (2.2) by β/N to explicitly include the force of infection. The results presented in Section 2.1.2 remain qualitatively the same.

Although the force of infection gives a more reasonable description of the infection process, the assumption of random mixing remains inappropriate for many real world systems. Due to the availability of contact data, the random mixing assumption can be improved in terms of contact networks. Even if the exact data of an epidemic system is not available, research on complex networks allows us to give more realistic models about mixing. In the next section, we briefly report important results in complex network research and focus on the interplay between networks and epidemics in Section 2.3.6.

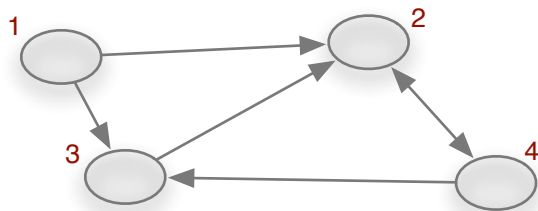
2.2 Network theory

As we have pointed out in the previous section, standard epidemic models make use of the random mixing assumption. This assumption holds, if no further information about the contact structure within a population is available. The random mixing assumption yields a worst case scenario of the infection dynamics. Even an overestimation of the outbreak size can be corrected by introducing smaller, effective disease parameters. However, the random mixing assumption does not allow for non homogeneous mixing, since each individual is considered equal. The equality of links between individuals is not a reasonable assumption for many epidemic substrates. Examples of epidemic substrates are contact structures of humans, livestock trade or links between computers. Apparently, connections are not purely random in these systems so that there are certain rules for the occurrence of links.

The main contribution of network science to epidemiology is that it allows for the analysis of detailed contact structures. If detailed information about the contact structure is available, the random mixing assumption is obsolete. Instead, the system can be treated using the underlying contact structure in form of a network. Since the beginning of the 21st century, large amounts of data about these contact structures have become

Figure 2.3. A simple directed network. The corresponding adjacency matrix is

$$\mathbf{A} = \begin{pmatrix} 0 & 1 & 1 & 0 \\ 0 & 0 & 0 & 1 \\ 0 & 1 & 0 & 0 \\ 0 & 1 & 1 & 0 \end{pmatrix}.$$



available for social, economic, transportation, and biological networks. Observations showed that many real-world networks share common topological properties, which are described in Section 2.2.2). Since the number of their non-trivial topological properties is considerable, they are often referred to as *complex* networks.

Modern network science is an interdisciplinary research field, because it addresses systems of diverse scientific affinity. Its roots lie in graph theory (mathematics) and social network analysis (social sciences). Social network analysis plays a particular role for the definition of local network measures (see Section 2.2.2), whereas the influence of graph theory is stronger in macroscopic problems as percolation or statistical properties in the thermodynamic limit. An important focus of network science is to find common features of different networks and to explore the basic principles behind their emergence. Applied network science makes extensive use of methods used in computer science. A brief introduction to efficient computer methods for network analysis is provided in Appendix A.1.

2.2.1 Matrix representations

A network is a system of nodes that are connected by edges. Edges can be undirected, directed and weighted. In principle, a network can consist of edges of different types. In this case, the network can be represented by multiple networks sharing the same set of nodes, but different edges.

Networks are called graphs in mathematical literature. A graph $G = (V, E)$ is a set of nodes (or vertices) V and edges (or arcs) E , where each edge is given by the tuple of nodes it connects, i.e. $e_1 = (u, v) \in E$ connects nodes u and v . An edge (u, v) being present in an undirected network implies the existence an edge (v, u) . Apparently, this does not hold in directed networks. In weighted networks, the edges carry additional information – such as their importance, capacity, number of transported items or the geographical distance between the nodes they connect.

Graphs can be represented by different graph matrices, where each matrix representation emphasizes typical properties of the network. The most common graph matrix is

the *adjacency matrix* \mathbf{A} with entries

$$a_{ij} \equiv (\mathbf{A})_{ij} = \begin{cases} 1 & \text{if } i \text{ is connected to } j \\ 0 & \text{else,} \end{cases} \quad (2.11)$$

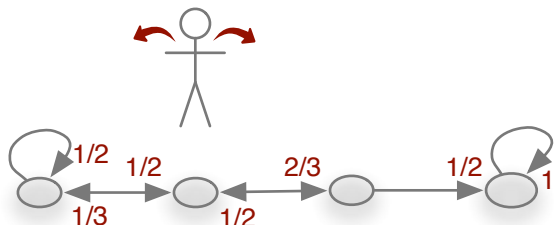
where the indices correspond to node labels. An adjacency matrix contains the edges of the graph and can be seen of the most fundamental graph representation. Figure 2.3 shows a simple example of a directed graph and its adjacency matrix. The corresponding matrix would be symmetric in the undirected case. Weighted networks can be represented by weight matrices, where the values of the entries in (2.11) are not restricted to 0 and 1.

The adjacency matrix of an undirected network is always symmetric, because every non-zero entry $a_{ij} = 1$ implies an edge into the opposite direction, $a_{ji} = 1$. Entries on the main diagonal a_{ii} correspond to nodes with self loops, i.e. nodes with edges pointing back to themselves. The i -th row the adjacency matrix contains non-zero entries $a_{ij} = 1$, wherever node i is connected to node j . Hence, every row can be interpreted as the neighborhood of one node. This holds for undirected and for directed networks. The columns of \mathbf{A} give the same information as the rows in the undirected case. In directed networks, however, rows contain the out-neighborhood of each node and columns contain the in-neighborhood, respectively.

Information about paths of a certain length can be obtained using the powers of the adjacency matrix. The adjacency matrix contains information about the number of paths of length 1 between node pairs. Evidently, the number of paths of length 2 between two nodes i and j is given by $(\mathbf{A}^2)_{ij}$. This applies also to paths of arbitrary length n using the elements of \mathbf{A}^n .

An important example for weighted network matrices is a *Markov chain*. A Markov chain is a random process without memory and with a discrete state space and discrete time. It is called time-homogeneous, if the transition rates are constant. Time-homogeneous Markov chains can be represented as weighted networks and the corresponding weighted adjacency matrix is the *transition matrix*. Transition matrices are stochastic matrices, i.e. the elements of every row sum up to unity. Each node represents a different state of the system and each edge is weighted with the probability to transition into the other state adjacent to the edge. It is obvious that a transition matrix representation is useful to describe random walks on networks. An example of such a process is shown in Figure 2.4. The figure shows a drunkard toddling randomly in the left or right direction. The underlying network represents a line of locations, where the drunkard can be located. At every time-step there is a certain probability to move to another location. The state of the random walker can be described by a probability vector \mathbf{p} , where the initial state of Figure 2.4 is $\mathbf{p} = (0, 1, 0, 0)$. The transition matrix \mathbf{M} is a weighted adjacency matrix as it follows from the figure. Given a state \mathbf{p}_t at time t , the state of the next time step is given by $\mathbf{p}_{t+1} = \mathbf{p}_t \mathbf{M}^T$. The equilibrium state \mathbf{p}_{eq}

Figure 2.4. Trajectory of a toddling drunk man as an example of a Markov chain. At every location there is a probability for the drunkard to go left or right. The node rightmost node is an absorbing state and could model a park bench. Weights at arrowheads mark the transition probability. (inspired by (Aldous and Wilson, 2000)).



follows in the limit $\lim_{t \rightarrow \infty} \mathbf{p}_0(\mathbf{M}^T)^t$, i.e. the equilibrium state is given by the dominant eigenvector of \mathbf{M} .

As a special case of transition matrices, the author would like to mention the *Google matrix*. It describes a random walk on a network, but allows for shortcuts to any node in the network with a certain probability. The eigenvectors of Google matrices are used for the computation of node rankings according to the PageRank-Algorithm (Page, 1997).

Finally, the *Laplace-matrix* of a network is an appropriate representation to model diffusion processes on networks. For undirected networks the Laplace-matrix is defined as

$$\mathcal{L} = \mathbf{D} - \mathbf{A}, \quad (2.12)$$

where \mathbf{A} is the adjacency matrix and \mathbf{D} is a diagonal matrix containing the degree $d_i = \sum_j a_{ij}$ of each node. The definition (2.12) has strong analogies to the discrete Laplace-Operator (Press et al., 1992). Consequently, it can be used to model diffusion processes on graphs in analogy to Laplace operators in continuous systems (see Section 3.2). The spectra of adjacency and Laplace matrices also contain information about the evolution/history of networks (Banerjee and Jost, 2009).

2.2.2 Network measures

Before we address ourselves to models of real world networks, we may introduce methods to measure structural properties of networks. On the microscopic scale, this can be done in terms of *node centrality* measures. These measures are crucial to assess the importance of single nodes in the network. On the macroscopic scale, we are interested in the large-scale properties of networks, i.e. percolation, distributions of centralities, connected components, or other large scale structures.

Implementations of appropriate data structures for the computation of network measures are briefly summarized in Appendix A.1.

Network terminology

Let $G = (V, E)$ be a graph consisting of a set of nodes V and a set of edges E . We denote the number of nodes in the network by $N = |V|$ and the number of edges by

$m = |E|$. Every route across a graph along its edges without repeating nodes is called a *path*. Each path is given by an ordered set of the nodes traversed, i.e. (v_1, v_2, \dots, v_l) , with $v_i \in V$ and all traversed edges are in E , i.e. $v_i, v_{i+1} \subseteq E$ for all i . A *shortest path* between a node pair is given by the smallest set of nodes connecting it. In general, there exist multiple shortest paths between nodes. If there is a path from every node in the network to any other node, the network is called *connected*. In directed networks, we have to consider two types of connectedness. A directed network is strongly connected, if there is a directed path between all node pairs and weakly connected, if the node pairs would be connected ignoring the direction of edges.

The *distance* between two nodes is the length of the shortest path between them and the longest distance between all node pairs is the *diameter* D of the network. Every closed path is called a *cycle*. Graphs that do not contain cycles are called acyclic graphs or *trees*. The neighborhood of a node u is the set of all nodes adjacent to it and the size of the neighborhood is the *degree* of the node. Hence, a node v is in the neighborhood of u , if $(u, v) \in E$. We distinguish between in-degree and out-degree in directed networks. Finally, $G_0 = (V_0, E_0)$ is a *subgraph* of $G = (V, E)$, if $V_0 \subseteq V$ and $E_0 \subseteq E$.

Microscopic measures

Given a network, an important question is, if some nodes are more important than others. Therefore, we summarize several measures of node *centrality*. The idea of centrality mainly goes back to social network analysis (Granovetter, 1973; Freeman, 1978; Wasserman and Faust, 1994), but has been widely adopted and extended in network science. We restrict ourselves to those measures, that are indispensable when describing networks. A more exhaustive overview of centrality measures is found in the review article (Martínez-López et al., 2009) or in online documentation of network analysis software, e.g. (Hagberg et al., 2008; Hagberg, 2012). In the following, N denotes the order of the network (the number of nodes) and m the number of edges.

Degree. The simplest centrality measure is the degree k of a node, which is the number of its neighbors. In directed network, we distinguish between in-degree k^- and out-degree k^+ . The degree follows immediately from the adjacency matrix, i.e.

$$k^-(i) = \sum_j a_{ji} \quad \text{and} \quad k^+(i) = \sum_j a_{ij}$$

is the in- and out-degree of node i , respectively. As an example, node 8 in Figure 2.5 has $k^+(8) = 4$ and $k^-(8) = 1$. In weighted networks, the degree is computed in the same manner using a weight-matrix and is called in-weight and out-weight, respectively.

The degree centrality (sometimes normalized by its maximum value $N - 1$) is used in a huge variety of applications. One of its most important applications is to measure the heterogeneity of network connections, i.e. the existence of hubs in the network. Hubs

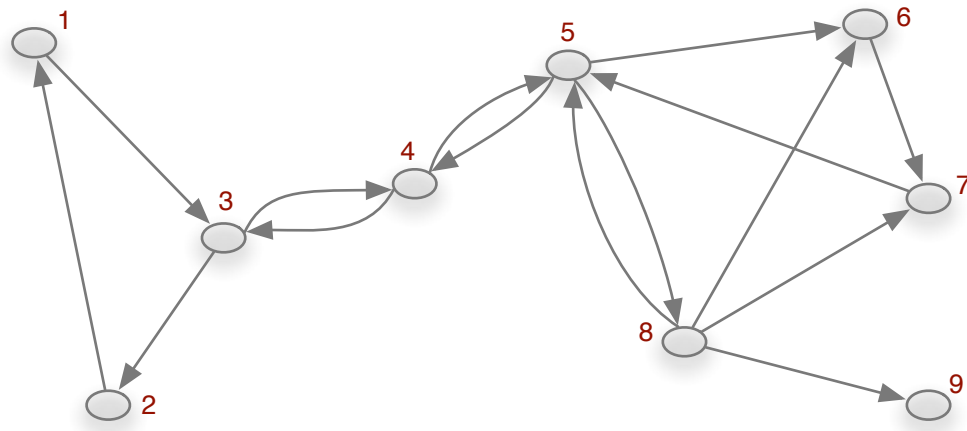


Figure 2.5. A directed network for the demonstration of different centrality measures.

are nodes with a degree much larger than the rest of the system. The heterogeneity of networks can be measured in terms of degree distributions. We discuss the role degree distributions in Sections 2.2.2 and 2.3.4.

Closeness. The closeness of a node i is the reciprocal average distance to all other nodes that can be reached from i . It can be normalized, so that the closeness is 1, if all other nodes are reachable within one step and 0 in the limit of infinite distances to all other nodes. The closeness of a node i in a network of order N is defined as follows:

$$c(i) = \frac{N - 1}{\sum_j d_{ij}} \quad (2.13)$$

where d_{ij} is the distance between nodes i and j . Some tools for an efficient computation of shortest-path distances are summarized in Section A.1. It should be noted that the distance between two nodes is defined to be infinite, if they are located in different components. In this case, the corresponding terms are ignored and do not contribute to the sum in Equation (2.13). Thus the closeness is computed for each connected component separately.

Closeness centrality is capable of identifying nodes with short average path lengths to other nodes in the network. Identifying high-closeness nodes is therefore reasonable for network navigation. This holds in particular, if the exact route to the destination is unknown, because nodes with high closeness are probable to reach many destinations quickly. In (Sudarshan Iyengar et al., 2012) it was shown that nodes of high closeness can act as efficient landmarks for navigation.

Betweenness. In order to identify nodes that act as bridges between two subgraphs, the measure of betweenness was developed. In Figure 2.5, node 4 plays such a role. It is characteristic for these nodes to contain a relatively large number of shortest paths that have to cross them. Therefore, betweenness of a node i is defined as

$$b(i) = \sum_{s \neq i \neq t} \frac{\sigma_{st}(i)}{\sigma_{st}} \quad (2.14)$$

where σ_{st} is the number of shortest paths between nodes s and t and $\sigma_{st}(i)$ is the number of shortest paths between s and t going through node i . The computation of betweenness is expensive using Equation (2.14) directly. Therefore, an efficient algorithm was introduced by Brandes (Brandes, 2001).

Note that bridge nodes might look ordinary in the first place, e.g. they could have only a few links. However, removing node 5 in Figure 2.5, for instance, would divide the network into two disjoint subgraphs with nodes $V_1 = (1, 2, 3)$ and $V_2 = (5, 6, 7, 8, 9)$ respectively. Therefore, removing nodes of high betweenness from the network has been proven useful in order to divide networks into smaller components (Girvan and Newman, 2002; Newman and Girvan, 2004).

Eigenvector centrality. The idea of eigenvector centrality can be easily captured recalling the Markov chains described in Section 2.2.1. Frequent iterative multiplication of the transition matrix \mathbf{M} with a random vector gives the largest eigenvector of \mathbf{M} . This relation is known as power method or von Mises iteration (von Mises and Pollaczek-Geiringer, 1929). The dominant eigenvector of the transition matrix gives the equilibrium state of the system. Using this state as a measure of centrality assigns every node with the probability to find a random walker there after a long period. The principle behind the dominant eigenvector of an adjacency matrix \mathbf{A} is that important nodes are likely to be connected to other important nodes. This recursive concept is reflected in the equation

$$x_i = \frac{1}{\lambda} \sum_j a_{ij} x_j,$$

where x_i is the centrality of i , $\sum_j a_{ij} x_j$ is the centrality of the neighborhood of i and λ is a constant. This equation can be written as

$$\mathbf{Ax} = \lambda \mathbf{x}. \quad (2.15)$$

It follows from the Perron-Frobenius-Theorem that λ must be the largest eigenvalue of \mathbf{A} in order to guarantee all entries of \mathbf{x} to be positive (Bonacich, 1972, 2007). The theorem guarantees unique solutions only for adjacency matrices of connected networks. Hence, eigenvector centrality is only defined for connected graphs. Nevertheless, the eigenvector centrality can be computed for each component separately, if a graph is not

connected (Bonacich, 2007). Two widely used variants of eigenvector centrality allowing for disconnected networks are the PageRank and HITS algorithm (Kleinberg, 1999; Page, 1997).

Node components and range. The component of a node is the set of nodes it is connected to by a path of any length. We call the size of this set the *range* of a node (Lentz et al., 2012). In directed networks, we distinguish between the out-component and in-component of a node. The size of the former is its range and the size of the latter is its reachability. Reachability measures the vulnerability of nodes against disease outbreaks in the network. Given a network $G = (V, E)$ of N nodes, the range of a node $v \in V$ is defined as

$$\text{range}(v) = \frac{|H|}{N}, \quad \text{where } H = \{u \in V : v \rightarrow u\}, \quad (2.16)$$

where $v \rightarrow u$ means that there exists a path from v to u . The reachability of a node is its range in the inverse graph $G^{-1} = (V, E^{-1})$, in which the directions of all edges are reversed.

Apparently, the range of a node is of major importance for any epidemiological problem on a network, because it defines an upper bound for the size of any outbreak starting at this very node. Although the range measure is rather simple, it can show an interesting distribution. The shape of its distribution is inherently related to percolation properties of the network. We discuss this relation in Section 3.1.

Macroscopic measures

In order to obtain a macroscopic view of a network, we discuss measures that capture its large scale properties. The central question for the analysis of real-world networks is, whether different networks share similar large-scale features or whether each network is unique. In principle, the distribution of any centrality measure could yield insights into the macroscopic network structure. As a matter of fact, the degree distribution of a network has been proven useful for the classification into different network types. Therefore, we restrict ourselves to a discussion of the degree distribution being the most representative centrality distribution.

Degree Distribution. In the simplest case, that all nodes of a graph have the same degree, the graph is called *regular*. These objects are also called regular lattices. In this case, the degree distribution collapses to a single peak without statistical variation.

Observations of real-world networks have shown that some networks exhibit exponential decaying degree distributions, i.e. there is a variance of degrees, but the system possesses a *typical degree*. Examples are social networks and technological and economic networks, such as electric power-grids and traffic networks (Amaral et al., 2000; Sen et al., 2003).

The nodes of the vast majority of large real-world networks, however, show a degree variation over several orders of magnitude. Examples are networks of internet routers (Faloutsos et al., 1999), links in the world-wide-web (Barabási and Albert, 1999), or scientific citations (de Solla Price, 1965). Their degree distributions are approximated by *power-laws* of the form

$$P(k) \propto k^{-\gamma}, \quad (2.17)$$

where $2 < \gamma < 3$ for most observed networks (Del Genio et al., 2011; Newman, 2003). The approximation is reasonable for the tails of the distributions, i.e. for large values of k . The identification of power-law distributions in empirical data is discussed in (Clauset and Newman, 2009).

Distributions of the form (2.17) are called *scale-free*, because they do not allow for a meaningful detection of a typical value. Instead, the network has a number of nodes with only a few neighbors and at the same time hubs with very large degrees. The structural difference between random and scale-free networks is sketched in Figure 2.6.

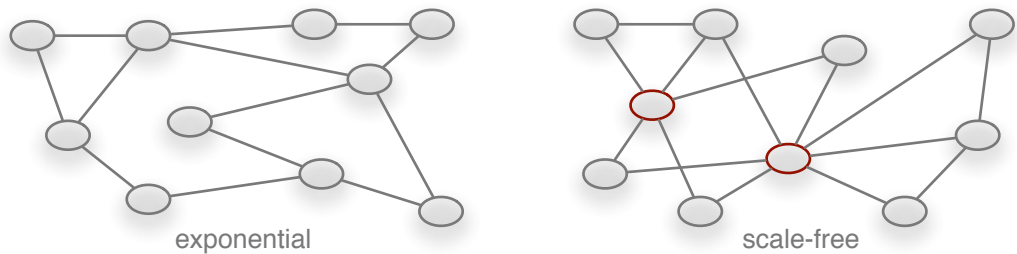


Figure 2.6. Structural difference between networks with exponential (left) and scale-free (right) degree distribution. All nodes have a similar degree in the network with exponential degree distribution, while the scale-free network shows hubs with a significantly larger degree than the average. Hubs are highlighted in red.

Scale-free networks have attained remarkable attention in the last years and many real-world networks have been conjectured as scale-free (Barabási and Albert, 1999; Newman, 2003). Important consequences of this classification were found to be a change in the threshold behavior of epidemic processes (Pastor-Satorras and Vespignani, 2001) and their topological resilience to node failures (Albert et al., 2000). The degree distributions of collaboration networks and others were well fitted by a scale-free distribution with a sharp cut-off (Newman, 2001; Albert and Barabási, 2002), where the distribution takes the form $P(k) \propto k^{-\gamma} e^{-k/\kappa}$ with fitting constants γ and κ . Amaral et al. suggest the aging of nodes as a possible explanation for the existence of an exponential cut-off, indicating that real systems possess a natural upper bound for their number of links (Amaral et al., 2000).

Clustering coefficient. The idea of the clustering coefficient comes from social networks and was first mentioned in (Milgram, 1967). It measures, whether a network contains a significantly large number of triangles. This behavior is conjectured to be typical for social networks and has the simple meaning: “a friend of your friend is likely to be your friend”. The clustering coefficient C is the number of connected triples ($A - B - C - A$) divided by the actual number of triples ($A - B - C$) in the network. Using the adjacency matrix \mathbf{A} , the clustering coefficient can be computed as follows:

$$C = \frac{\text{tr}(\mathbf{A}^3)}{\text{sum}(\mathbf{A}^2) - \text{tr}(\mathbf{A}^2)}, \quad (2.18)$$

where $\text{tr}(\mathbf{A})$ denotes the trace of \mathbf{A} and $\text{sum}(\mathbf{A}) = \sum_{ij} a_{ij}$ is the sum over all elements of \mathbf{A} . In this work, we focus on the clustering coefficient as a macroscopic property of networks. It should be noted that there is also a *local* clustering coefficient defined by $c_i = \sum_{jl} a_{ij} a_{jl} a_{li} / (k_i(k_i - 1))$ (Watts and Strogatz, 1998; Barrat et al., 2008). Thus, a network clustering coefficient can also be defined by averaging over all local clustering coefficients $\langle c_i \rangle$, which gives slightly different values than (2.18) and should not be mixed up with the latter.

The clustering coefficient plays an essential role in the small-world model of networks (Watts and Strogatz, 1998). We discuss this model in Section 2.3. In addition, significant clustering coefficients have been measured in social networks (Holland and Leinhardt, 1971), but also in many other real-world networks (Newman, 2003).

Average shortest path length. The elements of the distance matrix d_{ij} represent the distance between nodes i and j in the network. Ignoring those node pairs with infinite distance (i.e. setting $d_{ij} = 0$) gives the average shortest path length

$$l = \frac{1}{N(N - 1)} \sum_{i,j} d_{ij} \quad (2.19)$$

It is a common feature of many networks that the average shortest path length is much smaller than the number of nodes in the network, i.e. typically networks contain shortcuts (Albert and Barabási, 2002). An early and impressive example was shown by Milgram, where the average distance between two randomly chosen people in the united states was measured to be 6 (Milgram, 1967). This property is called *small world* phenomenon. It is an important building block of the Watts-Strogatz network model, which we discuss in Section 2.3.3.

Connected components. A connected component $G_{cc} = (V_{cc}, E_{cc})$ is a subgraph of $G = (V, E)$, where there is a path between any node pair in V_{cc} . In directed graphs, a connected component in the sense above is called *strongly connected*. A component is

called *weakly connected*, if it is connected ignoring the direction of edges. Many real-world networks contain a dominant *largest connected component* (LCC) that is typically much larger than all other components of the system. This component is therefore also called *giant component*.

In fact, the emergence of a giant component in a network is a second-order phase transition and is a graph theoretical percolation process (Newman, 2003). Components play an important role for epidemic processes, because the component membership of each node defines the maximum outbreak size of any epidemic started at this very node. The general component structure of directed networks is discussed in (Dorogovtsev et al., 2001) and we provide further discussion of their epidemiological relevance in Section 3.1.1.

Accessibility. If we directly connect each node of a network with all other nodes it is connected to by any path, we obtain the *accessibility* of the network. Accessibility measures the ability to reach destinations, which is of particular importance for transportation systems (Garrison, 1960; Mackiewicz and Ratajczak, 1996). Mathematically, we define the accessibility graph (also *transitive closure*) of a network as follows: Let $G = (V, E)$ be a network. Then $G^* = (V, E^*)$ is the accessibility graph of G with $(u, v) \in E^*$, if there is a path from u to v . The accessibility graph is typically dense, because it contains many more edges than the underlying network. A (weighted) adjacency matrix \mathbf{C} of G^* for a N -node network is given by the cumulative matrix

$$\mathbf{C} = \sum_{i=1}^{N-1} \mathbf{A}^i, \quad (2.20)$$

where \mathbf{A} is the adjacency matrix of G and the elements of \mathbf{C} contain the actual number of paths between each node pair. Consequently, we obtain the adjacency matrix $\tilde{\mathbf{C}}$ of the accessibility graph, when we normalize the elements c_{ij} of the matrix defined in (2.20), i.e.

$$\tilde{c}_{ij} = \begin{cases} 1 & \text{if } c_{ij} \neq 0 \\ 0 & \text{if } c_{ij} = 0. \end{cases} \quad (2.21)$$

2.3 Network models and epidemiology

The analysis of real-world networks in terms of the measures introduced in Section 2.2 has given useful insight into the structural properties of these systems. In particular, observations showed that many networks have heavy-tailed degree distributions and show non-vanishing clustering coefficients. In this section we review the results of some widely used network models. Neglecting higher order link correlations, most network models in this section are entirely defined by their degree distributions. They are therefore

generic realizations of ensembles with fixed $P(k)$. At the end of the section, we give a comparison between the different models and discuss their relevance in epidemiology.

2.3.1 Lattice model

Lattice models are inherently related to homogeneously distributed geographical positions of individuals. They show a high degree of regularity and their potential for SIS and SIR spreading processes has been studied in (Harris, 1974) and (Bak et al., 1990), respectively. The impact of the heterogeneous susceptibilities has been studied in (Sander et al., 2002). It was found that this heterogeneity introduces a broadening of the critical region and the outbreak threshold can be increased in the case of heterogeneous susceptibilities.

2.3.2 Erdős-Rényi model

The Erdős-Rényi model makes use of probabilistic methods to analyze network properties and is therefore a random graph model. A *random network* is generated by creating a set of N nodes and connecting each of the $\frac{1}{2}N(N - 1)$ possible node pairs² with a certain probability p . Networks generated this way are often called $G_{N,p}$ networks, although they are in the proper sense elements of a $G_{N,p}$ ensemble³.

Random graph theory addresses questions about typical properties of networks with an infinite number of nodes, i.e. networks in the thermodynamic limit $N \rightarrow \infty$. Consequently, the edge occupation probability p is the key parameter in random graph theory. Properties of particular interest are the average shortest path length or the distributions of degrees, component sizes (percolation) and the occurrence of special subgraphs such as triangles. Apparently, the expected number of edges in the network is $\langle E \rangle = \frac{1}{2} pN(N - 1)$, if p is the edge occupation probability. In addition, every edge increases the degree of two nodes, so that the *average degree* of a random network of N nodes is

$$\langle k \rangle = \frac{2 \langle E \rangle}{N} = (N - 1)p \simeq pN. \quad (2.22)$$

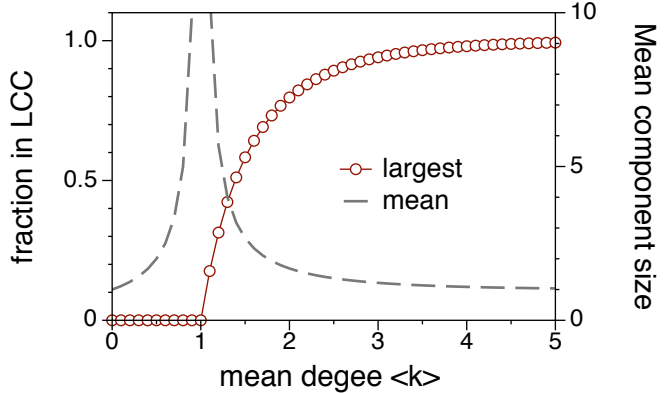
In the directed case, we would get the same result for both, in-degree and out-degree, since the factors 2 and $\frac{1}{2}$ would just disappear in (2.22). Equation (2.22) demonstrates that the system behavior for each value of p depends on the system size. We choose the mean degree as a convenient parameter for the analysis of random graphs, since it can be used to replace the explicit system size.

We obtain the *degree distribution* of $G_{N,p}$, if we realize that the probability to find a node with degree k is equal to the probability to find a node that is connected to k other nodes, but not to the $N - k - 1$ remaining nodes in the network. Thus, the degree

²We focus on undirected networks here. In the directed case, there are $N(N - 1)$ possible node pairs.

³A similar approach is to consider a fixed number of edges m instead, yielding a $G_{N,m}$ ensemble.

Figure 2.7. Emergence of the largest connected component (LCC) in an Erdős-Rényi graph as it follows from (2.25). The size of the largest component takes finite values for $\langle k \rangle > 1$. The mean cluster size is given by Equation (2.26) and diverges at $\langle k \rangle = 1$.



distribution is immediately given by a bimodal distribution

$$P(k) = \binom{N-1}{k} p^k (1-p)^{N-k-1}. \quad (2.23)$$

Provided that we are interested in large networks ($N \rightarrow \infty$), Equation (2.23) can be approximated by a Poisson distribution,

$$P(k) = \frac{\langle k \rangle^k}{k!} e^{-\langle k \rangle} \quad (2.24)$$

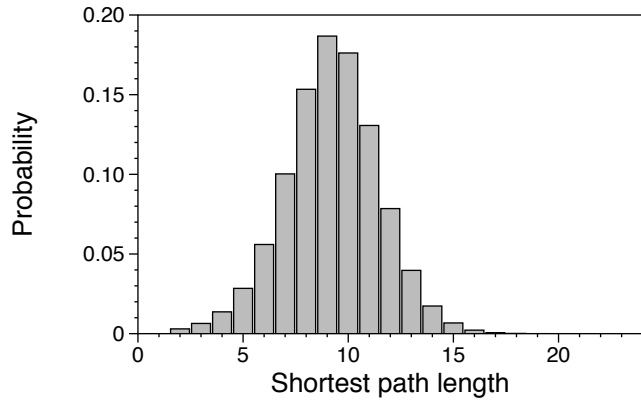
i.e. there is variation in the degrees, but there still remains a *typical degree* in the system.

It is an interesting feature of random graphs that for different edge occupation probabilities they show different phases. For low values of p , nodes tend to form small connected components, whereas for increasing p a *giant component* emerges. The giant component contains the majority of all nodes of the network. The behavior for large values of p has first been studied by Erdős and Rényi (Erdős and Rényi, 1959). One year later, Erdős and Rényi found thresholds for the emergence of subgraphs and a giant connected component (Erdős and Rényi, 1960, 1961). Their results for the occurrence of different subgraphs are summarized in (Albert and Barabási, 2002).

The size of the giant component and the mean component size can be computed analytically for random networks. Following Newman, we observe that the probability that a node is not in the giant component is equivalent to the probability that none of its neighbors is part of the giant component (Newman, 2003). If u is the fraction of nodes that are not in the giant component, this probability is given by u^k . An expression for u can be obtained by averaging u^k over all degrees k . The degree distribution is given by (2.24). Hence, the fraction of nodes not in the giant component is

$$u = e^{\langle k \rangle(u-1)}.$$

Figure 2.8. Shortest path length distribution for a realization of a directed Erdős-Rényi network of the ensemble $G_{N,p}$ for $N = 1000$ and $p = 0.002$. Equation (2.28) gives a mean value of 8.18, while the computed value is 9.08. The discrepancy vanishes in the limit of infinite graphs $N \rightarrow \infty$. The maximum shortest path length is 18 in this example. It defines the diameter of the network.



The size of the giant component is $S = 1 - u$ and consequently

$$S = 1 - e^{-\langle k \rangle S}. \quad (2.25)$$

One can use similar arguments to obtain an expression for the mean cluster size (Newman, 2003)

$$\langle s \rangle = \frac{1}{1 - \langle k \rangle + \langle k \rangle S}. \quad (2.26)$$

The mean cluster size (2.26) and a numerical solution of Equation (2.25) are shown in Figure 2.7. As the figure demonstrates, the system shows a second-order phase transition at $\langle k \rangle = 1$.

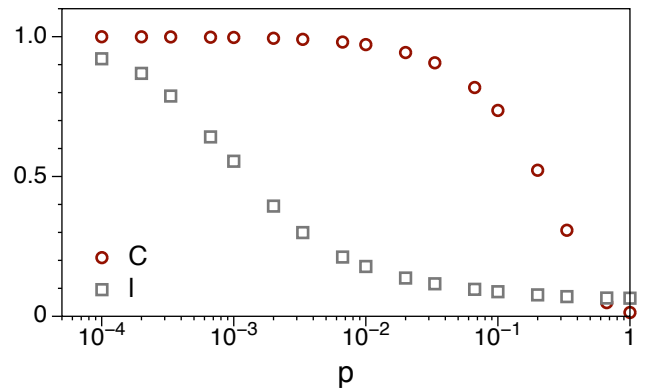
Since all edges in a random network are independent and identically distributed, the probability that a given node is part of a connected triple is p^2 . In analogy, the probability that a given node belongs to a closed triangle is p^3 . Consequently, the *clustering coefficient* (2.18) of a $G_{N,p}$ network is given by

$$C = \frac{p^3}{p^2} = p = \frac{\langle k \rangle}{N}. \quad (2.27)$$

Equation (2.27) implies that the clustering coefficient of random graphs vanishes in the limit of large networks.

We end this section by giving an approximation of the average shortest path distance in random graphs. Starting at some node in the network, the average number of nodes at distance 1 is given by the mean degree $\langle k \rangle$. Hence, the average number of neighbors at distance d is $\langle k \rangle^d$. In order to reach all N nodes in the network, we need r steps, where r is determined by $\langle k \rangle^r \simeq N$. Thus, r approximates the diameter of the network. Since we are only interested in the rough behavior of the average shortest path length

Figure 2.9. Clustering coefficient and average shortest path length in the Watts-Strogatz model. Both quantities are normalized to the corresponding value for $p = 0$. Results for networks with $N = 1000$ nodes and $m = 10$. Every data point is the average of 1000 realizations.



$\langle l \rangle$, we approximate it by r (Barrat et al., 2008) and obtain

$$\langle l \rangle \simeq \frac{\log N}{\log \langle k \rangle}. \quad (2.28)$$

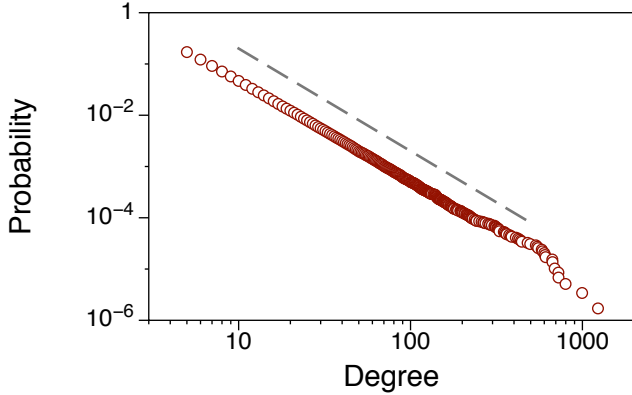
The average degree remains constant for different network orders, so that Equation (2.28) demonstrates that the average shortest path length grows logarithmically with the number of nodes in Erdős-Rényi graphs. Figure 2.8 shows the shortest path length distribution for one realization in the $G_{N,p}$ ensemble. Note that the mean value ~ 10 is relatively small compared with the number of nodes in the network (1000). This relation is found in many complex networks and is an indication for the small-world effect (see Section 2.3.3).

2.3.3 Watts-Strogatz model

We have seen that random graphs can reproduce some important properties of real-world networks, particularly the existence of a giant component and small average shortest path length. Nevertheless, Equation (2.27) demonstrates that the tendency to form connected triangles is absent in Erdős-Rényi networks. Observations show, however, that many real-world networks exhibit this feature (Milgram, 1967; Wasserman and Faust, 1994; Newman, 2003). It is characteristic for social networks in particular to have a high degree of clustering and at the same time short-cuts allowing for small average shortest path lengths. In this sense they can be seen as an intermediate structure between lattices (high local order) and random graphs (small shortest path lengths). Therefore, Watts and Strogatz introduced the *small-world model* in 1998 (Watts and Strogatz, 1998). We briefly summarize some of their main findings.

A Watts-Strogatz network interpolates between lattices and random networks by rewiring edges of a lattice. We start with a regular ring lattice of N nodes, where each node is connected to m of its nearest neighbors. Then, each edge is rewired randomly

Figure 2.10. Cumulative degree distribution of a Barabási-Albert graph with $N = 10^5$ nodes and $m_0 = m = 5$. The dashed line shows a power-law $P(k) \propto k^{-2}$.



with probability p . Keeping m constant from the beginning yields a scalable topology for different values of p . The clustering coefficient C and the average shortest path length $\langle l \rangle$ for different values of p are shown in Figure 2.9. Both values are normalized by their corresponding values in the initial lattice, i.e. C/C_0 and $\langle l \rangle / \langle l \rangle_0$ respectively.

The degree distribution collapses to a single peak for $p = 0$. In their paper on the properties of small-world networks (Barabási and Weigt, 2000), the authors showed that the degree distribution converges to a Poisson distribution in the limit $p \rightarrow 1$ and found an analytical approximation for the clustering coefficient for different values of p . The percolation threshold of small-world networks was investigated in (Ball et al., 1997; Sander et al., 2002), where the authors found the threshold to be reduced for increasing values of p .

There is no sharp criterion for a network to be called small-world network. Instead, a network is called small-world network, if it shows a sufficiently large clustering coefficient and a sufficiently low average shortest path length. This is the intermediate region in Figure 2.9.

2.3.4 Barabási-Albert model

Besides the critical behavior in Erdős-Rényi networks and the small-word effect in Watts-Strogatz networks, observations of real networks showed that they possess heavy-tailed degree distributions (Barabási and Albert, 1999; Liljeros et al., 2001). A central question is, where such distributions originate from. Therefore, Barabási and Albert introduced a network model in order to mimic the evolution of the world-wide-web (Barabási and Albert, 1999). The system under consideration is a network of websites that are connected by hyperlinks and should not be confused with the physical network of internet routers. The evolution of the www-network is reduced to two simple principles. (1) new nodes are added to the system over time and (2) the new nodes have a higher probability to link to existing nodes of higher degree. The second principle can be summarized as

a rich-get-richer phenomenon, i.e. the more links you have the more you will get. In network language, this mechanism is called *preferential attachment*. It can be seen as the network version of what is also known as Matthew-effect or cumulative advantage (Merton, 1968; de Solla Price, 1976).

The preferential attachment model for growing networks is as follows: Start with a small number m_0 of nodes and add a new node at every time step. Connect the new node to $m < m_0$ existing nodes, each with probability Π . Thus, $m = 1$ yields a tree and $m > 1$ gives a graph with cycles. The probability for an existing node i to be connected with the new one depends on the degree of i , i.e. $\Pi(k_i) = k_i / \sum_j k_j$.

Figure 2.10 shows the degree distribution of a network generated this way. We have to point out that it is generally more appropriate to plot the cumulative distribution of such distributions, because it is more robust against statistical fluctuations, particularly in the tail of the distribution (Clauset and Newman, 2009). As the figure shows, the distribution is well approximated by a power law of the form

$$P(k) \propto k^{-\xi}$$

with $\xi = 2$ for the cumulative distribution and $\xi = 3$ for the probability density function, respectively.

Barabási and Albert could show analytically that the resulting network has a power-law degree distribution of the form

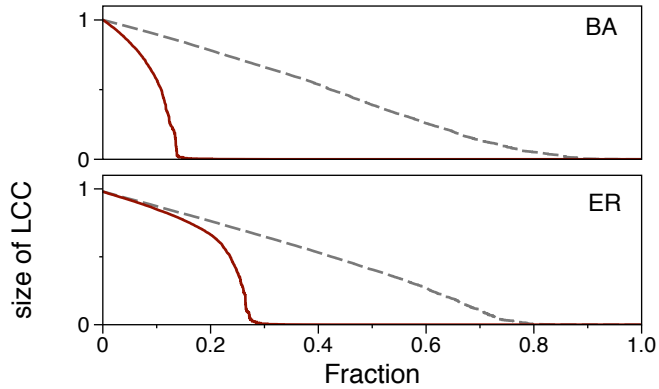
$$P(k) = 2m^2 k^{-3}. \quad (2.29)$$

Although the slope $\xi = 3$ does not match the power-law exponent of the world-wide web ($\xi = 2.1 \pm 0.1$ (Barabási and Albert, 1999)) the model explains the existence of a scale-free degree distribution.

Being a conceptional model, the Barabási-Albert model is extensively used for the investigation of theoretical questions. In fact, the power-law degree behavior is also reproduced by fitness models (Bianconi and Barabási, 2001; Fortunato et al., 2006) and copy models (Kleinberg et al., 1999). Fitness models allow for higher flexibility in terms of the power-law exponent. However, the range of possible exponents cannot take values in the interval $0 < \xi < 2$ (Del Genio et al., 2011).

Besides the models discussed above, there are other network models, such as the configuration model or exponential network models. The Barabási-Albert model can be extended a redirection algorithm in order to obtain other scaling exponents (Krapivsky and Redner, 2001). A model which is focused on real world data is the *configuration model*, a more sophisticated random graph model that allows for arbitrary degree distributions (Newman et al., 2001; Newman, 2010). Moreover, the degree sequence of a given network remains constant. In the configuration model one can consider higher order statistics, such as degree correlations and the clustering coefficient. *Exponential*

Figure 2.11. Robustness of a Barabási-Albert (BA) network and an Erdős-Rényi (ER) graph to random failure (grey dashed line) and targeted attack (red). Red lines represent the size of the largest connected component (LCC) under targeted removal of the most connected nodes. The size of the LCC remains finite for the Barabási-Albert network under random failure even for a large number of removed nodes.



random graphs are related to the concept of the micro canonical ensemble in statistical mechanics (Strauss, 1986). In this context, an Erdős-Rényi graph is just one realization of an ensemble of possible random graphs. Exponential random graphs are an elegant way of treating networks, but their mathematical treatment appears intractable for many cases of interest (Newman, 2003).

2.3.5 Resilience of different network types

A fundamental difference between complex networks and man made technological systems is their topologically induced robustness against failure. Failure can be modeled by *randomly* removing nodes of the system⁴. In this sense, network failure can be seen as an inverse percolation problem. The degree of failure is then given by the fraction of removed nodes f and the sensitivity of a network to random failure can be measured in terms of the size of its largest connected component, which is inherently related to its functionality. As an example, if only a few circuits in a computer would randomly fail, the largest connected component would disintegrate into smaller circuits and the machine is likely to malfunction. It is characteristic for complex networks, however, that randomly removing nodes does not drastically change the connectivity of the network. Albert et al. have measures the effect of network failure for different network types in (Albert et al., 2000). The authors found that Erdős-Rényi networks are more prone to random failure than scale-free networks. The robustness of scale-free networks against random node removal is explained by the huge number of low-degree nodes in the network, so that it is unlikely to remove a hub at random.

The situation changes dramatically, when nodes are not removed at random, but targeted, i.e. the most central nodes are removed first. This procedure models targeted *attacks* on the network. Albert et al. found that scale-free network are extremely vulnerable to attack of the most central nodes. Figure 2.11 shows the size of the largest

⁴Removing edges instead of nodes gives similar results.

connected component (LCC) vs. the fraction of removed nodes for an Erdős-Rényi network and a scale-free Barabási-Albert graph. The figure shows results for a Barabási-Albert network with $m = 2$ and a Erdős-Rényi network with $p = 0.0004$ at the beginning. Both networks have 10^4 nodes. Note that the Barabási-Albert network does not show a finite threshold for random node removal as the Erdős-Rényi network. Thus, the network shows finite connected components even if a very large number of nodes has been removed. The robustness against random removal comes at the price of high vulnerability against removal of the most connected nodes (red lines). After removing a relatively small fraction of high-degree nodes, the Barabási-Albert network disintegrates into small components.

A different measure of integrity of a network is how the diameter changes when nodes are removed at random or after a certain criterion. The differences between random and scale-free networks remain similar in this perspective. In addition, the definition of a targeted attack can be extended to any centrality measure. Although many centrality measures correlate in many network models (Barrat et al., 2008), different attack strategies may be effective in real networks (Holme et al., 2002).

2.3.6 Epidemics on networks

The spread of infectious diseases on networks is substantially related to network resilience. As we have seen in Section 2.1.2, individuals are removed from the population in an SIR-type disease. This corresponds to the failure of nodes as discussed previously. Moreover, results from attacking networks can be carried over to vaccination strategies. The central subjects of interest remain the same as in Section 2.1.2, namely the epidemic threshold R_0 and the outbreak size R_∞ .

We have seen in sections 2.1.1 and 2.1.2 how epidemics can be modeled under the assumption of homogeneous mixing of individuals. Nevertheless, data sources are available allowing for a more detailed analysis of an epidemic spreading process. We start by considering the network models as introduced in Section 2.2 and review some results about the impact of different topologies on spreading processes.

Epidemic models on homogeneous contact networks. To begin with, we consider a 2-compartment SI-model on a network of N individuals, where a fraction $i(t) = I(t)/N$ individuals are infected and the remaining fraction $s(t) = 1 - i(t)$ is susceptible. The force of infection ((2.10) in Section 2.1.3) models the effective interaction between susceptible and infected individuals in terms of passing on the infection. In a homogeneous network, e.g. an Erdős-Rényi or Watts-Strogatz network, the force of infection is $\lambda = \beta k i$, where $k i$ is the number of infectious contacts for a node of degree k and β is the probability of infection per time unit (Barrat et al., 2008). Consequently, $1/\beta$ is the spreading time scale of the process.

In order to obtain a rate-equation for the total number of infected in a homogeneous network, we replace the local degree k by the mean degree $\langle k \rangle$ and obtain

$$\frac{di(t)}{dt} = \beta \langle k \rangle i(t)[1 - i(t)], \quad (2.30)$$

where $1 - i(t)$ is the fraction of susceptible nodes. This model can easily be extended to a SIS model by adding a loss term $-\gamma i(t)$ to Equation (2.30). Setting $\gamma = 1$ without loss of generality, we obtain

$$\frac{di(t)}{dt} = -i(t) + \beta \langle k \rangle i(t)[1 - i(t)]. \quad (2.31)$$

The behavior of the SIS-model has been studied for Watts-Strogatz and Barabási-Albert networks in (Pastor-Satorras and Vespignani, 2001). Following Pastor-Satorras and Vespignani, we compute the steady state of (2.31) in order to find the epidemic threshold, that is

$$i[-1 + \beta \langle k \rangle (1 - i)] = 0.$$

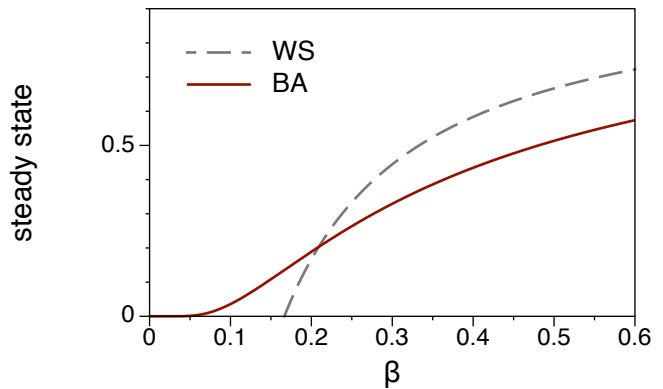
β being fixed as a local reaction constant, the average degree $\langle k \rangle$ remains the only parameter in this equation. We define the critical connectivity $\beta_c = \langle k \rangle^{-1}$ and obtain distinct regimes for different values of β . Thus, the density of infected in the endemic state is

$$\begin{aligned} i &= 0 && \text{if } \beta < \beta_c \\ i &= 1 - \frac{\beta_c}{\beta} && \text{if } \beta > \beta_c. \end{aligned} \quad (2.32)$$

This shows that the threshold behavior seen in Section 2.1.2 for homogeneously mixed populations remains unchanged for homogeneous networks. In fact, it has been shown that homogeneously mixed epidemic models can always be mapped onto a percolation process on a regular lattice (Grassberger, 1983; Sander et al., 2002).

Impact of heterogeneous connectivity. In order to consider networks with heavy-tailed degree distributions, we modify the SIS model above and include the heterogeneity of node degrees explicitly (Pastor-Satorras and Vespignani, 2001). Pastor-Satorras and Vespignani replaced the infected compartment $i(t)$ by the fraction of infected with a given degree, that is $i(t) \rightarrow i_k(t)$. The average degree in (2.31) is replaced by the actual degree and the force of infection is extended by the probability $\Theta(i(t))$ that a given link points to an infected node. The latter depends on the total density of infected and it depends only on β in the steady state. This gives the following SIS model for

Figure 2.12. Fraction of infected in the endemic state for an SIS model. The figure reveals the disappearance of the epidemic threshold for in Barabási-Albert networks (red). The epidemic threshold remains finite (here: $\beta_c = 1/6$) for homogeneous networks and $\beta_c \rightarrow 0$ for Barabási-Albert networks.



heterogeneous networks:

$$\frac{di_k(t)}{dt} = -i_k(t) + \beta k[1 - i_k(t)]\Theta(i(t)). \quad (2.33)$$

Pastor-Satorras and Vespignani found an analytic expression for the steady state by using statistical arguments to obtain an expression for $\Theta(i(t))$. After some calculations, the density of infected in the endemic state for a Barabási-Albert network with average degree $m = k/2$ reads

$$i \sim e^{\frac{-2}{\langle k \rangle \beta}} \quad (2.34)$$

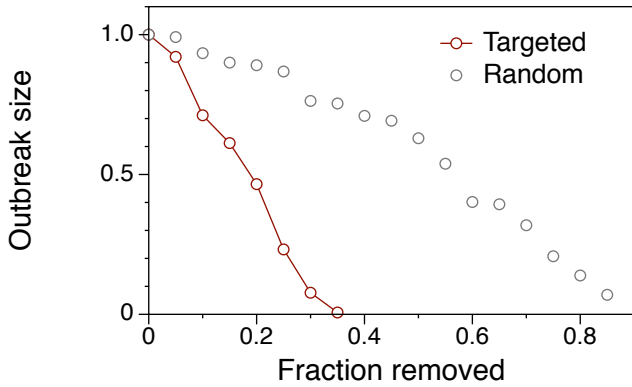
and the condition for the epidemic threshold is (Pastor-Satorras and Vespignani, 2002a)

$$\beta_c = \frac{\langle k \rangle}{\langle k^2 \rangle}. \quad (2.35)$$

A graphical comparison between (2.32) and (2.34) is given in Figure 2.12. It is an important result that the epidemic threshold vanishes in Barabási-Albert networks. As a consequence, random vaccination in Barabási-Albert networks does not suppress a disease outbreak (Keeling and Eames, 2005). Nevertheless, Figure 2.12 shows that for the outbreak size remains small for $\beta \rightarrow 0$. Finally, the absence of the epidemic threshold is generally found in infinite scale-free networks with degree distributions $P(k) \sim k^{-\xi}$ for $2 \leq \xi \leq 3$. It should be noted that a geographically embedded network with the same degree distribution can still show a finite outbreak threshold (Sander et al., 2003).

Vaccination strategies. As we have seen in the previous section, random immunization fails in scale-free networks, because it gives the same priority to low degree nodes and large hubs, while large hubs are unlikely to be chosen by chance. Random immunization effectively reduces the infection rate $\beta \rightarrow \beta(1 - g)$, where g is the fraction of vaccinated

Figure 2.13. Targeted and random vaccination for an SIS-type disease in a Barabási-Albert network with 10^5 nodes and $m = 4$. Infection parameters $\beta/\mu = 2$.



nodes. Therefore, the epidemic threshold condition (2.35) reads $\beta(1 - g_c) = \langle k \rangle / \langle k^2 \rangle$ with the critical immunization density g_c . It follows that

$$g_c = 1 - \frac{1}{\beta} \frac{\langle k \rangle}{\langle k^2 \rangle}. \quad (2.36)$$

Given a scale-free network with diverging $\langle k^2 \rangle$, the total population would have to be vaccinated in order to drop the infection rate below the epidemic threshold.

Nevertheless, scale-free networks are vulnerable to targeted removal of highly connected nodes, as we have seen in Section 2.3.5. Immunization of the mostly connected nodes is therefore an effective vaccination strategy on these networks. Numerical results for different vaccination strategies applied to a SIS-disease in a Barabási-Albert network are shown in Figure 2.13.

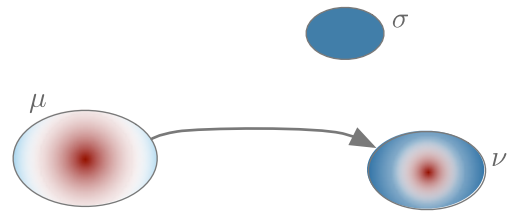
In analogy to (2.36), an analytic expression for the critical immunization density can be computed also for heterogeneous networks (Pastor-Satorras and Vespignani, 2002b). In this case, the fraction g of nodes with the highest degrees in the network is vaccinated. This introduces a cut-off degree $k_c(g)$ so that all nodes with degree $k > k_c$ do not contribute to the spread of the disease. For the case of a Barabási-Albert network Pastor-Satorras and Vespignani found an expression for the critical vaccination density to be

$$g_c \sim \exp(-2\mu/m\beta), \quad (2.37)$$

where m is the minimum degree of the network and μ and α are infection parameters, respectively. The exact value of g_c can be found by extrapolation of the curves in Figure 2.13. The striking feature of Equation (2.37) is, however, that the fraction of nodes that have to be vaccinated decreases exponentially with the spreading rate.

Besides the degree, we have to point out that any centrality measure (see Section 2.2.2) can be used in order to define a ranking of nodes. This node ranking can then be used to define a vaccination priority for all nodes. A generalized node ranking approach is

Figure 2.14. Three metapopulations μ, ν and σ of different size and infection status. The infection status is represented by the local color distribution. The edge (μ, ν) indicates migration from μ to ν .



of particular interest for networks, where the degree is not correlated to other centrality measures, as for example found in (Guimerà et al., 2005). A betweenness-based vaccination has been proposed in (Holme et al., 2002).

It should be noted that global knowledge about the network structure is needed in order to apply vaccination strategies as degree targeted vaccination. However, the detailed contact structure of many real systems – especially human contacts – is not known. Targeted immunization as described above can therefore be considered as an ideal vaccination strategy. This ideal strategy can be approximated using *nearest neighbor vaccination* (Cohen et al., 2003). The basic idea is to use local information by just asking for the neighbors of an individual, which gives some edges of the network. It is generally more probable that a randomly chosen edge is connected to a node of large degree, simply because these node class is connected to relatively many edges.

Metapopulations. The models and results discussed so far considered every node in the network as one individual. In many systems, however, the detailed internal contact structure is unknown, but information about contacts between whole subpopulations is available. A subpopulation can be a city in a mobility network, an agricultural holding in a livestock trade network or a habitat in ecology. A *metapopulation* is a set of subpopulations which are connected by migration processes (Grenfell and Harwood, 1997; Hanski, 1998; Barrat et al., 2008). Recent works have made use of metapopulation approaches to model large scale disease outbreaks (Colizza et al., 2006), such as influenza (Balcan et al., 2009) and SARS (Hufnagel et al., 2004).

The computation of outbreak thresholds in metapopulations was addressed in (Colizza and Vespignani, 2007; Colizza et al., 2007) and the spreading velocity was additionally analyzed in (Belik et al., 2011). The impact of network topology on disease spread in metapopulations was addressed in (Lentz et al. (2012), Section 3.2). Although metapopulation approaches provide a useful tool for the modeling of epidemics, they systematically overestimate the outbreak size when compared to individual resolved approaches (Keeling et al., 2010).

In the context of epidemics every subpopulation has a different infection status, i.e. a distribution of S , I and R . Additionally to the local infection model, we add a migration term so that the general form of a metapopulation SIR-infection-model for a

subpopulation μ is

$$\frac{dI_\mu}{dt} = R(S_\mu, I_\mu, R_\mu) + M(S_\mu, I_\mu, R_\mu, S_\nu, I_\nu, R_\nu, \tau). \quad (2.38)$$

The first term R in Equation (2.38) is a *local reaction* term, while the *migration* M to other subpopulations could depend on the local distribution and the infection status of other subpopulations connected to μ . Furthermore, the migration between subpopulations could occur on a time-scale τ different from the time-scale of the local infection. The impact of these time-scales on disease spread was analyzed in (Cross et al., 2005; Balcan and Vespignani, 2011; Lentz et al., 2012). We investigate the interplay between network properties and disease outbreaks in Section 3.2.

3 Static network analysis – Case study: Livestock trade network

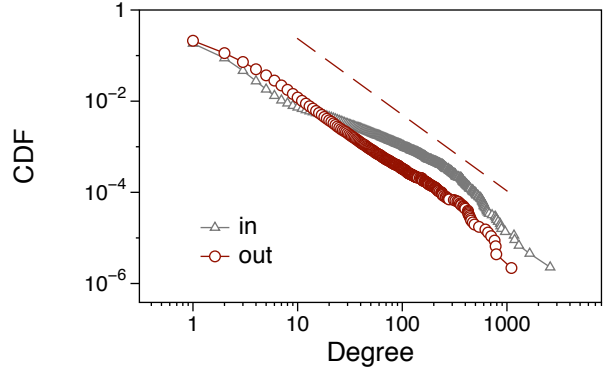
In this chapter, we analyze the pig trade between agricultural holdings in Germany as a static network and focus on the epidemic spreading potential of networks of this type. The epidemiological relevance of the pig trade network has been studied in (Fritzemeier, 2000) for the case of classical swine fever. Depending on the system under consideration, there are different approaches to data acquisition for different epidemiologically relevant networks. In the case of *human* contact structures, it is in most cases impossible to gather information about all possible paths of infection.

Therefore, different methods to extract the contact structure can be used (Keeling and Eames, 2005): *Contact tracing* is used to determine infection paths under the assumption that every contact has a high probability to cause an infection. This assumption is justified for highly contagious diseases, such as influenza or sexually transmitted diseases (Rocha et al., 2010, 2011). If more data is available, one can obtain an *infection tracing* network, where every contact definitely caused an infection. Infection tracing plays an important role for the analysis of HIV spread or food safety (Buchholz et al., 2011; Haydon et al., 2003). *Diary-based* methods make use of questionnaires to extract contact structures. The drawback of this method is that the subjects themselves are responsible for the information given and a considerable bias can be present in the data (Visser et al., 2003). Other diary-based methods make use of legislation in order to guarantee for a sufficient data quality. This holds in particular for livestock trade data. An example is the HI-Tier database, which records trade movements of livestock animals and is used for food safety and is a central subject of study in this work (EUR-Lex, 2000). The background of the dataset is described in more detail below.

It is beyond the scope of this thesis to provide a realistic disease model for any relevant infectious livestock disease. We therefore focus on a purely topological analysis of the maximum spreading domain. Fine-grained models including large sets of parameters and couplings are needed to model infectious diseases. A complex example for the transmission of classical swine fever is found in (Martínez-López et al., 2011). In general, a detailed knowledge about infection probability, contact probability and sensitivity to initial conditions is required to obtain a realistic epidemic model. Even if this information is available, results can not necessarily be generalized to other systems.

For this reason we restrict the epidemiological aspect of this work to a purely topological analysis of the underlying network, where detailed data about contact structures

Figure 3.1. Degree distribution of the livestock trade network. The out-degree distribution (red circles) is well approximated by a power-law of the form $x^{-1.67}$ (red dashed line). The in-degree distribution shows a bimodal behavior indicating the presence of large slaughterhouses (grey triangles). Power law exponent was computed using a maximum likelihood estimator (Clauset and Newman, 2009).



is available. In particular, we focus on a network of pig trade in Germany in the years 2006–2008. Each node in this network represents an agricultural holding and trade contacts between holdings are represented by directed edges. (An analogue analysis of a cattle network dataset was published in (Lentz et al., 2009)). This chapter is devoted to a static network analysis of this system and a general topological classification. In Section 4, we highlight the effects of a time-resolved treatment of this system.

Background of the dataset. After the BSE crisis in Europe in 2001, the EU member states established livestock trade movement databases to track potential pathways of pathogen spread. Since 2001, every holding in Germany is obliged to report every trade movement of live animals (pig, cattle, sheep and goat) to a federal database (Herkunftssicherungs und Informationssystem für Tiere (HIT), (StMELF, 2012)). Trade is recorded in a temporal resolution of 1 day. In the case of pig trade, the receiving holding and the pre-owner are reported in the database. In this section we aggregate the trade contacts yielding a static network, where a trade edge is present, if there was at least one trading contact during the observation period. Our data extract spans the trade within Germany between 01 June 2006 and 31 December 2008. This yields a static network with 121,223 nodes and 348,037 edges.

3.1 Network analysis

To begin with, we analyze the livestock trade data according to the measures introduced in Section 2.2.2. From the family of centrality measures we focus on the degree distribution, which is of major importance, since it allows for a topological classification of the network. Figure 3.1 shows the heavy-tailed degree distribution of the network. The in- and out-degree distributions span three orders of magnitude. Note that the network exhibits a maximum in-degree, which is significantly larger than the maximum out-degree. In addition, the in-degree distribution shows a bimodal behavior. This is attributed to

the existence of large slaughterhouses being supplied by a very large number of farms.

The majority of the other centrality measures reported in Section 2.2.2 are correlated with the degree. Depending on the specific question, most centrality measures are appropriate measures for the risk assessment of each node. We discuss the correlation between degree and other centrality measures for this particular network in Appendix A.2 and focus now on the possible infection paths given by the ranges.

3.1.1 Components and ranges

Ignoring the edge direction, the network has a giant component containing almost 99 % of the nodes. The second largest weakly connected component contains only 8 nodes. The size of the largest and second largest strongly connected components are 28,6 % (34,693 nodes) and 0.01 % (16 nodes), respectively. Sizes of the next smaller components decrease rapidly. All in all the network percolates ignoring the direction of links. Taking into account link directions, the giant component contains a considerable fraction of the network. The diameter of the giant strongly connected component is 21 and its average shortest path length is 6.03. This means that it takes typically 6 steps to infect every node of the network and never more than 21 steps.

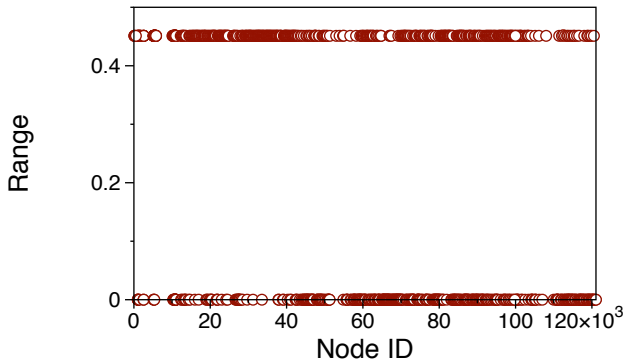
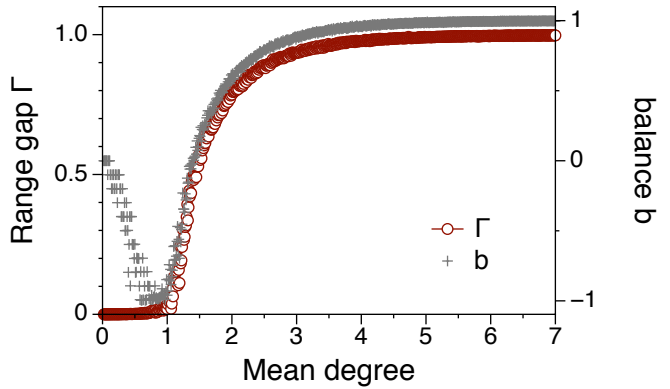


Figure 3.2. Range sequence for all nodes in the livestock trade network. Every 100th node with range larger than 0 is shown.

The giant strongly connected component has an interesting impact on the distribution of node ranges (and reachabilities) in the network. Note that the range of a node defines the upper bound for any disease outbreak starting from this very node. Following Equation (2.16), we compute the ranges of all nodes and focus for the moment on the *sequence* of these ranges. For most sequences of centralities in a network, we would find rather noisy sequences. These result in distributions such as the degree distribution in Figure 3.1. In contrast to most other centrality measures, the range shows a strikingly

Figure 3.3. Range gap Γ and balance b vs. mean degree for directed Erdős-Rényi graphs. Each datapoint is a mean value of 1000 networks. Network size: 1000 nodes. The range gap shows a similar behavior for undirected networks.



different behavior. The sequence of ranges for all nodes in the network is shown in Figure 3.2. The striking feature here is the *gap* in the distribution: no range in between $7 \cdot 10^{-4}$ (87 nodes) and 0.45 (54693 nodes) is present in the system. Consequently, a randomly chosen node can only belong to one of two classes, namely long ranged nodes and short ranged nodes. A node of the latter class is barely suitable to cause a considerable disease outbreak at all. Only a node of long range can act as a node for large scale disease outbreaks. The sizes of the classes in Figure 3.2 are as follows: 54,874 nodes belong to the short range and 66,349 nodes to the long range class, respectively.

For a general network we define the range gap Γ as the size of the largest interval, where the range distribution is identically zero (Lentz et al., 2012). The balance of the distribution around the gap is measured in terms of the variable

$$b = \frac{N_l - N_s}{N_l + N_s},$$

where $N_l + N_s$ is the number of nodes and N_l and N_s are the numbers of long and short ranged nodes, respectively. Apparently $b = 1$, if all nodes are long ranged and $b = -1$ for only short ranged nodes in the network. Figure 3.3 shows the range gap and balance for directed Erdős-Rényi networks of varying density. The figure demonstrates, that the size of the range gap and the balance are inherently related to the percolation properties of the system that we discussed in Section 2.3.2. A significant range gap in combination with similar sized range classes indicates that the system is in a critical state. For the dataset of Figure 3.2 we get $\Gamma = 0.45$ and $b = 0.095$ indicating that the system is only slightly above the critical point.

The explanation for the strong bi-modality of the range distribution is the existence of a giant strongly connected component (GSCC). Figure 3.4 shows a schematic picture of a directed network. Due to the giant component in the system, all nodes that belong to the GSCC can reach all other nodes in the component plus all nodes that the component

is connected to. If there is a path from a node to the GSCC, but the node itself is not

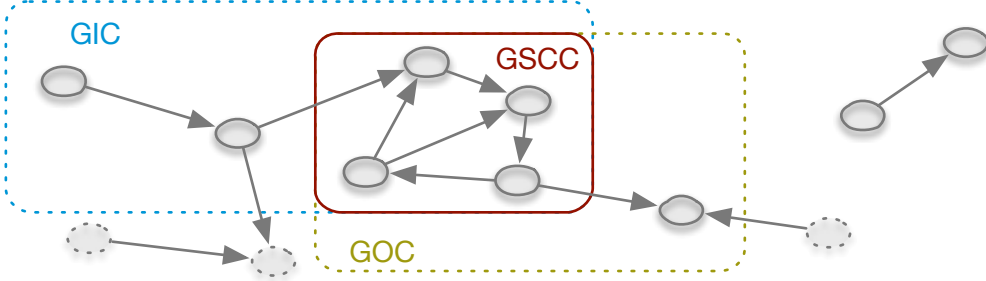


Figure 3.4. Schematic structure of a directed network. In the core region there is the giant strongly connected component (GSCC, red). All nodes reachable from the GSCC form the giant out-component (GOC, yellow) and the nodes with access to the GSCC define the giant in-component (GIC, blue). The union of GSCC, GIC, GOC and all tendrils is the giant weakly connected component (GWCC) of the network. Nodes that are not part of the GWCC belong to another component of the network (nodes on the upper right).

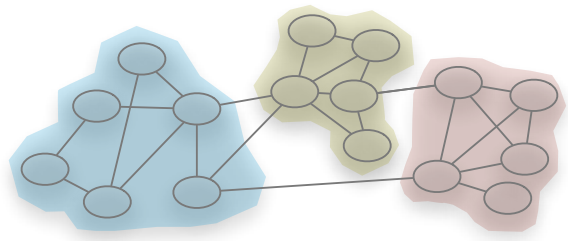
on this component, it belongs to the giant in-component (GIC) of the network. In analogy, nodes reachable from the GSCC that are themselves not part of the latter, belong to the giant out-component (GOC). All remaining nodes not belonging to one of the components mentioned above are called tendrils, if they are weakly connected to the GSCC. The nodes on the upper right (figure 3.4) are not even weakly connected to the GSCC and thus belong to another component of the network. A detailed discussion about these structures is provided in (Dorogovtsev et al., 2001).

As an explanation for Figure 3.2, the lower bound of the long range node class is formed by the nodes of the GSCC. Every node that belongs to the long range node class is either on the GSCC or on the GIC. The low range class is populated by nodes of the GOC, tendrils and nodes of other WCCs.

3.1.2 Modules

The network components analyzed above make a strict requirement to the connectivity between components, namely that no path exists between two different components. A weaker requirement would be to allow for the existence of *few* paths between components. More specifically, find partitions so that there exist less edges between them than expected by chance. The usage of such structures in the context management of disease risk has been suggested in (Martínez-López et al., 2009). Structures of this type are called *modules* or *communities*. The idea of finding communities in social networks has been proposed in (Coleman, 1964; Wasserman and Faust, 1994) and was mathematically formalized for general networks in (Girvan and Newman, 2002; Newman, 2006). In order

Figure 3.5. The nodes of modular networks are partitioned into modules of high edge density and edges between modules are rare.



to detect these structures, a cost function mapping every partition of the network onto a value between 0 and 1 has to be optimized. Newman proposed the modularity Q as an appropriate cost function defined as

$$Q = (\text{number of edges between communities}) - (\text{expected number of those edges})$$

or more formally (Fortunato, 2010; Newman, 2006)

$$Q = \frac{1}{2m} \sum_{ij} \left(\mathbf{A}_{ij} - \frac{k_i k_j}{2m} \right) \delta(c_i, c_j). \quad (3.1)$$

This equation gives the modularity for a network with adjacency matrix \mathbf{A} and m edges and k_i denotes the degree of the i -th node. The partition of the network is given in the Kronecker delta $\delta(c_i, c_j)$, which is 1, if nodes i and j are in the same community and otherwise 0. Hence, modularity measures the goodness of a particular partition of the network. $Q \sim 0$ implies that a given partition of a network does not yield a significant modular structure. Its maximum value is $Q = 1$ provided that a network has a strong modular partition and the latter is known for the computation of Q .

Finding the best possible partition that maximizes modularity has been shown to be NP-complete¹ (Brandes et al., 2007). However, several approximate methods – such as simulated annealing (Guimerà et al., 2004) and greedy algorithms (Clauset et al., 2004; Newman, 2004) – have been proposed to find approximate partitions that maximize modularity. In order to detect community structure in the pig trade network, we analyze the system using the method of Newman. The results presented in this section are published in (Lentz et al., 2011).

Note that although the concept of modularity can be generalized to the directed case in a straightforward manner using the definition (Leicht and Newman, 2008)

$$Q = \frac{1}{m} \sum_{ij} \left(\mathbf{A}_{ij} - \frac{k_i^- k_j^+}{m} \right) \delta(c_i, c_j), \quad (3.2)$$

¹NP-complete means that this problem is not exactly solvable for large network sizes. See (Skiena, 2008) and Appendix A.1 for brief discussions of NP-completeness.

there is still ongoing discussion about a systematic bias in this approach (Kim et al., 2010). Kim et al. point out that a straightforward generalization of modularity can not resolve nodes of different in and out degree. Hence, nodes of high total degree tend to form communities with their neighborhood regardless of how the links in the neighborhood are directed. We therefore focus on partitioning the undirected network only.

In order to find a partitioning maximizing the modularity function (3.1), we use the greedy method proposed in (Clauset et al., 2004). The algorithm is applied to the largest weakly connected component of the network, i.e. 119,858 nodes. It finds a partition where 96 % of all nodes and 98 % of all edges are assigned to 9 major clusters. The modularity value for this partition is $Q = 0.717$. After we computation of a suitable network partition, we add the geographical positions of the nodes as further meta information. The resulting map is shown in Figure 3.6. It should be noted that the community partition was done without spatial information in the first place. Thus, the figure demonstrates that in this case two nodes of the same community are likely to be geographic neighbors as well. An explanation for this correlation could be cultural affinity or simply economic reasons, since transport costs increase with geographical distance.

The right panel of Figure 3.6 shows the nine largest communities condensed into single nodes, where the size of each node represents the number of edges in the community. Node numbers are arbitrary IDs given by the used algorithm. Links between communities are weighted ranging from 6 (dashed lines) to 7251 (massive edge between 24 and 9). The positions of the nodes approximate the center of mass of the corresponding community on the left panel.

Module detection is a reasonable tool for capturing the large scale structure of networks. In fact, it has been shown that there is a resolution limit for community detection and the minimum size of the communities depends on the size of the network (Fortunato and Barthélemy, 2007). In general, additional meta information such as the geographical embedding of the network, is required to extract knowledge about the function of a network out of its large scale structure.

A particular partitioning of a network, however, is not guaranteed to give unambiguous information about the network. On the contrary, Equation (3.1) is a mapping from a high dimensional partition space to a scalar. The number of elements in a partition space of a set is given by the so called *Bell number*. It follows that the number of partitions of a network with 10 nodes is $\sim 10^5$ and it is already $\sim 10^{47}$ for 50 nodes! Adjacent partitions in the partition space can have huge differences in Q and it is not guaranteed that approximative algorithms are capable to find the global optimum. Furthermore, a huge number of different partitions can possess the same modularity Q .

Although a particular partition should in general be interpreted with caution, we can state that *at least one* partition of a certain value of Q is intrinsic in the system. I.e. the system is somehow modular, even if the best possible partition might be unknown.

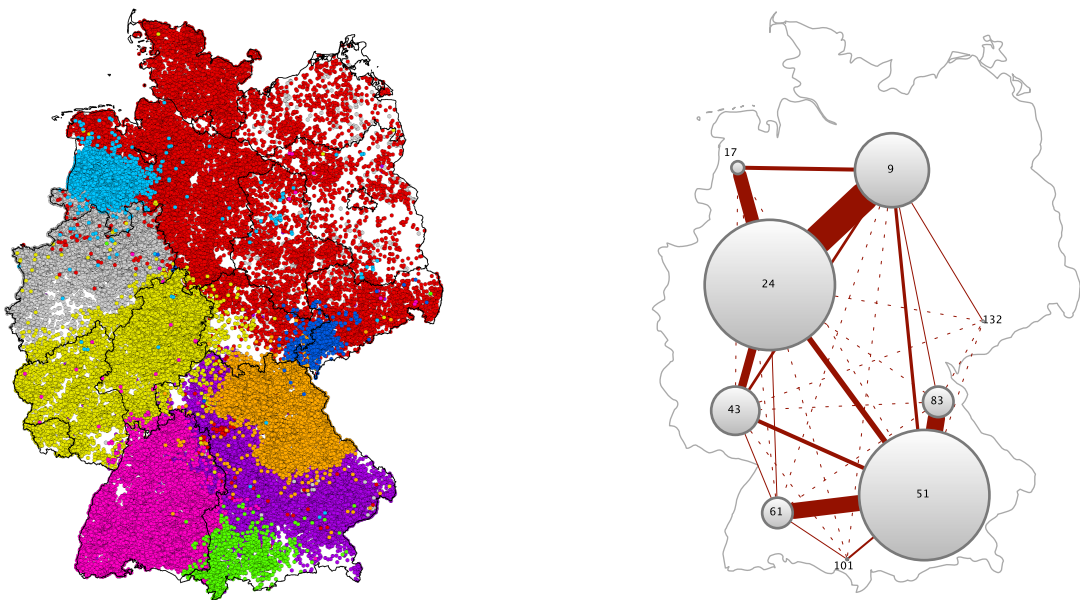


Figure 3.6. Geographical embedding of the communities found for the pig trade network (left). The nine largest (by number of nodes) communities are shown. A condensation of the communities is shown on the right. The edge width corresponds to the number of edges connecting different modules and the number of within module edges is reflected in the node size. Node IDs are arbitrary numbers. From Lentz et al. (2011).

We consider this line of thought in the next section, where we analyze artificial networks with distinctive structural features in order to gain insight into their impact on epidemic processes.

3.2 Range & modules: Spreading potential

In this section, we investigate the impact of directionality and modularity on the spread of infectious diseases on networks. Therefore, we use random network models that mimic the desired network properties. To begin with, we derive a system of equations that models an epidemic process as it would take place on the pig trade network of Section 3.1. Hereby we consider the agricultural holdings as metapopulations and the time scales between trade and infection are separated using a pacing of trade. All results presented in this section are published in (Lentz et al., 2012).

3.2.1 Epidemic model

We derive an infection model for agricultural holdings that are considered as metapopulations, each holding containing a certain number of animals. The coupling between the holdings is given by trade, which appears as transportation of livestock animals (see Figure 2.14). The union of all trade links is given by a trade network with adjacency matrix \mathbf{A} . Since transportation/trade is a non symmetric process in this system, we focus on *directed networks* in particular.

In each node of the network, a susceptible-infected-recovered (SIR) reaction takes place. Following Section 2.1.2, the infection model for each node μ in such a system reads

$$\begin{aligned}\partial_t s_\mu &= -\alpha s_\mu \frac{i_\mu}{n_\mu} \\ \partial_t i_\mu &= \alpha s_\mu \frac{i_\mu}{n_\mu} - \gamma i_\mu \\ \partial_t r_\mu &= \gamma i_\mu,\end{aligned}\tag{3.3}$$

where $n_\mu = s_\mu + i_\mu + r_\mu$ is the total population of node μ and we use the force of infection i_μ/n_μ as suggested in Equation (2.10). The *infection status* of node μ is given by the triple (s_μ, i_μ, r_μ) . Now we add the migration between the metapopulations by introducing a network with adjacency matrix elements $a_{\mu\nu}$.

The total *outflow* from node μ is given by its degree $\sum_\nu a_{\mu\nu}$ and branches into the different compartments

$$f_\mu^- = \frac{s_\mu}{n_\mu} \sum_\nu a_{\mu\nu} + \frac{i_\mu}{n_\mu} \sum_\nu a_{\mu\nu} + \frac{r_\mu}{n_\mu} \sum_\nu a_{\mu\nu}$$

according to the infection status of the node. The *inflow* of each node depends on the infection status of its predecessors in the network, i.e.

$$f_\mu^+ = \sum_\nu a_{\mu\nu}^T \frac{s_\nu}{n_\nu} + \sum_\nu a_{\mu\nu}^T \frac{i_\nu}{n_\nu} + \sum_\nu a_{\mu\nu}^T \frac{r_\nu}{n_\nu},$$

where $\sum_\nu a_{\mu\nu}^T = \sum_\nu a_{\nu\mu}$ is the in degree of node μ . We add the respective contributions

of inflow and outflow to equations (3.3) and get

$$\begin{aligned}\partial_t s_\mu &= -\alpha s_\mu \frac{i_\mu}{n_\mu} + \sum_\nu a_{\mu\nu}^T \frac{s_\nu}{n_\nu} - \frac{s_\mu}{n_\mu} \sum_\nu a_{\mu\nu} \\ \partial_t i_\mu &= \alpha s_\mu \frac{i_\mu}{n_\mu} + \sum_\nu a_{\mu\nu}^T \frac{i_\nu}{n_\nu} - \frac{i_\mu}{n_\mu} \sum_\nu a_{\mu\nu} - \gamma i_\mu \\ \partial_t r_\mu &= \sum_\nu a_{\mu\nu}^T \frac{r_\nu}{n_\nu} - \frac{r_\mu}{n_\mu} \sum_\nu a_{\mu\nu} + \gamma i_\mu.\end{aligned}\quad (3.4)$$

Regarding this equation system, we have to address the impact of directionality, i.e. the non-symmetry of the adjacency matrix. Considering the coupling term in equations (3.4), we have to make sure that the population of each node remains constant, i.e. $f_\mu^- = f_\mu^+$. Using that $\frac{s_\nu}{n_\nu} + \frac{i_\nu}{n_\nu} + \frac{r_\nu}{n_\nu} = 1$ this is equivalent to the condition

$$\sum_\nu (a_{\nu\mu} - a_{\mu\nu}) = 0.$$

In undirected networks, this condition is always satisfied. In directed networks, however, the condition implies that each node in the network has the same in and out-degree, respectively. This does not hold in the general case, so that the total flow of node μ is

$$\sum_\nu (a_{\nu\mu} - a_{\mu\nu}) = f_\mu^+ - f_\mu^- \equiv f_\mu \neq 0,$$

i.e. the difference between in-degree and out-degree. This difference is distributed over the infection status of the respective node so that

$$f_\mu = \frac{s_\mu}{n_\mu} f_\mu^s + \frac{i_\mu}{n_\mu} f_\mu^i + \frac{r_\mu}{n_\mu} f_\mu^r.$$

It follows that in the case of a directed network, we have to add a birth/death process in each node to keep the total population constant. Hence, the infection model becomes

$$\begin{aligned}\partial_t s_\mu &= -\alpha s_\mu \frac{i_\mu}{n_\mu} + \sum_\nu a_{\mu\nu}^T \frac{s_\nu}{n_\nu} - \frac{s_\mu}{n_\mu} \sum_\nu a_{\mu\nu} - \frac{s_\mu}{n_\mu} f_\mu^s \\ \partial_t i_\mu &= \alpha s_\mu \frac{i_\mu}{n_\mu} + \sum_\nu a_{\mu\nu}^T \frac{i_\nu}{n_\nu} - \frac{i_\mu}{n_\mu} \sum_\nu a_{\mu\nu} - \gamma i_\mu - \frac{i_\mu}{n_\mu} f_\mu^i \\ \partial_t r_\mu &= \sum_\nu a_{\mu\nu}^T \frac{r_\nu}{n_\nu} - \frac{r_\mu}{n_\mu} \sum_\nu a_{\mu\nu} + \gamma i_\mu - \frac{r_\mu}{n_\mu} f_\mu^r.\end{aligned}\quad (3.5)$$

In analogy to Section 2.2.1, we define the Laplace Matrix \mathbf{L} with elements

$$l_{\mu\nu} = a_{\mu\nu}^T - \delta_{\mu\nu} \sum_\sigma a_{\mu\sigma}. \quad (3.6)$$

Using vector notation, the status of the whole network is given by the respective vectors \mathbf{S} , \mathbf{I} and \mathbf{R} . Lowercase letters refer to normalized variables, i. e. the elements of \mathbf{s} are s_μ/n_μ . The system (3.5) now reads

$$\begin{aligned}\partial_t \mathbf{S} &= \mathbf{Ls} - \text{diag}(\mathbf{sF}_s) - \alpha \text{diag}(\mathbf{Si}) \\ \partial_t \mathbf{I} &= \mathbf{Li} - \text{diag}(\mathbf{sF}_i) + \alpha \text{diag}(\mathbf{Si}) - \gamma \mathbf{I} \\ \partial_t \mathbf{R} &= \mathbf{Lr} - \text{diag}(\mathbf{rF}_r) + \gamma \mathbf{I}.\end{aligned}\quad (3.7)$$

This system models an SIR-type epidemic on a metapopulation which is connected by a network structure given by the Laplacian \mathbf{L} . Terms of the form \mathbf{Ls} correspond to diffusion terms. In (3.7), vector-vector products are outer products. Thus, $\text{diag}(\mathbf{xy})$ denotes the main diagonal of the outer product of vectors \mathbf{x} and \mathbf{y} , i.e. the Hadamard-product.

In livestock trade systems, the trade between holdings is not frequent in time; it rather shows *bursty* behavior. This means that a local infection might evolve over some time and change the infection status of a node significantly until a trade link occurs. However, the infection time scale is the same as the trade time scale in (3.7). In order to separate these time scales, we modify the Laplacian (3.6) and define a *paced Laplacian*

$$\mathcal{L}(\tau) = \mathbf{L} \sum_{n=0}^{\infty} \delta(t - n\tau) \quad (3.8)$$

with pacing frequency τ . Thus, we obtain the requested model replacing the Laplacian in (3.7) by its paced counterpart. Finally, we use the following outbreak model:

$$\begin{aligned}\partial_t \mathbf{S} &= \mathcal{L}(\tau)\mathbf{s} - \text{diag}(\mathbf{sF}_s) - \alpha \text{diag}(\mathbf{Si}) \\ \partial_t \mathbf{I} &= \mathcal{L}(\tau)\mathbf{i} - \text{diag}(\mathbf{sF}_i) + \alpha \text{diag}(\mathbf{Si}) - \gamma \mathbf{I} \\ \partial_t \mathbf{R} &= \mathcal{L}(\tau)\mathbf{r} - \text{diag}(\mathbf{rF}_r) + \gamma \mathbf{I}.\end{aligned}\quad (3.9)$$

In order to analyze the impact of characteristic topological features – modularity and directionality in particular – on disease dynamics, we solve the system (3.9) numerically for different computer-generated networks with the desired properties.

3.2.2 Computer-generated networks

In this section we describe how networks with varying directionality and modularity can be generated on a computer. Although generating a sequence of graphs with a certain directionality is straightforward, we have to discuss how to quantify this property. Before we generate networks of a desired modularity, we address restrictions in the maximum value of Q .

Networks of varying directionality. The directionality of a given network is related to its fraction of bidirectional links. In principle, the strength of direction could be measured by this fraction alone. It has been shown, however, that this measure would yield finite values even for purely random networks (Garlaschelli and Loffredo, 2004). Therefore, Garlaschelli and Loffredo introduced the measure of *link reciprocity* ρ of a given network with N nodes and adjacency matrix \mathbf{A} as

$$\rho = \frac{\sum_{i \neq j} (a_{ij} - \bar{a})(a_{ij}^\top - \bar{a})}{\sum_{i \neq j} (a_{ij} - \bar{a})^2}. \quad (3.10)$$

The edge density is denoted as $\bar{a} = \sum_{ij} a_{ij}/(N(N - 1))$. In fact, Equation (3.10) is the correlation between the adjacency matrix and its transpose. Reciprocity is $\rho = 1$ for undirected networks, whereas $\rho \approx 0$ for directed random graphs. In the latter case the fraction of bidirectional links would take finite values, since some bidirectional links are placed by chance in random networks.

To investigate the impact of directionality on disease dynamics, we generate random networks with different values of ρ and solve the system (3.9) on these topologies. The networks are generated as follows: 1. generate an undirected Erdős-Rényi network, 2. replace all edges by bidirectional directed edge pairs and 3. remove one edge of the bidirectional edge pair with probability q . Consequently, the probability that an edge pair is connected by an undirected (bidirectional) edge is $p_{\text{rev}} = 1 - q$. The link reciprocity of the generated network can directly be computed using Equation (3.10). We have to point out that this analysis focuses on Erdős-Rényi networks for the sake of clarity.

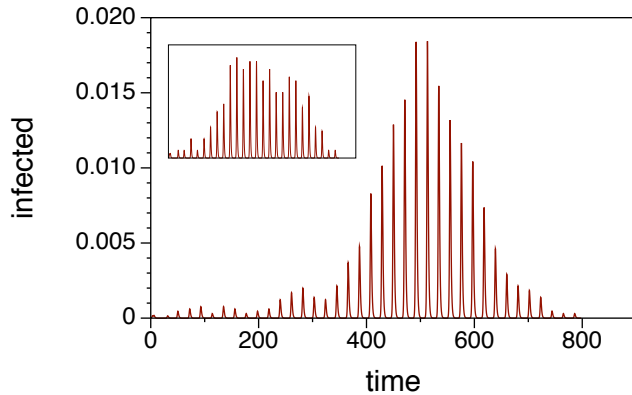
Modular networks. Following Newman and Girvan, a modular network can be realized as a union of independent subgraphs, that are afterwards sparsely connected (Newman and Girvan, 2004). In this work, we use random networks with fixed node number N and edge probability p as subgraphs. The connection of subgraphs is achieved by placing edges between them with probability p_{out} . Varying p_{out} allows for an adjustment of the modularity Q , which is computed using Equation (3.2).

It should be noted that a sufficiently large number of subgraphs is necessary to obtain large values of Q . We found an analytic approximation for the maximum possible modularity by maximizing Equation (3.1) (or (3.2), respectively) for different module numbers. For a network of n modules the maximum modularity is

$$Q_{\max} = 1 - \frac{1}{n}. \quad (3.11)$$

A full derivation of (3.11) is given in Appendix A.3. Derivation sketch: given a modular network with adjacency matrix \mathbf{A} , there is always a relabeling of indices \mathbf{P} so that $\mathbf{A}' = \mathbf{P}\mathbf{A}\mathbf{P}^{-1}$ is block diagonal. The blocks of \mathbf{A}' capture the number of edges within

Figure 3.7. Typical infection curve $\sum_\nu i_\nu(t)$ of a solution of Equation (3.9). The ratio of $1/\tau$ and γ results in a comb shape of the infection curve. Inset shows the more noisy infection curve obtained in a critical network. Networks: Erdős-Rényi network with 2000 nodes, $p = 0.05$, $p_{\text{rev}} = 0.5$ (inset: $p = 0.001$, $p_{\text{rev}} = 0.01$). From (Lentz et al., 2012).



and between the modules respectively and therefore allow for a simple computation of modularity. The maximum modularity can be derived from \mathbf{A}' , since the graphs of \mathbf{A}' and \mathbf{A} are isomorphic.

3.2.3 Impact of directionality

We solve the system (3.9) on a sequence of networks as generated according to the previous section. For the rest of this work, we keep the following parameters constant: The infection parameters are $\alpha = 3$, $\gamma = 1$ and the trade frequency is $\tau = 21$. The initial infection status of all nodes are $(s_\mu(0), i_\mu(0), r_\mu(0)) = (300, 0, 0)$. As initial conditions, we choose the node with longest range to avoid trivial solutions and set its initial state to $(299, 1, 0)$. Figure 3.7 shows a typical solution of the system on a random network.

Although the choice of parameters seems a bit arbitrary in the first place, the qualitative behavior of the system depends only weakly on the exact parameter values (Lentz et al., 2012). We have seen in Section 2.1.2 that the outbreak condition (2.6) determines whether an outbreak occurs at all. Above threshold, SIR-type outbreaks show quasi similar behavior. That is why the fraction α/γ in equations (3.9) is of minor importance as long as $\alpha/\gamma > 1$. In addition to that, the characteristic time scale of an SIR infection is given by $1/\gamma$ (see Equation (2.9)). If the pacing of the network coupling τ is too slow, a local infection dies out before it can be moved to the next node. Therefore, we choose τ and γ so that an infection can spread along the network. An analysis of the outbreak dynamics in the $(\tau\gamma)$ parameter space is given in (Lentz et al., 2012).

After integrating the system (3.9) on computer generated networks, we compute the final size of epidemic (see Section 2.1.2)

$$R_\infty = \lim_{t \rightarrow \infty} \sum_\nu r_\nu(t),$$

which is normalized by the population size P to yield the outbreak size

$$r_\infty = \frac{R_\infty}{P}. \quad (3.12)$$

Figure 3.8 shows the outbreak size for Erdős-Rényi networks with different values of link reciprocity. The plot shows networks of different densities determined by the edge occupation probability p . Note that p corresponds to the edge density before edge removal as described in Section 3.2.2. Hence, the edge density is further reduced for smaller values of ρ .

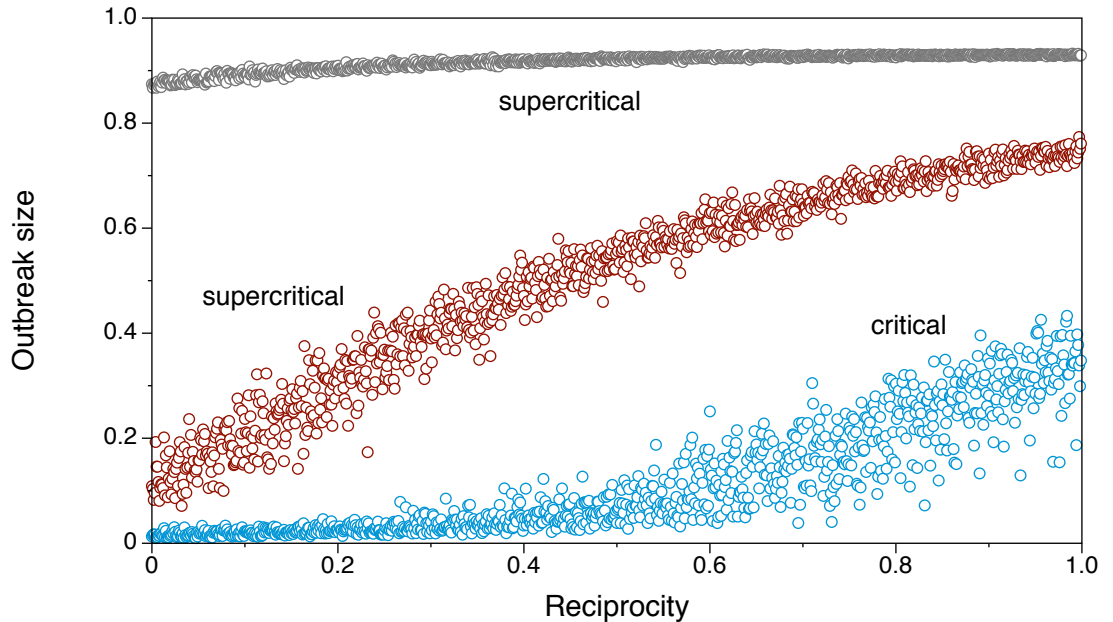


Figure 3.8. Effect of directionality for SIR outbreaks on random networks. Each point corresponds to one outbreak simulation on one network. All networks have 2000 nodes. Initial network densities: grey: $p = 0.003$, red: $p = 0.001$, blue: $p = 0.000625$.

Grey points in Figure 3.8 represent outbreaks in rather dense ($p = 0.003$) networks. This density is significantly larger than the percolation threshold of the network, which is $p_c = 0.0005$ and these networks are clearly supercritical. The figure demonstrates that the outbreak size is almost constant for all values of ρ , indicating that the number of infection paths in the network is not affected by a removal of some bidirectional links. The red points also represent outbreaks on supercritical networks, but the densities of the networks are only slightly above the critical point. As a consequence, the outbreak size is more sensitive to changes of reciprocity. Outbreak sizes range from 0.1 to 0.8 in

this case. The density of the blue outbreaks correspond to networks with initial density $p = 0.000625$. Consequently, the density is approximately $0.0005 = p_c$ for $\rho = 0.5$, i.e. the network undergoes a phase transition for $\rho = 0.5$. As shown in the figure, the outbreak size depends on the link reciprocity only in the supercritical regime.

The findings of Figure 3.8 demonstrate, that the structure of the underlying network affects the outbreak size. In particular, critical networks show a strong sensitivity to changes in directionality. Nevertheless, it can be shown that the effect behind the results in Figure 3.8 can in fact be explained by purely topological arguments. In fact, decreasing the reciprocity of a random network reduces the range of the primary infected node in the same manner as observed in Figure 3.8 (Lentz et al., 2012). This can be shown by comparing the range of the initially infected node with the actual size of the disease outbreak. A deviation between the two would indicate that back-mixing of recovered into the population is responsible for a decrease in outbreak size. In this case, recovered would not contribute to the infection process and would act as infection firewalls.

3.2.4 Impact of modularity

Before we study the impact of modularity, we define the *time of outbreak peak* in order to quantify the time period of the main epidemic. The peak time of the epidemic is defined as the time, that divides the infection curve into two equal areas, i.e. the “median” of the infection curve. Hence this corresponds to the time, where half of the final infection size is reached. It follows from the SIR model (2.2) that the time of infection peak can also be computed using

$$t : i(t) = R_\infty / 2. \quad (3.13)$$

Using the term “median”, the number of recovered is – up to a constant – the “cumulative distribution” of the infection curve, i.e. $dR/dt = \gamma I$.

As in the previous section, we compute the outbreak sizes and the infection peak times for networks of different modularity generated according to Section 3.2.2. For each outbreak, we compute the outbreak size r_∞ following (3.12) and the time of infection peak as defined in (3.13). The results are shown in Figure 3.9.

As the figure demonstrates, the outbreak size increases with modularity (red circles). This can be explained by the distribution of recovered and infected: In the early phase, the epidemic is localized in the initial module, while it is unlikely that other modules become infected in the first place. Modules have a high link density by definition so that an infection is likely to infect large parts of the initial module in the early phase. In the moment when a path is accessible to another module, the new module is likely to comprise of a large number of susceptible population. Therefore, the recovered subpopulation cannot act as a firewall against infection spread.

It should be noted that the effect is marginal over a wide range of modularity. The inset shows that a very high modularity causes a significant drop of the outbreak size,

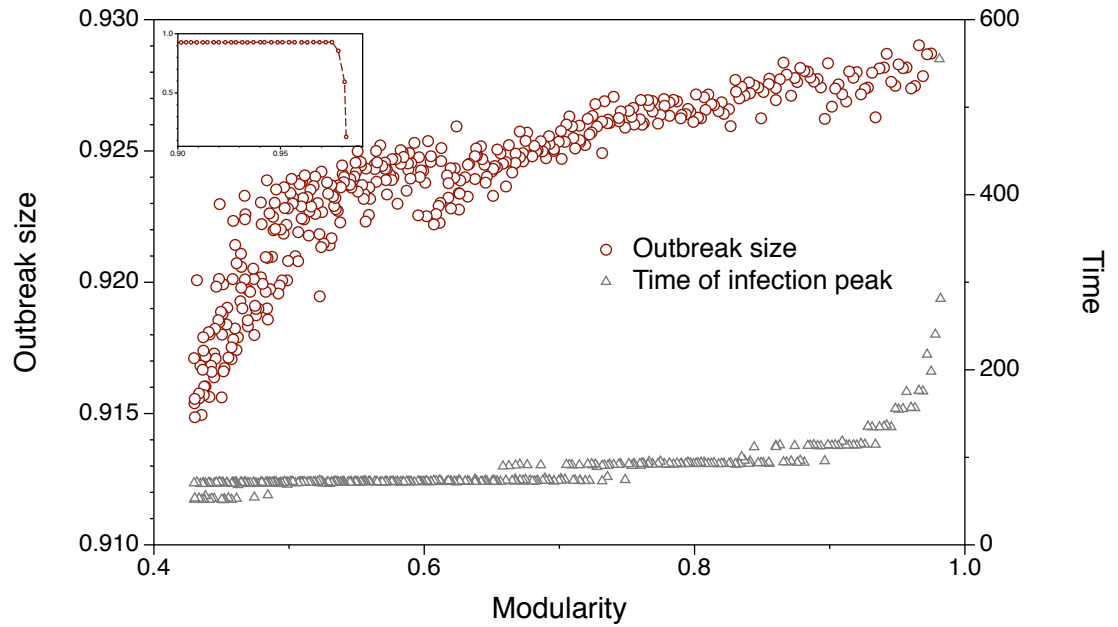


Figure 3.9. Impact of modularity Q on the outbreak size r_∞ . The outbreak size (red circles) is affected by an increase of modularity, although the effect is rather weak. The inset shows the disintegration of the network resulting in a drop of the outbreak size for very large values of Q . Grey triangles demonstrate that increasing modularity can cause significant delays of the infection peak.

since the network disintegrates into disconnected components in this limit. In contrast to the effect discussed above, the drop of outbreak size in the limit $Q \rightarrow 1$ is a purely topological one (Lentz et al., 2012). This can be shown with the same arguments as in Section 3.2.3.

In addition to that, Figure 3.9 shows the time of infection peak for different modularities (grey triangles). For small and intermediate values of Q , we observe a slight delay of the outbreak peak. The discontinuous behavior of the plot stems from the pacing τ of the network. The main finding of the figure is that large values of modularity cause a significant delay of the outbreak peak. This knowledge could be useful for the implementation of counter measures, such as vaccination strategies. Consequently, there is more time to react in high modular networks.

3.2.5 Impact of reciprocity in modular networks

In this section, we focus on modular networks with varying link reciprocity, i.e. we combine the properties studied in sections 3.2.3 and 3.2.4. We generate a number of modular networks and change their link reciprocity afterwards. Solving the infection

model (2.2) on these topologies gives outbreak sizes for different reciprocities. The results are shown in Figure 3.10.

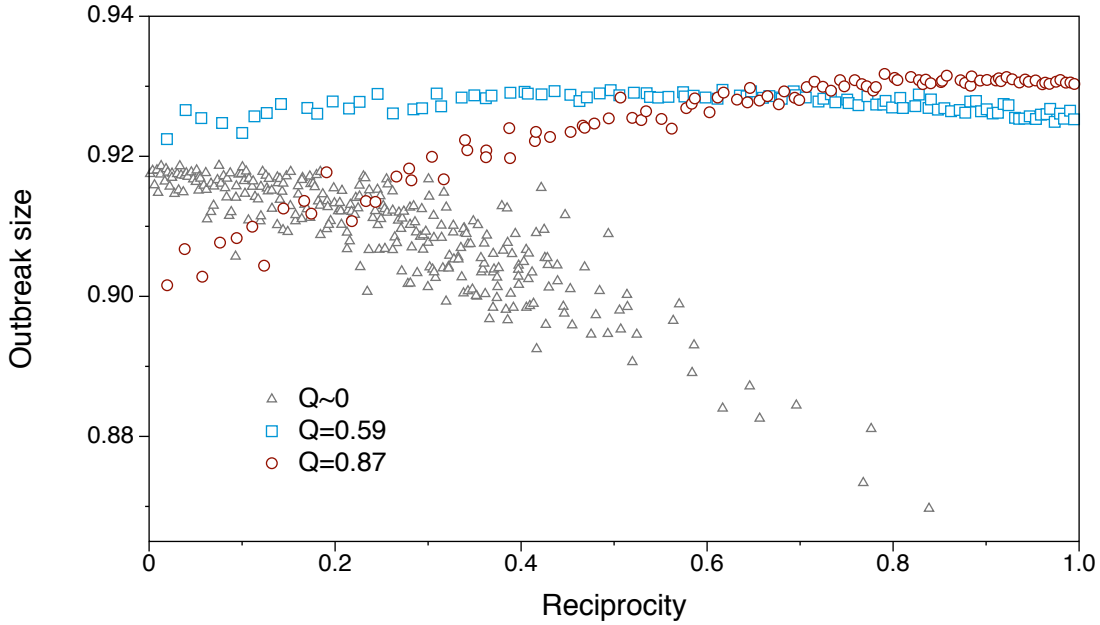


Figure 3.10. Outbreak size vs. link reciprocity for modular networks. Changing reciprocity in intermediate modular networks (blue squares) does not affect the outbreak size significantly. Highly modular networks (red circles) act as isolated modules and show a behavior similar to that of Figure 3.8. The correlation between outbreak size and reciprocity is reversed for very low modular networks (grey triangles).

The red circles in Figure 3.10 represent networks with $Q = 0.87$, i.e. highly modular networks. The outbreak size shows a behavior comparable to that of the supercritical Erdős-Rényi graphs in Figure 3.8. This provides evidence for the hypothesis that the modules of highly modular networks act as isolated subgraphs. For networks of intermediate modularity ($Q = 0.59$, blue squares), there is almost no correlation between outbreak size and link reciprocity.

Interestingly, the correlation between outbreak size and link reciprocity becomes even negative for networks of very low modularity ($Q \sim 0$, grey triangles). The networks behind the grey triangles should not be confused with random networks. In fact, they are generated as modular networks, but with very high inter-module edge probabilities p_{out} , i.e. they possess an internal structure. This structure can not be resolved by modularity and can be seen as the limit $Q \searrow 0$. It is an interesting feature of these networks that they show a smaller outbreak size for increasing reciprocity.

A possible explanation for this counter-intuitive behavior is that there is a high probability that an infected subpopulation M is highly connected to the module M_0 where the infection originated from. As a matter of fact, the module M_0 is at this stage in an “older” infection state, i.e. it is dominated by recovered subpopulations. Consequently, the effective number of susceptible population is decreased and forms an impermeable boundary for the infection path.

Conclusion of the section. The German pig trade network was analyzed in terms of static network measures. Our main observations are the following: First, the system possesses a heavy-tailed degree distribution (Figure 3.1) indicating that the system is heterogeneous. This implies that the network is epidemiologically stable to random vaccination and targeted vaccination should be efficient (see Section 2.3.6).

Second, the network components and the distribution of ranges result in a node classification into either long range or short range nodes. Any ranking of nodes according to their potential of disease spread is reduced to the class membership of the nodes in this context. In addition to that, the balance b of the range distribution provides evidence that the system considered here is in a critical state ($b = 0.069$, see also Figure 3.3). The directionality of the network results in a rather complex large scale structure, when compared to an undirected network.

Third, the network under consideration can be partitioned into modules, i.e. relatively densely connected subgraphs. By adding meta information (in this case geographical information) to the network partition, we found a reasonable partition into compact geographical regions (see Figure 3.6). The large scale trade structure of the system can be revealed this way.

Finally, the observations above raise two questions for the context of epidemics on networks: 1. How do link directions affect an epidemic outbreak? and 2. Given a network is somehow modular, does this have any impact on disease dynamics? In order to answer these questions, we generated random networks that allow for a variation of the desired properties – directionality and modularity – and solved an infection model tailor made for a livestock trade network on these topologies. Our main findings are that modularity can cause a significant delay of an outbreak, and stronger link directionality generally reduces the outbreak size. In special topologies this effect can be reversed.

4 Temporal network analysis – Case study: Livestock trade network

The previous chapter has demonstrated that network analysis provides a deep insight into the processes behind epidemic spreading. Given a sufficient amount of data, a contact network is capable to capture all possible infection pathways in the system. The potential of static network analysis lies in the huge toolbox of methods that has been developed in the last decades. As depicted in Section 2.2, there exist conclusive definitions for both their large scale topological features and local centrality measures allowing for node rankings.

Nevertheless, the concept of static networks neglects temporal variations in the system, i.e. the edges of a particular network are not necessarily present at all times. Networks showing a sparse and heterogeneous temporal occurrence of edges are said to show *bursty* behavior (Holme and Saramäki, 2012). This chapter addresses some of the conceptional problems owing to bursty links occurrence, the most central one being the *causality* of paths. Section 4.2 focusses on the computational analysis of the full temporal representation of the network analyzed in Section 3.1. In Section 4.3, we present a novel formalism mapping the causality of temporal networks onto a mathematical graph.

4.1 Introduction

To begin with, we highlight the most fundamental difference between static and temporal networks. In particular, we compare the static to the temporal representation of the system. Figure 4.1 shows a temporal network and its aggregated graph. Although the edges of the temporal network are present also in the aggregated graph, the existence of paths of length greater than one is not as obvious. The aggregated graph (right panel in Figure 4.1) suggests that the network is connected, i.e. there is a path between every node pair. As an example, there are two different paths from node 3 to 4 in the aggregated system. However, this does not hold for the temporal view of the system. Consequently, paths in an aggregated graph of a temporal network have to be treated with care.

Before we give a formal definition of temporal networks, we briefly discuss the different terms used for temporal networks in the literature. Hereby, we have to distinguish between temporal networks in the sense above and other systems, which have a different focus.

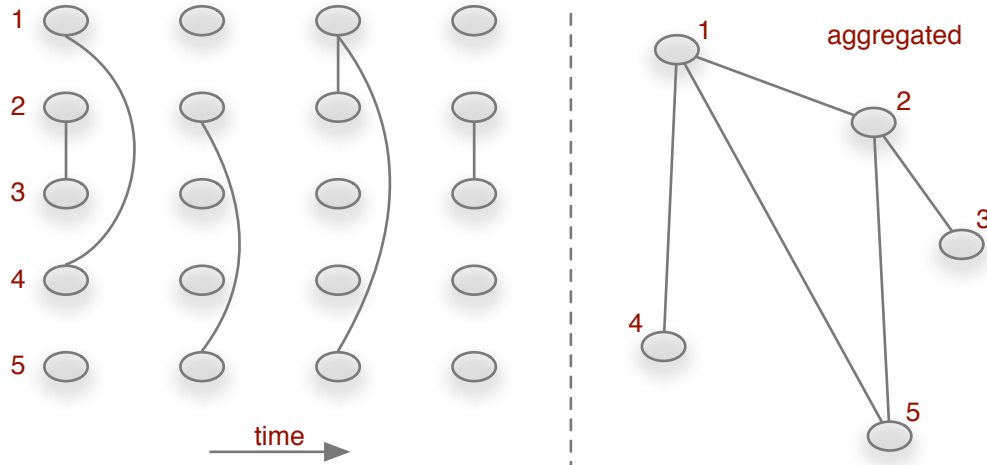


Figure 4.1. Role of causality in a temporal network with 5 nodes and 4 snapshots. The left panel shows snapshots of the system at different times and the right panel shows the corresponding aggregated network. Although there is a path from node 3 to 4 (and vice versa) in the aggregated network (right panel), there is no causal path between 3 and 4 in the temporal network (left panel).

Disambiguation. Since the analysis of temporal networks is an interdisciplinary field, there is still no consistent designation for what we refer to as *temporal networks* (Holme and Saramäki, 2012). Different phrases, such as temporal graphs, dynamic graphs, dynamic networks are used in the literature. In addition to that, there are other classes of networks seeming to be related to temporal networks, i.e. adaptive networks, growing networks, evolving graphs. The analysis of the latter has a strong focus on network growth, i.e. the process behind the evolution of static networks. A central question for these systems is what is the fundamental process that has formed the network. An example is the Barabási-Albert network, where the underlying process is a rich-get-richer principle that results in a scale free degree distribution. The striking difference between growing networks and temporal networks is that the snapshots of a temporal network can in principle be arbitrary. Correlations between two snapshots of the system (if any) could be over arbitrary periods of time. We prefer the term temporal network, since *temporal* is not so easily confused with dynamic systems. Furthermore, the systems under consideration are not mathematical graphs; therefore, we use the more general term *network*.

4.1.1 Formal definition

A temporal network $\mathcal{G} = (V, \mathcal{E}, T)$ consists of a set of nodes V and a set of edges \mathcal{E} , where each edge in \mathcal{E} is given by a triple (u, v, t) and connects nodes u and v at time

$t \in T$. T is the observation period of \mathcal{G} , where $T \subset \mathbb{N}^+$ for time discrete systems and $T \subset \mathbb{R}^+$ for continuous systems¹. Using discrete time steps, a temporal network can be represented as a sequence of static snapshots, i.e. $\mathcal{G} = G_1, \dots, G_T$. The aggregated graph $G = (V, E)$ of a temporal network simply ignores the occurrence times of the edges in \mathcal{E} and the set of nodes V is the same in both representations. In analogy to static networks, we denote the *transitive closure* of $\mathcal{G} = (V, \mathcal{E}, T)$ by $\mathcal{G}^* = (V, \mathcal{E}^*, T)$, where \mathcal{E}^* contains an edge (u, v, t) , wherever there is a causal path from node u to v arriving at time t and having started at some time $t_0 < t$. Following (Casteigts et al., 2012), the *horizon* \mathcal{H} of node u is defined by the set

$$\mathcal{H}_u = \{v : \exists u \rightsquigarrow v\}, \quad (4.1)$$

where $u \rightsquigarrow v$ means that there is a causal path from node u to v .

4.1.2 Viewpoints and implementation

As in the case of static networks, temporal networks can be interpreted and implemented in different ways (Casteigts et al., 2012). A brief report of different implementations of static networks is given in Appendix A.1. Besides the adjacency matrix, edge lists and adjacency lists are appropriate network representations. Considering a temporal network as a sequence of static networks (called snapshots or graphlets) can be seen as a *graph centric* view on the system. It is the analogue of the adjacency matrix in static networks. More formally, a temporal network \mathcal{G} can be represented by a sequence of adjacency matrices

$$\mathcal{A} = \mathbf{A}_1, \dots, \mathbf{A}_T, \quad (4.2)$$

where T is the observation time and the increment is the temporal resolution.

In analogy to the edge lists of static networks (see Appendix A.1), an *edge centric* view on a temporal network is represented by an edge set respecting the occurrence times of the edges. Let $\mathcal{G} = (V, \mathcal{E})$ be a temporal network. Then the set of edges \mathcal{E} is represented by a sequence of triples

$$\mathcal{E} = (u_1, v_1, t_1), (u_1, v_1, t_2), (u_2, v_2, t_2), \dots .$$

Alternatively the set of edges can be expressed in the form

$$\mathcal{I}((u_1, v_1)) = t_1, t_2, \dots ,$$

where \mathcal{I} is called edge presence function. This point of view is particularly convenient

¹In this thesis, we focus on time discrete systems, since a continuous time process can be approximated by a discrete one by choosing an appropriately small increment. Furthermore, edge weights and a latency functions for edge traversal could be added to the definition (Casteigts et al., 2012). This is, however, beyond the scope of this thesis.

for the time randomization of temporal networks that we will use in Section 4.3.5.

Finally, a *node centric* view of a temporal network considers the neighborhood \mathcal{N} of a node v over time, i.e. $\mathcal{N}(v, t)$. This view is the counterpart of the adjacency list in static networks (see Appendix A.1). The temporal degree of each node immediately follows from $d(v, t) = |\mathcal{N}(v, t)|$. The edge centric and node centric network view is considered as a microscopic perspective, while the graph centric view provides a macroscopic perspective.

We make use of microscopic perspective implicitly in computer implementations as in Section 4.2. Furthermore, we focus on the graph centric view (4.2) in Section 4.3 to analyze macroscopic path structures in temporal networks.

4.1.3 Paths in temporal networks

A causal sequence of edges between two nodes in a temporal network is called (causal) path. A path between two nodes u and v starting at node u at time t_1 is given by a sequence of edges, i.e.

$$\text{path}(u, v, t_1) = \{(u, x, t_1), (x, y, t_2), \dots, (z, v, t_n)\},$$

where $t_1 < t_2 < \dots < t_n$ and x, y and z are nodes on the path. It is important to note that paths in a temporal network are in general *not transitive*. Transitive means that the existence of a path from node u to v and a path from v to w implies that there is a path from u to w , i.e.

$$(u \rightarrow v) \wedge (v \rightarrow w) \implies (u \rightarrow w). \quad (4.3)$$

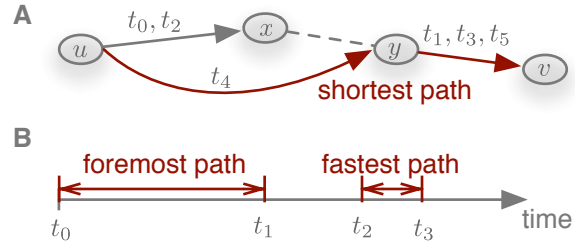
This property is obviously satisfied in all static networks. In temporal networks, however, paths are in general not transitive, since a path from u to v could simply exist only at a later time than the path from v to w , so that

$$(u \rightsquigarrow v) \wedge (v \rightsquigarrow w) \not\implies (u \rightsquigarrow w) \quad (4.4)$$

in general. The reasons why paths in temporal networks can not be easily represented as paths in static networks originate from property (4.4). In Section 4.1.4 we briefly discuss some conceptional problems that arise from this circumstance.

Note that possible paths between nodes depend on time in general. This has crucial implications on the shortest path distance known from static networks (see section 2.2.2). As a matter of fact, there are three different shortest path types in temporal networks. Just like in the static case, the *shortest* path distance between two nodes measures the topological distance between the nodes. It counts the number of edges used to traverse the shortest path. In addition, the *duration* of a path can be measured in temporal networks. This duration can be measured in two different time frames (Casteigts et al.,

Figure 4.2. Topological shortest distance and temporal shortest durations for a path between nodes u and v . The shortest path (Panel A) counts the number of edges between the nodes. Panel B demonstrates that although the fastest path could take $t_3 - t_2 < t_1 - t_0$, the foremost path arrives already at $t_1 < t_2$.



2012): First, the *fastest* path between two nodes is the path of shortest duration, no matter when the path starts in time. Second, the *foremost* path between two nodes is the path that arrives earliest in a global time frame.

Figure 4.2 demonstrates the difference between the foremost, fastest and shortest path concepts, respectively. Edge labels are edge occurrence times, which are ordered so that $t_1 < t_2 < t_3 < t_4 < t_5$. The dashed edge (x, y) indicates that these nodes are not connected directly, but by other nodes of the network. Panel A shows that the shortest topological path between nodes u and v is (u, x, v) and the distance is 3. It can be seen from panel B that the first (foremost) path starts at node u at time t_0 and arrives at node v at time t_1 . Although the fastest path takes less time to traverse ($t_3 - t_2 < t_1 - t_0$), it arrives later ($t_3 > t_1$) than the foremost path. Note that shortest path and temporal shortest path do not coincide in this example, since the shortest path connection can be at times t_4 and t_5 which are greater than t_1 and t_3 .

Throughout the rest of this work, we use a global time scale, which is defined by the first time in the dataset under consideration. Consequently, we measure shortest path durations in terms of *foremost* path durations, if not explicitly stated.

4.1.4 Conceptional problems in temporal networks

Before we focus on different methods to analyze temporal networks, we have to point out that many static network measures, such as centrality or components, are in general time-dependent and can not be summarized to static measures. As an exception, Grindrod et al. defined a time-independent centrality measure for temporal networks (Grindrod et al., 2011). In addition, time-scales of node dynamics and network dynamics can be of the same order and cause significant interactions between the dynamics. We consider the relation between node dynamics and edge dynamics in Section 4.2.

The most essential difference between static and temporal networks lies in the importance of causality of paths in temporal networks. Although it is possible to analyze paths in temporal networks systematically (see Section 4.3) we have to stress that generalizing the concept of connected components is far more complex in temporal networks as it is in the static case. Nicosia et al. point out that finding connected components in temporal networks is NP-complete in general (Nicosia et al., 2012). In addition to that,

the authors demonstrate that components in temporal networks can be *degenerated*, i.e. there are multiple possible partitions of connected components and nodes can belong to two multiple components at the same time.

We take up this point at the end of Section 4.3. In order to get an impression about the path structure in temporal networks, we start with a pure data-analysis of a temporal network dataset.

4.2 Data-driven network analysis

In this section we analyze the livestock trade data set as introduced in Section 3.1, but we explicitly take into account temporal information². Each edge in the system is only present at certain days, i.e. the network can show bursty behavior and long waiting times between edge occurrences can be present in the system.

As in the case of static networks, the concept of centrality plays an important role for risk assessment and the implementation of vaccination and surveillance strategies also in time-varying topologies. The maximum spreading potential of each node is given by its range as discussed for static networks in Section 3.1. In this section we analyze the ranges of the network nodes according to their constance over time. The results shown in this section are published in (Konschake et al., 2013).

4.2.1 Representative sample

Before we analyze the ranges of the nodes in the network, we estimate the time span needed to cover the temporal properties of the system. Figure 4.3 A shows the activity of the nodes and edges in the network over the observation period. The red line shows the number of active nodes on a daily resolution. We observe that 25 % of all nodes and 10 % edges are active every day on average. The plot shows decreased activity during the summer month and on public holidays such as easter and christmas. In addition, there is a slight trend to a decrease of the number of nodes, which reflects a centralizing process in the system.

Figure 4.3 B gives a picture about the convergence of the network during the aggregation process, i.e. summing up the snapshots of the temporal system step by step to obtain the static network representation. Dashed lines show the fractions of nodes and edges in the aggregated network, respectively. The solid lines show the respective aggregation rates. Since the latter are derivatives of the aggregation fractions, we show a local regression of the aggregation rate to reduce noise in the signal.

²In order to be congruent with the datasets used in the publications, we use the pig trade dataset of (Konschake et al., 2013) in this chapter. This dataset differs slightly from the static network dataset used in Section 3.1. It covers the period from 01 January 2008 to 31 December 2009. The results do not change qualitatively and hereby the results of (Konschake et al., 2013) and (Lentz et al., 2013) are comparable.

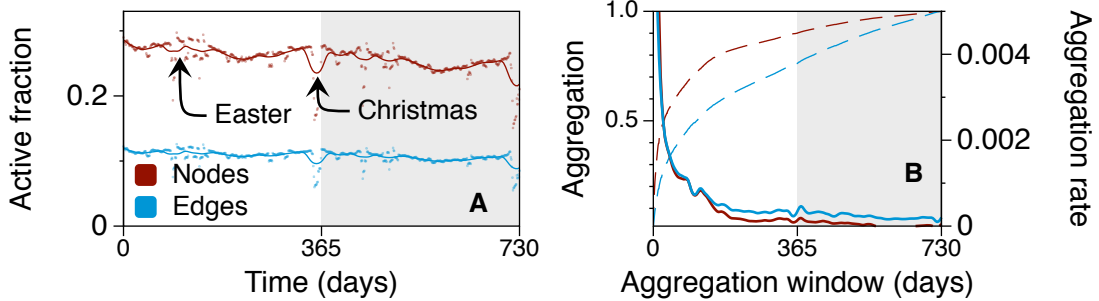


Figure 4.3. **Panel A:** Daily activity of the livestock trade network over two years. Original data is shown as points and solid lines are local regressions of the original data.

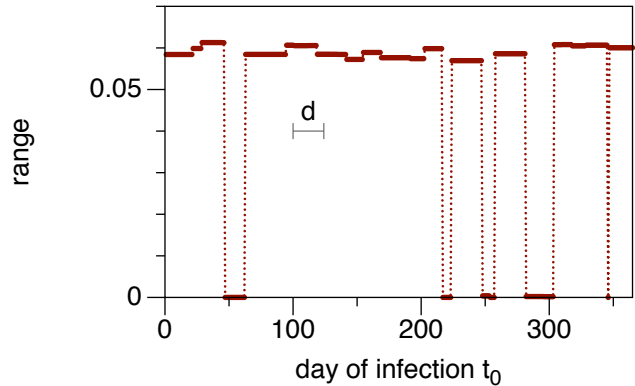
Panel B: Time aggregation of the network for different aggregation windows. Dashed lines show the fractions of nodes/edges in the aggregated network. Solid lines are local regressions of the aggregation rates.

The figure demonstrates that the aggregation rates for both nodes and edges becomes negligible after 1 year. Therefore, we can assess a period of 1 year sufficient to provide stationarity of the system, i.e. the time span, after which only few more edges are added to the network.

4.2.2 Simulated disease outbreaks

Node rankings are of major importance for epidemiology. We try to answer the question, if a constant ranking of node makes sense in this particular temporal network. As a generic measure for the spreading potential of a node, we consider its range. In analogy to Section 3.1, we define the range of a node in a temporal network as the size of its temporal out-component. It is important to note that the out-component of each node depends on the time t_0 , when it is measured. In addition to that, the range of a node can depend on the particular spreading process, e.g. an epidemic, a chemical reaction or rumor spread. More specifically, a spreading process can have a finite memory d that shortens the ability of a node to remain in a certain state over time. In our context, this memory corresponds to the *infectious period* d of a disease, i.e. the time period, before the infection dies out if it is not carried over to another agent. Computing the range combined with a finite infectious period mimics an SIR-type process, where the infectious period is related to the reciprocal recovery rate as discussed in Section 2.1.2. For clarity reasons we do not solve differential equations for epidemics in this section, but reduce the infection dynamics to assigning a discrete infection state – susceptible, infected or recovered – to each node in the network. An infected node remains infected over the infectious period d . Thus, the infection state of the whole network is given by the number of susceptible $S(t)$, infected $I(t)$ and recovered $R(t)$ nodes, respectively.

Figure 4.4. Temporal variation in the range $r(v, d, t_0)$ of an exemplary node v in the network over one year. Although the range remains rather constant for most infection times, it vanishes for certain periods. The grey interval corresponds to the fixed infectious period $d = 24$ days.



We define the *temporal range* of a node v by explicitly taking into account the time of (primary) infection and infectious period, i.e. $r(v, d, t_0)$. Since there are no mixing states of nodes as in meta populations and we assume an infection probability $p = 1$ for every contact edge, the range of a node is identical to the outbreak size $R(t = \infty)$.

In summary, range and infectious period are intrinsically entangled on temporal networks

$$\text{static network: } r(v) \rightarrow \text{temporal network: } r(v, d). \quad (4.5)$$

For the rest of this work, we therefore use the notion *range* and *outbreak size* synonymously. Although the temporal range should approach the static range for infinite memory, i.e. $r(v, d = \infty) \rightarrow r(v)$, the static range of a node is in general not reached even in this case. This is caused by causality of paths in temporal networks as explained in Figure 4.1.

Single outbreaks

We address the outbreak pattern caused by single outbreaks in this section, while we discuss the properties of the set of all possible outbreak scenarios in the next section. In order to analyze node ranges in the pig trade network, we use a modified breadth-first-search algorithm (see Appendix A.1 for a brief summary of search algorithms for static networks). Given a fixed infectious period, we mark a particular node v to be infected at time t_0 . For every time step t in the interval $[t_0, t_0 + d]$, we identify the neighborhood $\mathcal{N}(v, t)$ and mark all susceptible nodes in $\mathcal{N}(v, t)$ as infected. Infected nodes are marked as removed after the infectious period d and do not contribute to further infections. This procedure is repeated for all infected nodes as long as there are still infected nodes in the system.

Figure 4.4 shows the range of an exemplary node in the network for different infection times t_0 . The infectious period is $d = 24$ days. For most infection times the example node can infect about 6 % of the network. The range distribution over time shows a

similar bimodal pattern similar to the distribution over nodes for the static network in Figure 3.2. This provides evidence that there is an infection path from the exemplary node to a connected component in the network. It is important to stress that the concept of connected components does not translate to temporal networks in a straightforward manner (see Section 4.1.4). Besides the bimodality itself, it is remarkable that the majority of adjacent primary infection times cause outbreaks of similar size.

This feature can be explained, if we underline the temporal sparsity of edges, i.e. nodes are likely to have only few contacts within one infectious period. If the primarily infected node v has no trade contact during the infectious period, the disease dies out. Even if the disease is transferred to a successor node w at a time t_1 within the interval $[t_0, t_0 + d]$, the disease dies out, if there is not further trade contact within the period $[t_1 + d]$ and so forth. The regions of small/vanishing range in Figure 4.4 correspond to these scenarios. On the other hand, if all successors of node v have one or more trading contact within their respective infectious periods, the disease can be transferred to a larger number of nodes. The majority of small variations in t_0 implies stable ranges in the order of d (the infectious period is shown by the grey line in Figure 4.4). If the degree of v or a successor node in the infection chain is even larger than 1, even more secondary outbreaks are triggered and manifest themselves in smaller range fluctuations as for the long range values in Figure 4.4.

We have seen in this section that a temporal degree of freedom adds a significant amount of complexity even to the outbreak pattern of a single node. Now we focus on the set of *all* outbreak scenarios, i.e. the set of all initial conditions and variations in the infectious period as a parameter.

Set of outbreak scenarios

We apply the method discussed in the previous section to all nodes in the network. As primary infection times, we consider all times within the first year in the dataset. This ensures that even if a particular outbreak penetrates the second year, it will have died out within the observation period. We restrict ourselves to infectious periods $d < 56$ days, since this interval covers the infectious periods of the major livestock diseases (Horst, 1998; Konschake et al., 2013). Considering all nodes in the network as potential starting points for infections and all days in the first year of the dataset as possible starting times yields 10^9 different initial conditions. We denote the *set of all outbreak scenarios* by \mathcal{S} . More formally, let $\mathcal{G} = (V, \mathcal{E}, T)$ be the temporal network of our dataset. Then the set of all outbreaks is given by all possible initial conditions and parameters and the corresponding outbreak size, where the latter is identical to the range for our model:

$$\mathcal{S} = \{(v, t_0, d, r(v, d, t_0)) : v \in V, t_0 \in T/2, d \leq 56\}. \quad (4.6)$$

In what follows, we will average over this set in different ways to immediately obtain information about the impact of infectious period, primary infection time or the starting node on disease spread. Table 4.1 shows a table representation of the set (4.6).

Table 4.1. Tabular data structure of the set of outbreak scenarios as defined by (4.6). We analyze 103,490 starting nodes for 365 times of primary infections and 56 different infectious periods yielding 10^9 rows.

Starting node ID	initial conditions & parameter		outbreak size $r(v, d, t_0)$
	time of primary infection t_0	infectious period d	
1	1	1	58
1	2	1	276
⋮			
103,490	365	56	72

Considering static networks, every node can cause an epidemic, if it is connected to other nodes in the network. We have seen in the previous section that in temporal networks the time of primary infection has to be in an appropriate interval. In addition, the range also depends on the infectious period, since a disease with long infectious period is more likely to spread over the network than a disease with low infectious period. We define the *outbreak probability* $p_s(d)$ as the fraction of elements in \mathcal{S} that causes a secondary outbreak at all, that is

$$p_s(k) = \frac{|\{x \subset \mathcal{S} : r(v, d, t_0) \in x > 0, d = \text{const.}\}|}{|\mathcal{S}|}. \quad (4.7)$$

Note that we compute the outbreak probability for each infectious period separately.

Figure 4.5 A shows the outbreak probability for different infectious periods. For comparison, the outbreak probability in the static network is shown by the dashed line. This is just the fraction of nodes with finite out degree and apparently the outbreak probability has no dependence on the infectious period in the static case. The outbreak probability saturates for sufficiently large infectious periods, but it is still only half as much as in the static case even for $d = 56$.

In addition to the probability of an outbreak, we compute the expected size of the outbreaks. The *mean outbreak size* is an average over all starting nodes and all starting times in \mathcal{S} , i.e. $\langle r(v, d, t_0) \rangle_{v,t_0}$. Figure 4.5 B shows the mean outbreak size and the 50 % confidence interval (solid line and grey shaded area) and the mean outbreak size in the static network (dashed line). As for the outbreak probability, we observe significant outbreak sizes only for $d > 14$ days and the outbreak size is 6 times smaller than in the static case even for $d = 56$ days. In summary, the infectious period must be larger than

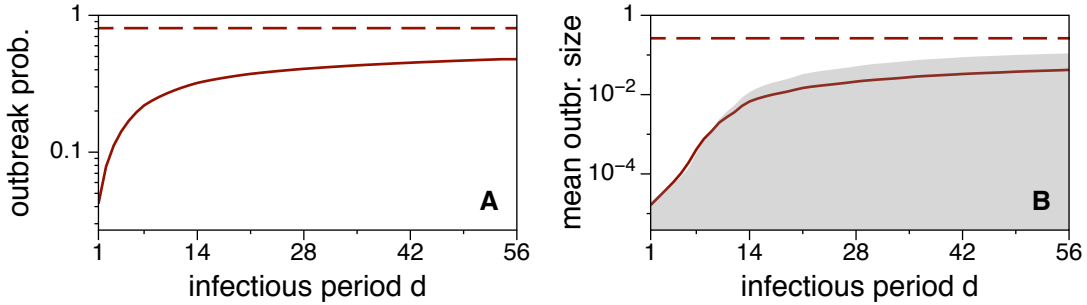


Figure 4.5. Outbreak probability (A) and mean range (B) for different infectious periods d as solid lines. Dashed lines correspond outbreak probability and mean outbreak size of the static network, respectively. The grey shaded area in panel B shows the 50 % confidence interval.

14 days to cause a severe outbreak and the static network approximation overestimates the size of outbreaks significantly.

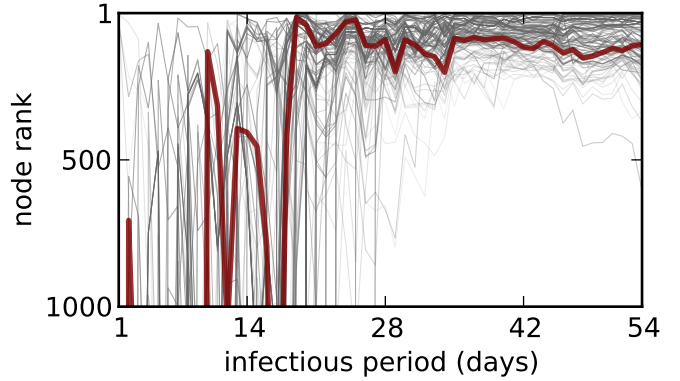
4.2.3 Node rankings

This section is devoted to the analysis of the node ranking according to their respective ranges. Rankings are very important for the implementation of vaccination and surveillance strategies, where the exact value of a certain measure for each node is not important. For every infectious period d , we average over all times of primary infection in (4.6). Thus, the quantity $b(v, d) = \langle r(v, d, t_0) \rangle_{t_0}$ is a function of the node and infectious period. Ordering $b(v, d)$ for every d in descending order gives a ranking $R(d)$ of the nodes according to their outbreak sizes, where $R(d)$ is an ordered set of nodes for every infectious period. The question is, whether these rankings remain stable, if the infectious period is changed.

Figure 4.6 shows the ranking trajectories over different infectious periods of the top 100 nodes in the network. We define the top 100 nodes as the nodes with the largest outbreak size in \mathcal{S} averaged over both t_0 and d , i.e. $\langle r(v, d, t_0) \rangle_{d, t_0}$. An arbitrarily chosen node is shown in red for illustration purposes. It should be noted that the rank of each node in the top 100 set can take any value in the figure, since the top 100 nodes are determined by averaging out the infectious period.

As the figure suggests, the ranking of nodes is unstable for small infectious periods ($d < 21$ days). This region is dominated by temporal fluctuations of the infection paths in the network. Interestingly, the ranking approaches a stable region for $d > 21$ days. For $d > 28$ days most nodes in the top 100 sample do not undergo significant rank changes any more. This means that a ranking of nodes is reasonable for sufficiently large infectious periods.

Figure 4.6. Node ranking of the top 100 nodes over different infectious periods. Rankings are computed by averaging (4.6) over the time of primary infection. Top 100 nodes are the nodes with the largest outbreak sizes averaged over d and t_0 . The rankings of an arbitrary node are shown in red for illustration purposes.



4.2.4 Inaccurate infectious periods and the robustness of node rankings

Finding exact values of the infectious periods of a certain disease is often unachievable in real world scenarios. Therefore, we look into the impact of variations in the infectious period on the ranking of nodes. We consider pairs of rankings as defined in the previous section with different infectious periods, i.e. $R(d_1)$ and $R(d_2)$.

In order to compare two rankings, we could use measures of rank correlation, such as Spearman or Kendall rank correlation coefficients. These turn out, however, to be very sensitive to even small differences between two rankings. Figure 4.6 suggests that even in the stable region where $d > 28$ days node ranks remain similar, but not equal. Computing Spearman or Kendall rank correlation coefficients for different infectious periods (k_1, k_2) in our dataset would give vanishing values for almost all pairs (d_1, d_2) . For that reason, we relax the requirements for similarity between two rankings. Thus, we consider the Jaccard index – i.e. the *intersection* between the sets of the respective upper samples of each ranking. In other words, we examine whether the same nodes appear in the upper ranks of both the R_{d_1} and the R_{d_2} rankings.

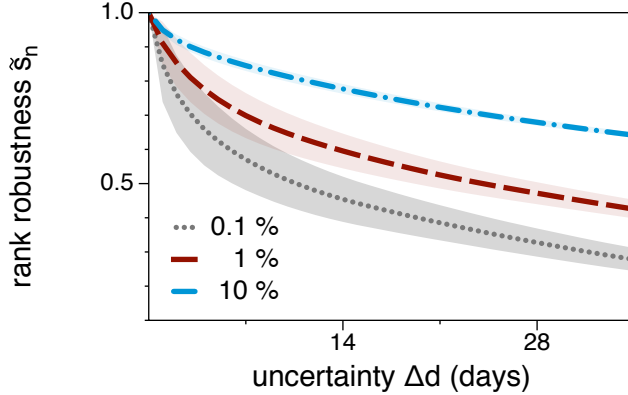
We denote the subset of the upper τ ranks of $R(d)$ by $R_\tau(d)$. As a similarity measure, we define the *rank intersection* between two rankings $R_\tau(d_1)$ and $R_\tau(d_2)$ as

$$s_\tau(d_1, d_2) = \frac{|R_\tau(d_1) \cap R_\tau(d_2)|}{|R_\tau(d_1)|}, \quad (4.8)$$

that is the intersection between the sets of nodes normalized by the size of the top n sample. We get $s_\tau(d_1, d_2) = 1$, if the upper τ nodes in the rankings $R(d_1)$ and $R(d_2)$ are identical. On the other hand, $s_\tau(d_1, d_2) = 0$ implies that ranks for d_1 and d_2 are completely different.

Using Equation (4.8) yields a similarity matrix with 1540 different combinations of infectious periods for our outbreak scenarios (4.6). Since particular combinations of infectious periods are less relevant, we analyze the ranking as a function of the *uncertainty*

Figure 4.7. Rank robustness vs. uncertainty in the infectious period for the upper 0.1 % (grey), 1 % (red) and 10 % (blue) of nodes in the network. Shaded areas correspond to the 50 % confidence intervals.



of the infectious period

$$\Delta d = |d_1 - d_2|. \quad (4.9)$$

Now we average the entries of the similarity matrix over uncertainties and get the rank intersection

$$\tilde{s}_\tau(\Delta d) = \langle s_\tau(d_1, d_2) \rangle_{|d_1 - d_2| \leq \Delta d}. \quad (4.10)$$

This rank intersection measures the robustness of a certain ranking against changes in the infectious period. Therefore, we call this measure the *rank robustness* a given uncertainty in the infectious period.

For convenience, we express (4.10) in terms of the upper *fraction* of nodes instead of the upper nodes themselves. That is, we replace the top τ nodes by the top fraction of nodes n :

$$\tilde{s}_n(\Delta d) = \langle s_n(d_1, d_2) \rangle_{|d_1 - d_2| \leq \Delta d}. \quad (4.11)$$

The same is implicitly done for rank intersection $s_n(d_1, d_2)$ (4.10) and the node ranking $R_n(d)$.

We show the rank robustness for the fraction of the 0.1 %, 1 % and 10 % upper nodes in Figure 4.7. These fractions correspond to approximately 100, 1000 and 10,000 nodes, respectively. The 50 % confidence intervals of each curve are shown as shaded areas. As expected, larger uncertainty in the infectious period generally leads to a decrease of rank robustness. The decrease is small for the largest sample (blue), since the number of nodes in this sample is relatively large. This guarantees that the same nodes are likely to be in all rankings $R_{10\%}(d)$ for all d . Consequently, the variation in rank robustness is relatively small (blue shaded area). Considering the 0.1 % sample (grey), it is remarkable that even for an uncertainty of 14 days, the robustness is still 50 %. As a smaller sample is more prone to fluctuations, variations of rank robustness are relatively large (grey shaded area). The red curve shows an intermediate behavior.

4.2.5 Temporal vs. static representation

Since the analysis of a temporal network using a data-driven approach is computationally expensive, we compare the node rankings $R_n(d)$ to centrality measures for the static network representation as defined in Section 2.2.2. We denote the upper τ nodes according to a static centrality measure as C_τ . Note that C_τ does not depend on the infectious period, since the latter plays no role in static networks. In this work, we consider betweenness, closeness, degree centrality and range as centrality measures. Following Equation (4.8), we define the *centrality intersection* between the outbreak size ranking $R_\tau(d)$ and C_τ as

$$I_\tau(d) = \frac{R_\tau(d) \cap C_\tau}{|C_\tau|}, \quad (4.12)$$

where C_τ is a substitute for the upper τ nodes of one particular centrality measure listed above.

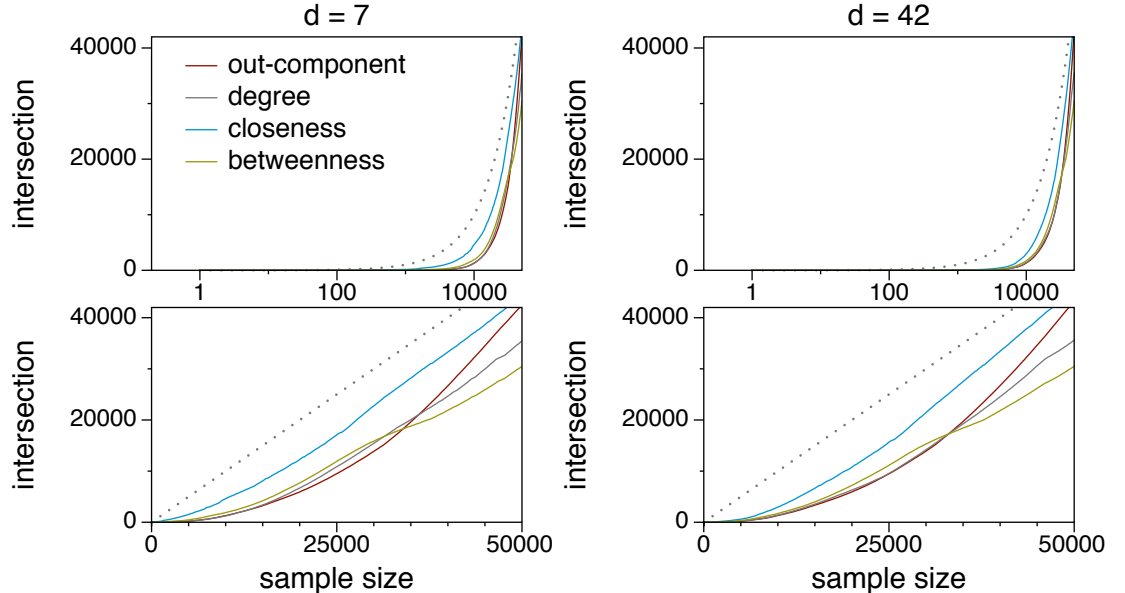
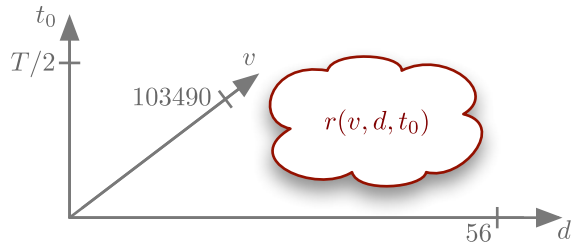


Figure 4.8. Intersection between outbreak size and different static centrality measures. **Left panel:** infectious period $d = 7$ days. **Right panel:** infectious period $d = 42$ days. Top panels show x -log versions of the bottom panels. Dotted lines show data accordance $y = x$ for comparison. The top panels demonstrate that finite intersections appear only for sample sizes of more than 1000 nodes.

In Figure 4.8, we plot the centrality intersection (4.12) for different static centrality measures and two exemplary infectious periods. Upper panels are identical to the lower

Figure 4.9. Scalar field representing the set of outbreak scenarios as defined in (4.6). Each combination of starting node v , starting time t_0 and infectious period d yields an outbreak size $r(v, d, t_0)$. The domain is bounded as defined in (4.6).



panels, but use logarithmic x -axes. The upper figures show that non vanishing intersections are taken for samples of at least 1000 nodes. Consequently, the upper part of the ranked nodes does not coincide with high ranked nodes in any static centrality measure. Intersections between outbreak size and static centrality measures become significant only for sample sizes of more than 10,000 nodes, i.e. about 10 % of the network! Although this fraction is rather large, the coincidence of centrality and outbreak size is still relatively small, as can be seen when comparing the centrality curves to the dotted line on the lower panel. The different centrality measures show similar intersections with the outbreak size. An exception is closeness centrality, which performs significantly better than the other measures. An explanation for this special role is that nodes with high closeness are likely to infect other nodes within only few steps as it follows from the definition of closeness. This way long static paths are avoided, i.e. the chance that one of these static paths is disrupted by causality is relatively low. It should be noted that all features discussed above are almost identical for both infectious periods.

Conclusion of the section. We simulated an SIR-type disease on the livestock trade dataset and explicitly took into account the temporal dynamics of edges. This yields a set of outbreak scenarios, which can be thought of as a scalar-field $r(v, d, t_0)$, where each triple (v, d, t_0) is assigned an outbreak size r , if $r > 0$. A schematic sketch of this scalar-field is given in Figure 4.9. Using the state space of Figure 4.9, we can summarize the different aggregation techniques used in this section as follows:

Exemplary outbreak: All outbreak sizes for a cut through r for constant d and v (see Figure 4.4).

Outbreak probability: State density of r for every d -slice of the state space (see Figure 4.5 A).

Mean outbreak size: The mean value of the field in every d -slice (see Figure 4.5 B).

Node ranking: First, average over the t_0 -axis. Afterwards ordering of nodes by largest outbreak size for every d -slice. See Figure 4.6.

Infectious period uncertainty: Comparison between pairs of node rankings. See Figure 4.7.

The comparison to the static network representation (figure 4.8) is obtained using intersections between pairs of node rankings in analogy to the estimation of uncertainty of the infectious period.

We conclude that although the temporal nature of the system results in strong fluctuations of the paths in the network, a ranking of nodes according to their range appears reasonable for sufficiently large infectious periods. This ranking could not be reproduced using classical static centrality measures. In addition to that, a static network view systematically overestimates disease outbreaks in the network. Even for large infectious periods, we found the mean outbreak sizes to be six times smaller as for the static case.

4.3 Graph centric temporal network analysis

The previous section has shown that even the analysis of simple measures such as node ranges is a complex endeavor. While the previous section implicitly used a node centric approach to the system, we now introduce a *graph centric* approach to temporal networks. It is important to emphasize that the capability of static network analysis originates from the fact that the adjacency matrix provides a graph centric (“big picture”) of the system. Therefore, a graph centric view for temporal networks contributes a key element for a theoretical framework for temporal systems.

As we have seen in Section 4.1.3, the static approximation of a temporal network leads us to believe that all paths are transitive and therefore lacks a differentiation between causal and non causal paths. We make use of adjacency matrix sequences as defined by Equation (4.2) and derive a method for the computation of causal paths.

This yields first the ranges of all nodes in the network and second information about the mutual *accessibility* between nodes. In analogy to the static range defined in Equation (2.16), the range of a node v in a temporal network $\mathcal{G} = (V, \mathcal{E}, T)$ can formally be defined as

$$r(v) = \frac{|\mathcal{H}(v)|}{N}, \quad \text{where } \mathcal{H}(v) = \{u \in V : v \rightsquigarrow u\}, \quad (4.13)$$

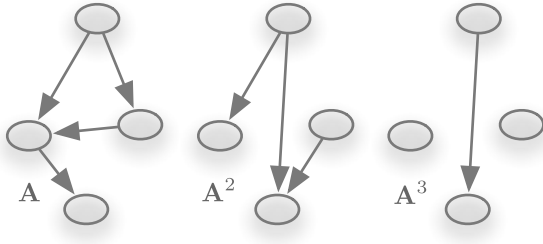
where $\mathcal{H}(v)$ is the horizon of node v and N the number of nodes in the network.

The set of all horizons in a network defines its *accessibility graph*. For static networks, the concept of accessibility was defined at the end of Section 2.2.2. We extend the static accessibility approach to the explicit step by step derivation of accessibility in Section 4.3.1. This novel procedure is called *unfolding* of accessibility. Finally, we generalize the unfolding accessibility approach to temporal networks in Section 4.3.2. The results presented in this section are in part published in (Lentz et al., 2013).

4.3.1 Accessibility of static networks

We consider a static network $G = (V, E)$ with N nodes and adjacency matrix \mathbf{A} . The accessibility graph (or transitive closure) of G is denoted by $G^* = (V, E^*)$, where E^*

Figure 4.10. Graph representations of different powers of an adjacency matrix. The left panel shows the original graph G with adjacency matrix \mathbf{A} . Node pairs with distance 2 in G are connected by an edge in the graph of \mathbf{A}^2 (middle). The analogue for distance 3 is shown on the right panel.



contains an edge (u, v) , whenever $u \rightarrow v$. The accessibility matrix – i.e. the adjacency matrix of the accessibility graph – can be computed using the cumulative matrix defined by

$$\mathbf{C}_n = \mathbf{A} + \mathbf{A}^2 + \cdots + \mathbf{A}^n = \sum_{i=1}^n \mathbf{A}^i. \quad (4.14)$$

Every term \mathbf{A}^i corresponds to a network where nodes are connected that have shortest path distance i in G . Figure 4.10 illustrates this observation.

In general, each power of an adjacency matrix contains the number of paths between node pairs as entries. Since we are not interested in the actual *number* of paths, we can treat the adjacency matrix as Boolean and use Boolean arithmetic and normal algebra. Thus, the normalized cumulative matrix can be computed using

$$\mathbf{P}_n = \bigvee_{i=1}^n \mathbf{A}^i, \quad (4.15)$$

where the i -th power of the adjacency matrix is computed using the matrix product of two Boolean matrices \mathbf{A} and \mathbf{B} defined by

$$\begin{aligned} (\mathbf{AB})_{ij} &= (a_{i1} \wedge b_{1j}) \vee \cdots \vee (a_{iN} \wedge b_{Nj}) \\ &= \bigvee_{k=1}^N a_{ik} \wedge b_{kj}. \end{aligned} \quad (4.16)$$

In Equations (4.15) and (4.16), \vee denotes a Boolean OR and \wedge a Boolean AND, respectively.

The adjacency matrix of the accessibility graph is given by $\mathbf{P}_{n=N-1}$. We call \mathbf{P}_{N-1} the *accessibility matrix* of G . Note that the index $N - 1$ corresponds to the maximum path length in the network. The graph G^* given by \mathbf{P}_{N-1} is called fully exploited accessibility graph. We focus on accessibility for values other than $N - 1$ below.

Properties of accessibility graphs. In a *connected* network G , the graph G^* contains links between all node pairs, since all nodes are connected by a path. Thus, G^* is fully

connected and the matrix \mathbf{P}_{N-1} has only nonzero entries. It follows from the transitivity of paths that also all entries $(\mathbf{P})_{ii}$ are unity, since there is always a path from node i to some other node j and vice versa. Consequently, \mathbf{P}_{N-1} has N^2 nonzero entries in this case. If the network G is *not connected*, the accessibility matrix can be transformed into a block diagonal form, where each block has only nonzero entries. The total number of nonzero elements in this case is smaller than N^2 .

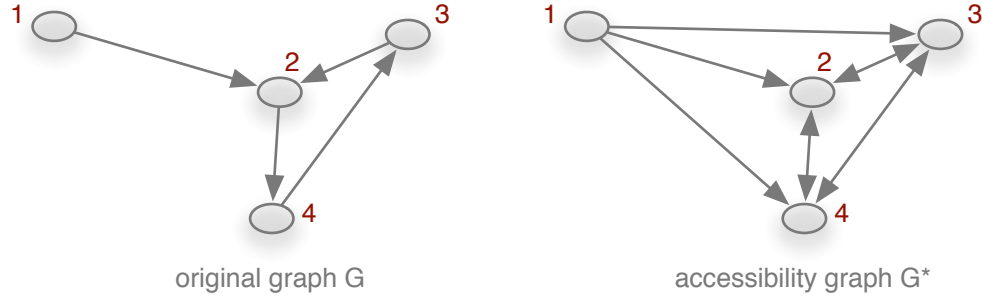


Figure 4.11. A static network G and its accessibility graph G^* . The nodes 2, 3 and 4 are strongly connected in G and form a clique in G^* .

Figure 4.11 shows the accessibility graph of a static network. The corresponding accessibility matrix is

$$\mathbf{P}_N = \left(\begin{array}{c|ccc} 0 & 1 & 1 & 1 \\ \hline 0 & 1 & 1 & 1 \\ 0 & 1 & 1 & 1 \\ 0 & 1 & 1 & 1 \end{array} \right).$$

The nodes of the connected components in the adjacency matrix \mathbf{A} form blocks in \mathbf{P}_N so that nodes 2, 3 and 4 form a fully connected subgraph (clique) in G^* .

If the network G is *undirected*, every \mathbf{P}_n has a non vanishing main diagonal for $n \geq 2$, if there are no isolated nodes. This corresponds to the fact that there is always a path of length 2 from a node back to itself. For the directed case, the main diagonal of \mathbf{P}_{N-1} can contain 0 or 1 entries.

Shortest paths and unfolding accessibility. Now we focus on the properties of the accessibility graph for the steps $\mathbf{P}_{n \leq N}$. We explicitly take into account different values of n , i.e. we *unfold* the accessibility graph. Each \mathbf{P}_n is the adjacency matrix of a preliminary accessibility graph, which we denote by G_n^* . The graph G_1^* (with adjacency matrix \mathbf{P}_1) gives a graph containing paths of length 1, i.e. the adjacency matrix itself. Analogues to Figure 4.10, the graph G_2^* contains paths of length 1 *and* paths of length 2. In principle, the procedure $\mathbf{P}_n \rightarrow \mathbf{P}_{n+1}$ corresponds to traversing the graph by paths of one more edge. This is equivalent to a breadth-first-search (BFS) algorithm in the

network, which is a standard procedure in computational network analysis. The BFS technique is explained in Appendix A.1. A similar method was used in early algorithms for computing shortest path lengths in networks (Floyd, 1962; Warshall, 1962). At the moment, when the BFS-algorithm approaches the diameter D of the network, the matrix \mathbf{P}_n saturates and does not change for higher values of n . Moreover, the accessibility matrix of a network is reached for $n = D$, so that

$$\mathbf{P}_D \equiv \mathbf{P}_{D+1} \equiv \mathbf{P}_{N-1}. \quad (4.17)$$

Hence, it is sufficient to compute only the first D term in Equation (4.15).

The relation between the computation of accessibility and the BFS-algorithm suggests that this procedure contains information about the shortest path length distribution. In order to reveal this correlation, we define the *density* of a matrix \mathbf{M} as the number of its nonzero elements, i.e.

$$\rho(\mathbf{M}) = \frac{\text{nnz}(\mathbf{M})}{N^2}. \quad (4.18)$$

In Equation (4.18) the number of nonzero elements is $\text{nnz}(\mathbf{M})$ and N is the dimension of \mathbf{M} . As a special case, we define the *path density* of a network as the density of its accessibility matrix

$$\rho(\mathbf{P}_n) = \frac{\text{nnz}(\mathbf{P}_n)}{N^2}. \quad (4.19)$$

Note that the normalization in (4.18) and (4.19) is not $N(N - 1)$, since we explicitly take into account self loops in the accessibility graph. These self loops guarantee that the maximum path density is unity in connected graphs.

Now we address the relation between path density and shortest path distribution. In the case of the adjacency matrix, Equation (4.18) gives the edge density of the network, which is equivalent to the probability that two randomly chosen nodes are connected by an edge. It follows that the probability that two nodes are connected by a path of length n is given by $\rho(\mathbf{A}^n)$.

Since the path density $\rho(\mathbf{P}_n)$ follows from a cumulative procedure, it corresponds to the probability that two randomly chosen nodes are connected by a path of length $l \leq n$. Consequently, the path density is the cumulative distribution of shortest path lengths

$$\rho(\mathbf{P}_n) = F(l \leq n) \equiv F_n. \quad (4.20)$$

The shortest path length distribution follows from Equation (4.20) by differentiation. Since the step length is 1 by definition, the probability for a shortest path length n is given by $f_n = (F_n - F_{n-1})$ and $F_0 = 0$.

It should be noted that the probabilities considered here are normalized to unity only for connected networks, because for connected networks $\rho(\mathbf{P}_{N-1}) \equiv \mathbf{P}_D = 1$. In the case of disconnected networks, the saturation value is in general smaller than 1. Therefore,

we treat the distribution (4.20) as an “improper” probability distribution, which is in general not normalized to unity. In addition, we define the *median* of F_n as the value n where $F_n = 1/2 F_D$.

We make use of the relations discussed above in order to obtain information about the shortest path distribution. We call this procedure *Unfolding Accessibility*, because we explicitly analyze the step-by-step derivation of the accessibility matrix. Although the concept of unfolding accessibility seems to make things unnecessarily complicated, it can be generalized to temporal networks.

But before we generalize the approach explained above to temporal networks, we illustrate the concept exemplarily for a static Erdős-Rényi network. We compute the shortest path length distribution of a directed Erdős-Rényi network of 1000 nodes and 2000 edges. Figure 4.12 shows the path density $\rho(\mathbf{P}_n)$ and the shortest path distribution. The shortest path length distribution is identical to that of Figure 2.8 (section 2.3.2).

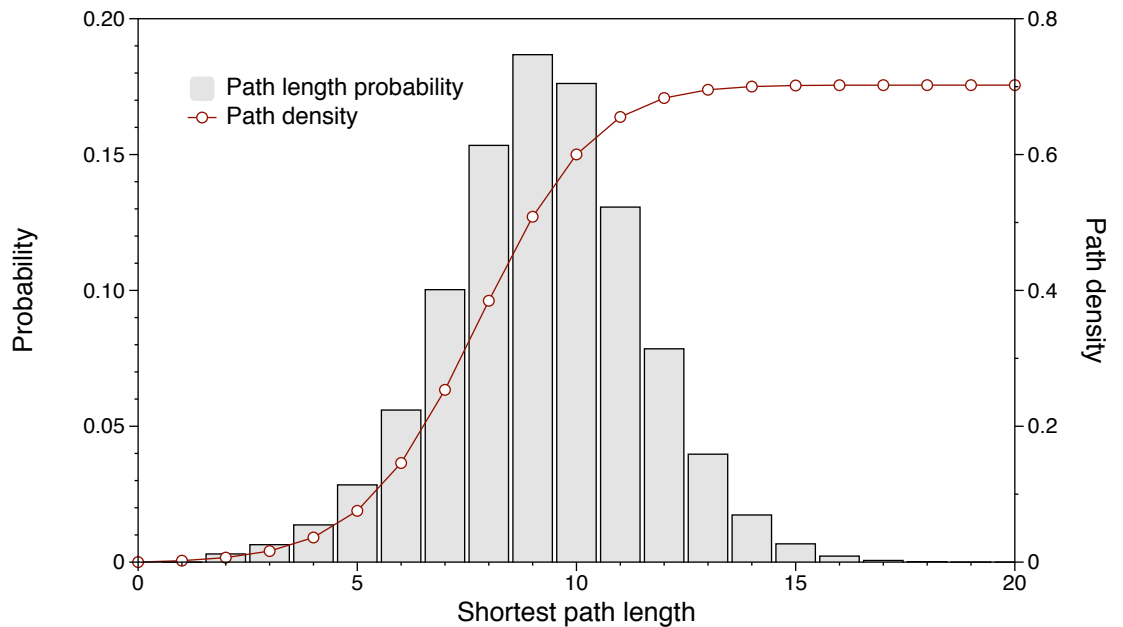


Figure 4.12. Path density (red line) and shortest path length distribution (grey histogram) for a directed Erdős-Rényi network with 1000 nodes and 2000 edges. Mean value 8.18, median $n = 8$, diameter $D = 18$, maximum path density $\rho(\mathbf{P}_D) \approx 0.7$. The histogram is identical to that in Figure 2.3.2, where a standard BFS algorithm was used.

4.3.2 Unfolding Accessibility of temporal networks

We generalize the definition of the static accessibility matrix (4.15) to the case of temporal networks. The basic problem is how to generalize different powers of an adjacency matrix to the case, where the adjacency matrix is not constant. Let us consider a temporal network $\mathcal{G} = (V, \mathcal{E}, T)$ with adjacency matrix sequence as defined in (4.2)

$$\mathcal{A} = \mathbf{A}_1, \dots, \mathbf{A}_T. \quad (4.21)$$

Treating each element \mathbf{A}_t in \mathcal{A} as Boolean, the aggregated network is given by the Boolean sum of the matrices

$$\mathbf{A} = \bigvee_{t=1}^T \mathbf{A}_t. \quad (4.22)$$

Before we derive an expression for the accessibility graph $\mathcal{G}^* = (V, \mathcal{E}^*, T)$, we have to discuss the meaning of matrix multiplication in temporal networks. In particular, we have to discuss the role of causality in paths generated by matrix products. As shown in Figure 4.10, a product of adjacency matrices gives information about paths of a certain length in static networks. The multiplication of two different matrices \mathbf{A}_1 and \mathbf{A}_2 yields nonzero entries, i.e. paths of length 2, wherever nodes of the graph of \mathbf{A}_1 receive links at time 1 and cast forth links at time 2. An example is illustrated in Figure 4.13. If we

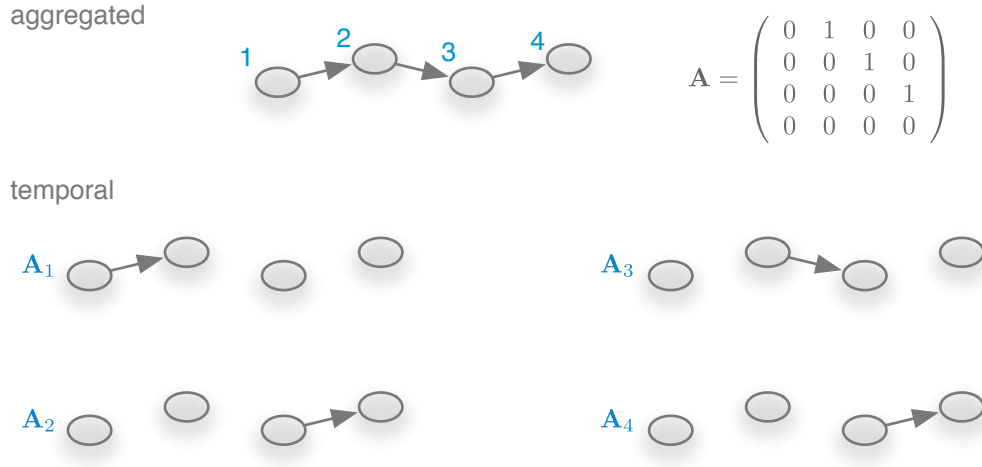


Figure 4.13. Snapshots of a temporal network. Each snapshot is given by an adjacency matrix \mathbf{A}_t . The aggregated network and adjacency matrix are shown in the top panel.

exemplarily multiply the two snapshots \mathbf{A}_2 and \mathbf{A}_3 , we get

$$\mathbf{A}_3 \mathbf{A}_4 = \begin{pmatrix} 0 & 0 & 0 & 0 \\ 0 & 0 & 1 & 0 \\ 0 & 0 & 0 & 0 \\ 0 & 0 & 0 & 0 \end{pmatrix} \begin{pmatrix} 0 & 0 & 0 & 0 \\ 0 & 0 & 0 & 0 \\ 0 & 0 & 0 & 1 \\ 0 & 0 & 0 & 0 \end{pmatrix} = \begin{pmatrix} 0 & 0 & 0 & 0 \\ 0 & 0 & 0 & 1 \\ 0 & 0 & 0 & 0 \\ 0 & 0 & 0 & 0 \end{pmatrix}. \quad (4.23)$$

Thus, there is a two-step-path from node 2 to 4 via node 3. It follows that multiplication of different matrices is a reasonable operation for the computation of paths also in temporal networks. Therefore a straight-forward temporal generalization of the accessibility matrix could be to replace the power of adjacency matrices by products of different snapshots. Defining $\tilde{\mathcal{C}}_n$ as the temporal generalization of (4.14) and $\tilde{\mathcal{P}}_n$ as its Boolean version, this approach reads

$$\tilde{\mathcal{C}}_n = \sum_{i=1}^n \prod_{j=1}^i \mathbf{A}_j = \mathbf{A}_1 + \mathbf{A}_1 \mathbf{A}_2 + \mathbf{A}_1 \mathbf{A}_2 \mathbf{A}_3 + \dots$$

and

$$\tilde{\mathcal{P}}_n = \bigvee_{i=1}^n \bigwedge_{j=1}^i \mathbf{A}_j = \mathbf{A}_1 \vee \mathbf{A}_1 \mathbf{A}_2 \vee \mathbf{A}_1 \mathbf{A}_2 \mathbf{A}_3 \vee \dots, \quad (4.24)$$

respectively. Although this naive approach shows great similarities with the accessibility matrix of a static network, it turns out that it has a crucial drawback: If we compute the product $\mathbf{A}_1 \mathbf{A}_2$ in Figure 4.13, we would get a zero matrix

$$\mathbf{A}_1 \mathbf{A}_2 = \mathbf{0}. \quad (4.25)$$

It follows from Equation (4.24) that $\tilde{\mathcal{P}}_n = \mathbf{A}_1$ for all $n = 2$. As opposed to this, Figure 4.13 suggests that the accessibility graph should contain other paths than $1 \rightsquigarrow 2$ only, for example $1 \rightsquigarrow 4$. Apparently, the elements of the matrix products in (4.24) become zero, if the requirement of receiving links at time t and casting forth links at time $t+1$ is violated. In a more general sense, the accessibility matrix given in Equation (4.24) gives meaningful results in the case that temporal correlations are only between successive snapshots of the system. Systems with this property can be considered as Markovian temporal networks.

Many systems, however, show a *bursty* behavior, i.e. significant waiting times between periods of node activity. As an example, a typical trade pattern in the pig trade network used in sections 4.2 and 3.1 would be that animals remain at different holdings for certain periods of time for breeding or fattening. In these systems, consecutive matrices are not

correlated and their products would vanish, i.e.

$$\lim_{n \rightarrow \infty} \bigwedge_{t=1}^n \mathbf{A}_t = \mathbf{0}. \quad (4.26)$$

Equation (4.26) implies that all long time information would be lost. This dilution of the path density occurs, if the temporal resolution of the dataset provides many snapshots over the typical timescale of the node waiting times. As a consequence, these snapshots show relatively low edge densities. Bajardi et al. reported a maximum path length of 8 days for a temporal cattle trade network, when edge sequences are at successive time steps (Bajardi et al., 2011).

In order to overcome the drawbacks of Equation (4.24), we explicitly take into account products of matrices over distant time steps. In the example of livestock trade networks, a subset of nodes of the system could for instance fatten livestock animals for a timespan τ . Thus, these nodes receive links at time t_1 and cast forth links at time $t_2 = t_1 + \tau$. More general, the time span τ could correspond to a production time in value chains or the period of stay at one place in human mobility networks.

On the whole, we have to include *all* possible higher order products into the computation of the accessibility matrix. It turns out that this is equivalent to adding a memory into the system, i.e. the ability of each node to keep edge information over time. This can be done using self-loop so that we add an identity matrix \mathbf{I} to each matrix in the sequence \mathcal{A} . Then the unnormalized accessibility matrix of a temporal networks reads

$$\begin{aligned} \mathcal{C}_n &= \prod_{i=1}^n (\mathbf{I} + \mathbf{A}_i) \\ &= \mathbf{I} + \underbrace{\mathbf{A}_1 + \mathbf{A}_2 + \mathbf{A}_3 + \cdots + \mathbf{A}_n}_{\mathbf{A}} + \\ &\quad + \underbrace{\mathbf{A}_1 \mathbf{A}_2 + \mathbf{A}_2 \mathbf{A}_3 + \mathbf{A}_1 \mathbf{A}_3 + \mathbf{A}_1 \mathbf{A}_2 \mathbf{A}_3 + \cdots}_{\mathcal{O}(\mathbf{A}_i^2)}. \end{aligned}$$

As the author noticed recently, a similar expression also appears in the temporal generalization of a centrality measure as it was independently found in (Grindrod et al., 2011). Since the actual number of paths are not important in this work, we define the the *accessibility matrix of a temporal network* in Boolean notation

$$\begin{aligned} \mathcal{P}_n &= \bigwedge_{i=1}^n (\mathbf{I} \vee \mathbf{A}_i) \\ &= \mathbf{I} \vee \mathbf{A}_1 \vee \mathbf{A}_2 \vee \mathbf{A}_3 \vee \cdots \vee \mathbf{A}_n \vee \\ &\quad \vee \mathbf{A}_1 \mathbf{A}_2 \vee \mathbf{A}_2 \mathbf{A}_3 \vee \mathbf{A}_1 \mathbf{A}_3 \vee \mathbf{A}_1 \mathbf{A}_2 \mathbf{A}_3 \vee \cdots. \end{aligned} \quad (4.27)$$

In Equation (4.27), the linear terms correspond to the aggregation of the network over n time steps. These are all paths of length 1, which are always causal. The higher order products always respect the temporal correct order of snapshots, that is $i < j$ for all $\mathbf{A}_i \mathbf{A}_j$ and $\mathbf{A}_i \cdots \mathbf{A}_j$. Analogue to Section 4.3.1, we define the accessibility graph to path duration n as \mathcal{G}_n^* .

It should be noted that in general the “real” accessibility graph of a temporal network is given by \mathcal{G}_∞^* , since the observation time is limited and might not capture the real timescale of a system. Also some systems could be periodic, i.e. $\mathcal{A}_{t+T} = \mathcal{A}_t$, but this can not be assumed in the general case. Since the upper limit of time is predefined by the dataset under consideration, we consider the fully unfolded accessibility graph as $\mathcal{G}^* = \mathcal{G}_T^*$. Using Equation (4.27), we can now unfold accessibility just like for the case of a static network reported in Section 4.3.1.

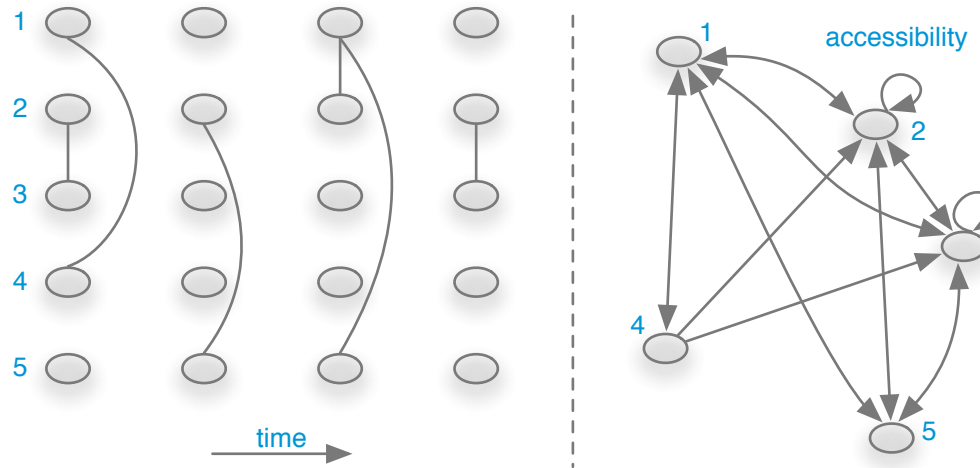


Figure 4.14. A temporal network (left panel) and its accessibility graph (right panel). The network is taken from Figure 4.1. Only nodes 3 and 4 have self loops in this example. Note that even though the temporal network is undirected, its accessibility graph is directed (edge (4,2) is unidirectional).

Before doing so, we have to point out that the identity matrix \mathbf{I} on the right-hand side of Equation (4.27) is an artifact of the introduced memory. This does not make a huge difference for undirected networks, as we have discussed for the static case in Section 4.3.1. A similar argument can be used in the temporal case, since there is always a path from a node back to itself after 2 contacts at different time steps. Consequently, whenever an edge between two nodes appears twice, both nodes have a self loop in the accessibility graph. In directed networks, the identity matrix could indeed cause discrepancy from the real accessibility matrix. Nevertheless, this discrepancy is small, since the contribution of the diagonal is small compared to the total number of elements in \mathcal{P}_n . This holds in particular, since accessibility matrices are in general not sparse.

Therefore, the deviation is ignored throughout this work.

It is important to emphasize that the index n in Equation (4.27) does not have the meaning of a length of a shortest path as in the static case. In fact, n measures the *duration* of a path. Therefore, unfolding an accessibility graph does not yield a shortest path length distribution, but rather the distribution of shortest path durations. Even if a particular temporal network might be a small-world network in the topological sense – say it still takes only a few edges to traverse the whole system – the traversal could take a long time. In general, even a small world network could be a “slow world” network.

Finally, it should be noted that the accessibility graph of a temporal network is in general directed, even if every snapshot is an undirected network. Figure 4.14 shows the accessibility graph of the network used in Figure 4.1. As the figure demonstrates, the accessibility graph is directed, even though the underlying temporal network is undirected. This property reflects the “arrow of time” in temporal networks. In addition to that, the accessibility graph does not show global transitivity as opposed to the static case (compare to Figure 4.11). In our example, the existence of the paths $4 \rightsquigarrow 2$ and $2 \rightsquigarrow 3$ does not imply that $4 \rightsquigarrow 3$, as it would be in the static case.

4.3.3 Representative sample / characteristic time scale

We come back to the findings of Section 4.2.1, where we determined the typical timescale of the livestock trade network using data-driven methods. Thus, we apply the unfolding accessibility method to the livestock trade network dataset, i.e. we take more and more snapshots to obtain information about the path density. From the derivative of the path density we obtain the distribution of shortest path durations in the network. The result for the livestock trade network is shown in Figure 4.15. The path density is relatively low along the whole observation period, since the pig trade network is directed. We have seen in Section 3.1.1 that even the static network representation is fragmented, i.e. the largest strongly connected component is relatively small. Since the components of the aggregated network define an upper bound for the components in the temporal view, the temporal path density is confined.

Although the shortest path durations show a broad distribution, Figure 4.15 shows that this distribution has a global maximum. It follows that there is a typical timescale in the system, which is in the region of 180 days. This means that the typical spreading time of any process on the network is in the order of 100 days. In fact, this timescale is a manifestation of the underlying process taking place on the network, i.e. the production of livestock pigs. The time scale detected in Figure 4.15 is in agreement with the representative sample found using a data-driven approach as reported in Figure 4.3 (see Section 4.2.1). We conclude that the representative sample size of 180 days can be explained by the characteristic time scale of the system.

The underlying process follows a production chain as shown in Figure 4.16. As the figure illustrates, the pig trade network is a union of many disjoint production chains.

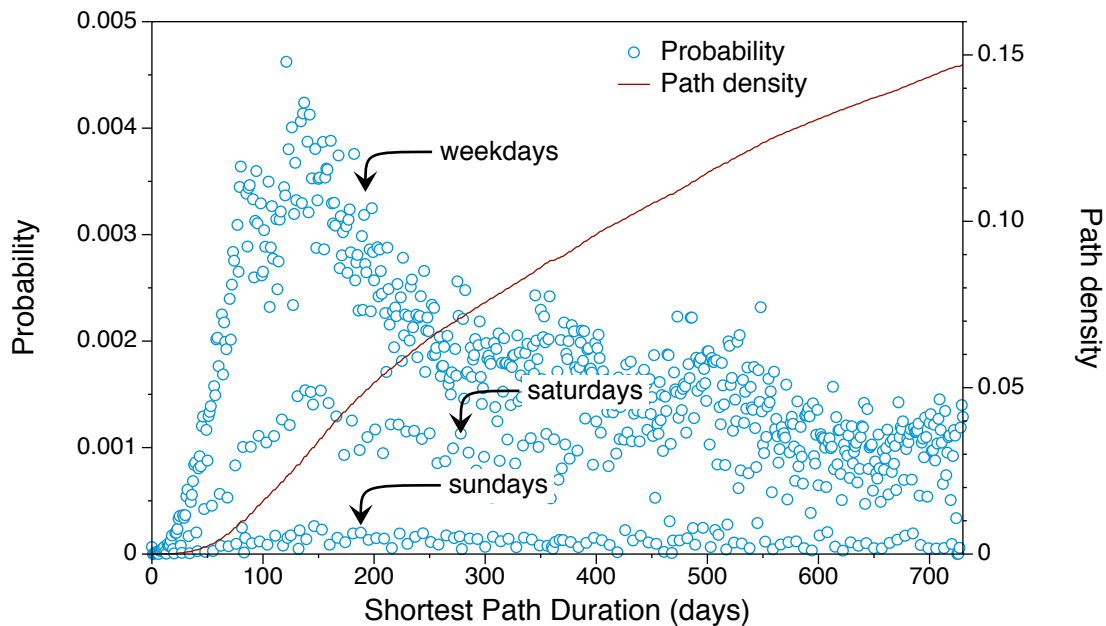


Figure 4.15. Path density (red) and distribution of shortest path durations (blue) for the pig trade network. Multiples of weekdays are generally more likely for shortest path durations, since trade is less on sundays and almost absent on sundays.

In addition, there are trade links in the network, which do not follow the exact production path and are shown as dashed lines in Figure 4.16. The timescale of each production chain is strictly determined by the biological properties of pig production. Most pigs are slaughtered in the age of 180 days. This period defines the *temporal diameter* of the production chain, which gives an explanation for the existence of a typical time scale observed in Figure 4.15.

4.3.4 Causal fidelity

A large number of tools and measures has been developed for static networks and some of which were reported in Section 2.2. For this reason, temporal networks are often aggregated and treated as static networks. The penalty of such an approximation is that it allows for paths that do not follow a causal sequence of edges. In other words, the most fundamental difference between a temporal network and its aggregated approximation lies in the difference between the number of possible paths. The question is how closely does an aggregated network reproduce the path properties of the temporal network. In

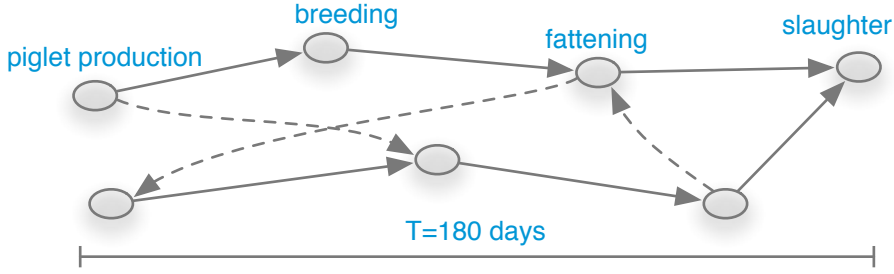


Figure 4.16. Simplified representation of the pig trade network. The system consists of multiple distinct production chains plus a certain degree of “random” trade connections indicated by the dashed arrows. The total production time of one single production chain is 180 days, which defines its temporal diameter.

order to quantify this ability, we define the measure of *causal fidelity*

$$c = \frac{\rho(\mathcal{P}_T)}{\rho(\mathbf{P}_T)}, \quad (4.28)$$

where $\rho(\mathcal{P}_T)$ is the path density of the fully unfolded temporal accessibility graph and $\rho(\mathbf{P}_T)$ its static counterpart. The causal fidelity lies in the range $0 \leq c \leq 1$. Large values of c indicate that an aggregation of the temporal network gives a good approximation of the temporal system from a causal point of view. A low value of c implies that most paths in the static network can not be taken in the temporal system, since their edges do not form causal sequences. Consequently, temporal networks with small causal fidelities should not be treated as static systems.

If a temporal network with low causal fidelity is treated as a static network, any spreading process on the system would be significantly overestimated. The ability to quantify this error is an important contribution to risk assessment in epidemiology.

For the pig trade network, we measure 2,202,369,723 paths in the static network and only 1,575,699,560 paths in the temporal network. Hence, the causal fidelity of this network is

$$c = \frac{1,575,699,560}{2,202,369,723} \approx 0.715. \quad (4.29)$$

Thus, about 72 % of the paths exist in both network representations. We state that the aggregated network captures the causality of the system sufficiently well.

It should be noted that Equation (4.28) computes the causal fidelity for the fully unfolded accessibility graph $\mathcal{G}_{n=T}^*$. In principle, the causal fidelity can also be computed for intermediate steps of the unfolding procedure. This approach can be used in order to quantify the size of a minimal aggregation window that guarantees for a sufficiently

large causality in the approximation.

4.3.5 Randomization techniques

In order to assess the strength of topological and temporal correlations in the network, we make use of randomized models of the original dataset to remove specific correlations. A standard procedure to remove correlations on a *static* network is randomizing its edges. This procedure keeps the degree sequence constant and is similar to the configuration model. Time as an additional dimension in temporal networks requires for a large number of randomizing procedures in order to systematically remove correlations. We briefly report, how different randomization procedures affect the temporal network \mathcal{G} and its aggregated counterpart G . Random models for temporal networks have been introduced in (Pan and Saramäki, 2011; Holme and Saramäki, 2012). We use these models and translate them into our formalism based on the adjacency matrix sequence of a temporal network, i.e.

$$\mathcal{A} = \mathbf{A}_1, \dots, \mathbf{A}_T. \quad (4.30)$$

The following random models are applied to our dataset:

RE – randomized edges. Each snapshot in sequence (4.30) is randomized according to the following procedure. Choose two edges (u, v) and (w, x) in the network randomly. If the edges are disjoint, i.e. $u \neq w$ and $v \neq x$, then swap the nodes v and x . Thus, the new edges are (u, x) and (w, v) . This procedure is repeated until every edge in the original network has been swapped.

The RE model is similar to the configuration model mentioned in Section 2.3.4. It keeps the degree sequence constant and removes higher order topological correlations from the network. Affected are properties as the clustering coefficient or generally any specific subgraph in the original system. In the context of the pig trade network, these subgraphs are the production chains illustrated in Figure 4.16. Since the RE model places new edges almost randomly, it adds a significant amount of mixing to the network. Consequently, a large deviation between the original network and the RE network indicates that the initial system was not well mixed. Note that the RE model does explicitly affect *topological* correlations.

The RE procedure also affects the aggregated network. Since new, random edges are placed for every snapshot, the new aggregated network can have a significantly larger edge density than the original aggregated network. Models for the removal of temporal correlations are discussed next.

TR – time reversal. The TR model considers the network evolution backwards in time. Using the adjacency matrix sequence, the TR procedure yields a new sequence of

adjacency matrices given by

$$\mathcal{A}^{-1} = \mathbf{A}_T^\top, \dots, \mathbf{A}_1^\top, \quad (4.31)$$

i.e. every matrix in the sequence is transposed and the order of the sequence are reversed. Transposing the matrices reverses the direction of all edges in a network. This step is of course obsolete in undirected networks.

If the path density of a temporal network is significantly affected by time reversal, the network has a significant temporal directionality. This behavior occurs in particular, if the activity of the network monotonously changing over time, e.g. during a growing or shrinking process. The TR procedure also reverts the aggregated network, i.e. $G_{\text{TR}} = G^{-1}$.

GST – globally shuffled times. The occurrence time of each snapshot of the network is placed randomly. This can be directly implemented using a random order of the matrix sequence, i.e.

$$\mathcal{A}_{\text{GST}} = \text{shuffle}(\mathcal{A}), \quad (4.32)$$

where the function $\text{shuffle}(X)$ returns a random order of a sequence X . Although this model keeps the single snapshots constant, it explicitly removes *temporal* correlations in the system. These correlations manifest themselves in bursty behavior, such as a broad distribution of waiting times. Consequently, waiting times in the system are strongly affected by the GST model.

Since the GST procedure does not affect the topology of the snapshots, the aggregated network remains unchanged, $G_{\text{GST}} = G$.

LST – locally shuffled times. Instead of placing snapshots of the system at random times, the LST model randomly assigns the occurrence times of single *edges*. This model is very similar to the GST model. It can be efficiently implemented using an edge centric network representation as discussed in Section 4.1.2. To give an example, a particular edge (u, v) could be present at times t_1 and t_5 , i.e. using the edge occurrence function $\mathcal{I}((u, v)) = t_1, t_5$. The LST model assigns new occurrence times, but keeps the number of edge occurrences constant, e.g. $\mathcal{I}_{\text{LST}}((u, v)) = t_3, t_{12}$.

As the GST model, the LST model does not change the aggregated network so that $G_{\text{LST}} = G$.

RT – random times. The RT model uses the aggregated network $G = (V, E)$ and places random subsets of E as snapshots. As the GST and LST models, the RT procedure removes temporal correlations from the system. In addition to that, the random occurrence of edges mimics a contact rate between the nodes in the system. The RT model is therefore similar to a weighted static representation of the system. Different rules for the number of edges per snapshots are possible: First, every time step could be

treated equally so that the number of edges is constant over all snapshots on average. Second, the distribution of edge densities over all time steps remains constant. The first and the second variant correspond to the $G_{N,p}$ and the $G_{N,m}$ ensembles known from Erdős-Rényi networks, respectively. Consequently, the third variant can more efficiently implemented, since the number of edges is known from the beginning.

Since the RT model removes bursty behavior in every path of the network, it affects *scheduled* systems in particular. These are systems, where paths follow strict time schedules and the systems are temporally sparse. This is typical for production networks such as the livestock trade network discussed in this thesis. Being related to a weighted static network, the RT model does not affect the topology of aggregated network, so that $G_{\text{RT}} = G$. It should be noted that due to the impact of chance, a small number of edges might not be chosen in the snapshots of E . Consequently, $G_{\text{RT}} \approx G$ up to negligible statistical fluctuations. A summary of the used randomization models is shown in Table 4.2.

Table 4.2. Effects of the different randomization models.

Model	Effects
RE	addition of topological mixing removes specific topological subgraphs static network changed
TR	reverts arrow of time static network reversed
GST	graph-centric conserves bursty occurrence of edges homogenizes edge occurrences over the observation time removes characteristic time scales static network unchanged
LST	edge-centric conserves bursty occurrence of edges homogenizes edge occurrences over the observation time removes characteristic time scales static network unchanged
RT	removes bursty occurrence of edges static network (almost) unchanged

4.3.6 Temporal and topological mixing patterns

In order to reveal temporal and topological correlations in the livestock trade dataset, we apply the randomization techniques from the previous section to the network. Every deviation from the original dataset hints to a particular correlation in the network. Figure 4.17 shows the path density for the original dataset and for the randomized versions. The red curve shows the original network.

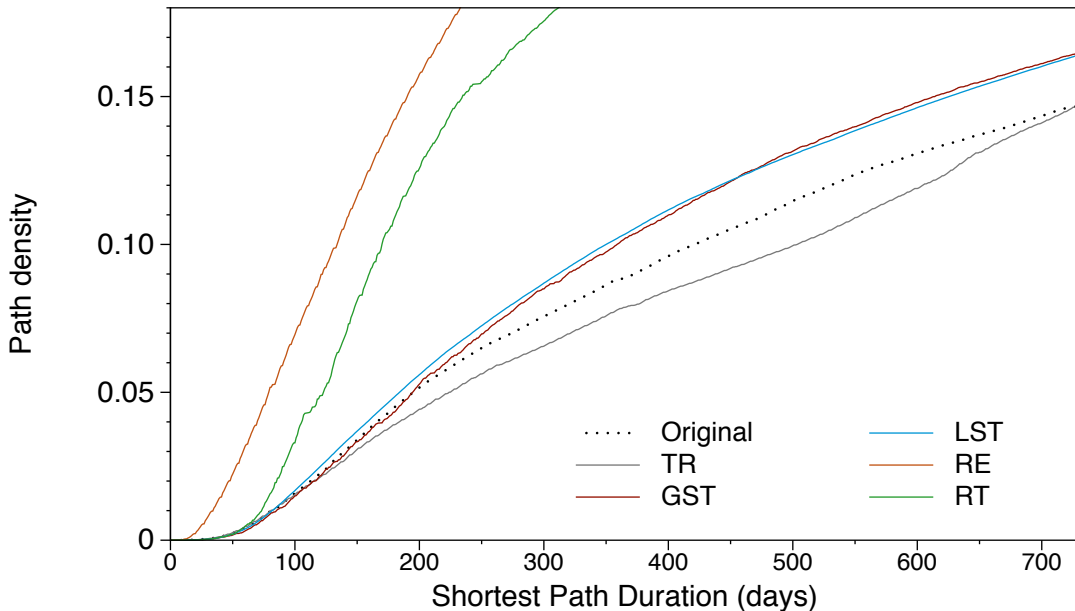


Figure 4.17. Path densities of randomized networks of the livestock trade dataset. Black points represent the original dataset. The randomization models are TR – time reversal, GST – globally shuffled times, LST – locally shuffled times, RE – randomized edges and RT – random times.

As the figure demonstrates, time reversal has a measurable effect for shortest path durations larger than about 100 days (grey line). Overall, the path density is lowered over a wide range of times. This shows that causal chains are less frequent, when the network is traversed backwards in time. This feature reflects the temporal directionality of the underlying production chain. In addition, the lower path density implies that a significant fraction of paths with duration between 100 and 700 days are “single events”, i.e. they do not form highly frequented lanes. More specifically, a single event path is a causal chain of edges, where each edge has only few occurrence times. These structures are particularly sensitive to time reversal.

The role of temporal correlations can be examined using time shuffling models. In Figure 4.17, the GST and LST models are shown as dashed blue and red lines, respec-

tively. Both lines show no significant differences from each other, indicating that the application of both procedures has a similar effect. The figure shows that time shuffling significantly increases the path density over a large period of shortest path durations. Since the GST and LST models remove temporal bursty behavior from the system, we conclude that the node waiting times restrict the number of paths in the original system.

The random times (RT) model removes scheduling from the network. The consequence is a significant increase of the path density (green line). An explanation for this behavior is that most paths in the system show a bursty behavior. It should be noted that the path density of the RT model almost approaches the path density of the aggregated network – i.e. $\rho(\mathbf{P}_T) \approx 0.206$ – in this case study. This high path density is caused by the relatively high activity of the system. As we have observed in Section 4.2.1, about 10 % of the edges are active every day.

It is a salient feature of this dataset that edge randomization (RE model, orange line) considerably increases the overall path density. The reason is that the underlying production chain strongly determines the network. As we have seen in Figure 4.16, the livestock trade system basically consists of a number of disjoint production chains as basic units. These basic units are interconnected by few “random” links. As a consequence, the whole system is by far not well mixed. Applying the RE model to the network provides strong mixing of the trade contacts. This mixing results in a large number of possible paths, also the aggregated network has a path density of $\rho(\mathbf{P}_T) \approx 0.449$, which is more than twice as much as the original data.

In summary, the underlying production chain of the livestock trade network is ubiquitous in the path structure of the network. The most salient feature in this context is the poor topological mixing of the network. Another striking feature is that bursty trade transactions seem to dominate the traversal of the system. Temporal correlations and temporal directionality play a role, but these features are not as striking as mixing and scheduling.

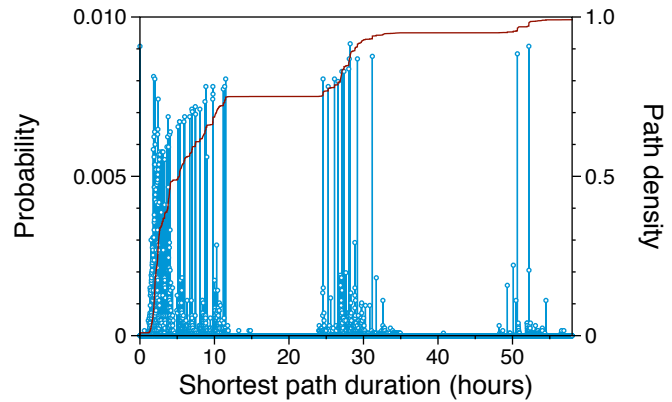
4.3.7 Further case studies

In order to demonstrate the capability of the unfolding accessibility method for the study of other systems, we apply the methods discussed before to two other datasets: First, a network of face-to-face contacts measured during a conference and second, a network of sexual contacts between prostitutes and their customers measured via an online rating platform for escorts. Both networks are undirected. As the pig trade network, both networks are possible substrates for the spread of infectious diseases – in this case, droplet transmitted diseases (e.g. flu) and sexually transmitted diseases, respectively. Both datasets are available online. Further information on the conference network is found in (Isella et al., 2011; Sociopatterns, 2012) and the sexual contact network is analyzed in (Rocha et al., 2010).

Figure 4.18 shows the path density and the distribution of shortest path durations for

4.3 Graph centric temporal network analysis

Figure 4.18. Unfolding accessibility of a conference contact network. The fast saturation behavior and the high maximum of the path density suggest a high degree of mixing in this system.



the conference contact network. The observation period of three days separated by periods of weak interaction (nights) are clearly resolved in the figure. Overall, this network is particularly active. This is reflected by the relatively high maximum path density of $\rho(\mathcal{P}_T) \approx 0.99$, i.e. almost all possible paths are traversed within the observation period. As we have discussed in Section 4.1.4, the high overall path density indicates that there

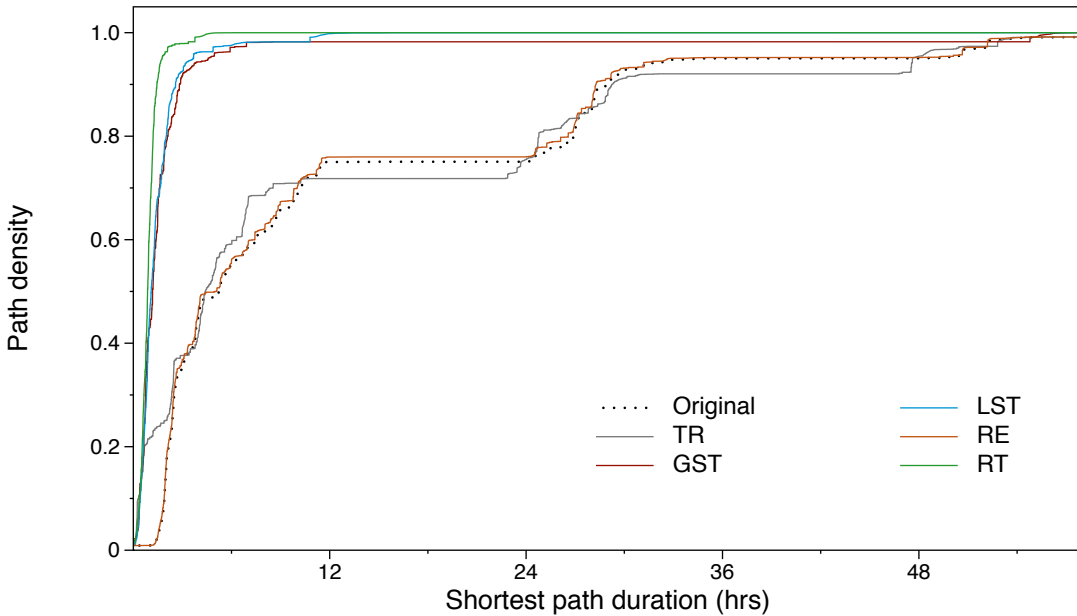
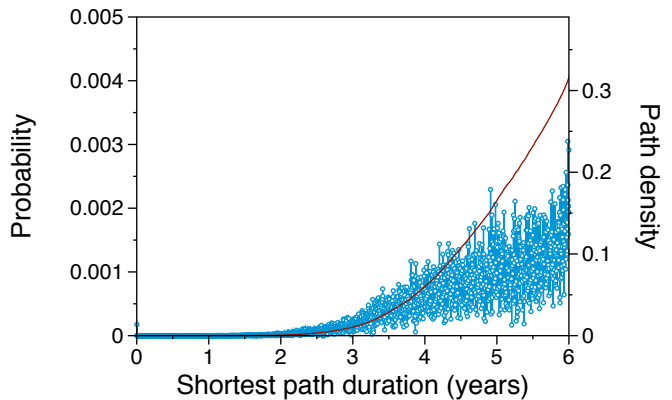


Figure 4.19. Path densities of randomized networks of the conference contact network. Removing temporal correlations (GST, LST, RT) removes periods of no activity (nights) from the network and significantly decrease the characteristic time scale and the temporal diameter.

Figure 4.20. Path density and shortest path duration distribution for a network of sexual contacts. Despite the long observation period, the path density does neither saturate nor it reveals a characteristic time scale.



exists a giant causally connected component in the system. However, the question of mutual connectivity cannot be answered in detail using the accessibility graph alone.

It can be read immediately from the path density that within the first day of the conference, more than 70 % of all possible paths have been traversed. The median of the shortest path duration distribution is reached within the first 6 hours. Thus, we conclude that 6 hours is a typical timescale for spreading processes in this system.

Following Section 4.3.4, we use Equation (4.28) and compute the causal fidelity of the conference network. As can be conjectured from the high path density, the causal fidelity attains the relatively high value $c \approx 0.99$. This implies that an aggregated network gives a good approximation of the real system from the causal point of view.

In order to assess the mixing properties of the conference contact network, we apply the randomization techniques of Section 4.3.5 to the dataset. The result is shown in Figure 4.19. As the figure demonstrates, time reversal (TR) and randomizing edges (RE) do not significantly change the behavior of the path density. The small effect of the RE model implies that the system is already (topologically) well mixed. Also the time reversal invariance can be attributed to the strong mixing and the high activity of the system. Note that both models preserve the plateaus caused by night-times.

Removing temporal correlations has a similar effect for the GST, LST and RT model. All three models show a steep increase of the path density and within only a few hours the maximum path density is reached. This effect originates from the fact that all three models remove the night periods from the system and thus the edge activity is distributed over the whole time period.

We now focus on a network of sexual contacts between escorts and customers over a time span of 6 years. Figure 4.20 shows the unfolding path density of the temporal network. The accessibility graph is very sparse during the first 2 years of observation. Even after the 6 years it remains difficult to extrapolate the path density and estimate a saturation behavior. Hence, no characteristic time scale can be observed during the observation period. Although the dataset does not give clear results, we can state that

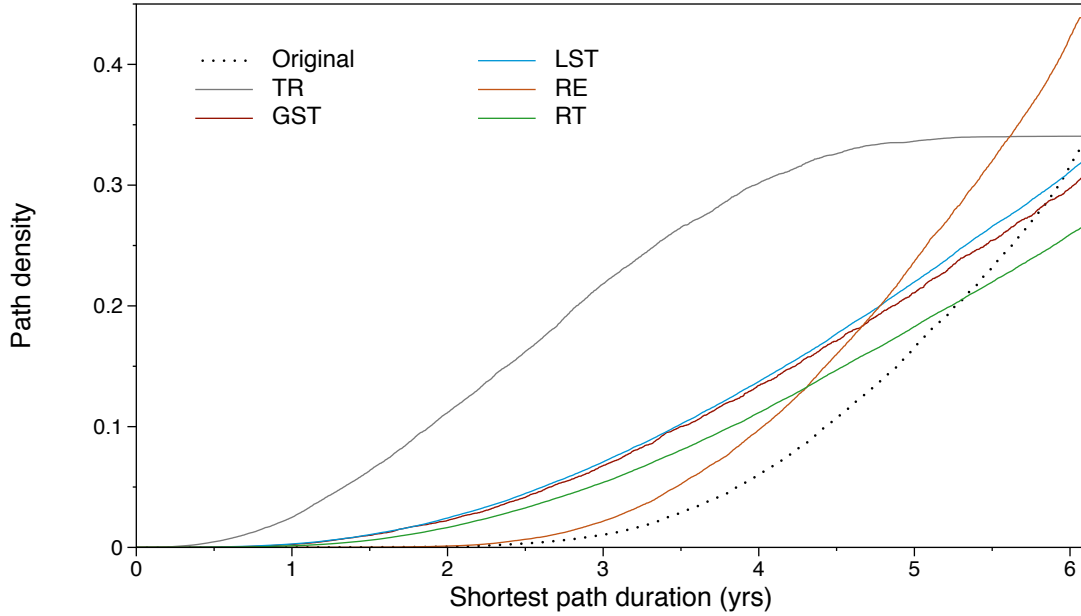


Figure 4.21. Path densities of randomized networks of the sexual contact network. The system is not well mixed (RE model, orange) and not time reversal invariant (TR model, grey). The path density of the TR model indicates that the data density is monotonously increasing in the original data.

any disease takes more than 2 years to infect a finite fraction of the network. The results are also valuable for further studies, since we have demonstrated that longer observation periods are needed in order to measure the characteristic spreading time in this system

In addition, the causal fidelity of this network is $c = 0.38$. This clearly provides support for treating the system from a temporal perspective – as done in (Rocha et al., 2010) – since a static approximation would significantly overestimate the size of any disease outbreak.

Finally, the path densities of randomized models of the sexual contact network are shown in Figure 4.21. A salient feature of this figure is that time reversal significantly changes the behavior of the path density (grey line). In fact, the edge density of the system increases monotonously over time and it has been shown that this circumstance alone can cause this behavior in the supplementary information of Lentz et al. (2013). The impact of removal of temporal correlations – i.e. GST (red), LST (blue) and RT (green) model respectively – can be explained in a similar fashion. All of these procedures homogenize the edge density over time resulting in a systematic increase of the path density. Due to the overall sparsity of edge data, the RT model places relatively

sparse networks as snapshots in this case. This impedes the formation of causal chains. Therefore, the path density of the RT model is slightly smaller than in the case of the time shuffling models.

Interestingly, the path density of the time shuffling models fall below that of the original data in the long term. It is not clear, whether this can be attributed to the increasing edge density or whether it reflects an intrinsic property of this system. A longer dataset would be needed in order to answer this question.

As it was the case for the livestock trade network, the sexual contact network is not well mixed. This is measured in terms of a strictly higher path density in the RE model (orange line) than it was in the original data.

5 Conclusion

In this thesis we have examined the role of paths for the spread of infectious diseases on networks. A path is a route through the network along its edges. The importance of paths in the context of disease spread has been demonstrated for the case of static networks and was then extended to the temporal case. As a central result, we have introduced the method of unfolding accessibility for temporal networks in order to analyze the path structure of these systems.

Concerning the spread of infectious diseases, detailed knowledge about the parameters governing the dynamics of disease transmission is not known in most real-world scenarios. It turns out, however, that the mere topology of contact patterns is of major importance in this context. In contrast to the infection parameters of most diseases, the contact patterns can be measured to great detail for a large number of real-world systems. Although these contact structures form complex networks, it turns out that solely the structure of paths defines the domain for any spreading process. On the one hand, the range of a node defines an upper limit for the size of disease outbreaks. On the other hand, the path structure of the whole system can be mapped onto the accessibility of the network.

In Section 3.1, we have for the first time analyzed pig trade in Germany as a **static network** systematically. We found that – among other features – the network exhibits a giant component and a significant modular structure. The existence of a giant component strikingly affects the spreading potential of the network nodes. Whenever a network is close to the percolation threshold, its nodes can be divided into long ranged and short ranged nodes, which define a high risk and a low risk class, respectively. As we have discussed in Section 3.1.1, this result is valid for all networks close to the percolation threshold. Modules are a weaker restriction on the path-connectivity between subgraphs than components, since they allow for a small number of paths between subgraphs. We have seen in Section 3.1.2 that the pig trade network shows a modular structure which is also related to the geographical positions of the nodes.

The impact of these structural features on the spread of infectious diseases was analyzed in Section 3.2. First, the directed nature of the trade network has lead to the question, how directionality affects disease spreading. We have seen in Section 3.2.3 directed networks show smaller outbreak sizes than undirected ones, since they statistically allow for a smaller number of paths.

As we have demonstrated in Section 3.2.4 a modular structure has a relatively weak effect on the outbreak size. This is particularly true for meta population networks,

where nodes are permeable for disease spread, if they are not fully recovered. However, a modular network is likely to show a significantly delayed outbreak peak, i.e. the “median” of the infection curve. This result could be useful for the implementation of counter measures, since it does not depend on a particular partitioning of a network, but only on the fact that the network is to a certain extent modular.

Treating a system as a static network, however, is not a reasonable assumption, if the links in the system vary over time. This is true for many real-world systems and livestock trade networks in particular. A static network view neglects preserving of chronology of edges, which is essential for any path in the network. Edge chronology is particularly important in systems showing a bursty occurrence of links. This consideration is fundamental for a realistic model of disease spread. In Section 4.2, we systematically analyzed data about pig trade in Germany including temporal resolution for the first time. We found that even if the network shows temporal fluctuations, it is still possible to define a relatively stable ranking of nodes according to their potential of disease spread. Data-driven approaches are indispensable tools to extract information from temporal network data. Nevertheless, their use does not provide a deeper understanding of the reasons for the observed results.

Therefore, special emphasis should be placed on the methods introduced for the analysis of **temporal networks**, i.e. systems where the occurrence of edges varies over time. These systems are particularly challenging due to the importance of preserving causality for any path. In Section 4.3.2, we have introduced a novel method to obtain the accessibility graph of a temporal network. We believe that the definition of accessibility contributes a key element for a theoretical framework for the macroscopic analysis of temporal networks, because it maps the whole causal path structure of the system onto a single mathematical object. Moreover, we have introduced the explicit *unfolding* of accessibility as a novel formalism for the evaluation of shortest path durations in temporal networks in Section 4.3.3. This approach is able to reveal characteristic timescales for the traversal of temporal networks. Knowledge of these timescales is of fundamental importance for the estimation of realistic spreading times, since nodes can be connected by slow paths, even if they seem close in the aggregated network.

In addition, the accessibility graph of a temporal network can be compared to its aggregated, static counterpart. Using this concept, we have defined the novel measure of *causal fidelity* in Section 4.3.4. Causal fidelity quantifies the goodness of the static approximation of a temporal network from the causal point of view. This measure is of major importance, since due to the lack of established temporal network analysis tools, a static approximation can provide useful insights into the real system. On the other hand, temporal networks with low causal fidelities should be analyzed with care, when static network tools are used. In particular, a low causal fidelity implies that disease outbreaks are systematically overestimated in the static approximation.

Finally, the unfolding of accessibility contains implicit information about temporal and topological mixing properties of the network under consideration. This information can

be revealed when the path density of the network is compared to randomized versions. We used different randomization techniques in Section 4.3.6 to reveal mixing properties of the livestock trade network. Hereby, we found that the network is first, poorly topologically mixed and second, link occurrence is temporally sparse, i.e. the system shows bursty behavior. Additionally, we demonstrated the capability of the method introduced above by application to other temporal network datasets.

Outlook. The idea of the *clustering coefficient* for temporal networks introduced by Tang et al. (2010) is the persistence of links over time. On the other hand, it is straightforward to generalize the concept of closed triangles known from static networks as it was introduced by Equation (2.18). Using different snapshots of the temporal network, the author suggests the following definition of the temporal clustering coefficient:

$$C_{ijk} = \frac{\text{tr}(\mathbf{A}_i \mathbf{A}_j \mathbf{A}_k)}{\sum_{\mu, \nu \in \{i, j, k\}: \mu < \nu} [\sum_{\mu\nu} (\mathbf{A}_\mu \mathbf{A}_\nu) - \text{tr}(\mathbf{A}_\mu \mathbf{A}_\nu)]},$$

where \mathbf{A}_i is a snapshot of the network at time i . The clustering coefficient is then computed for all snapshot triples with indices $i < j < k$ and yields a 3-dimensional object. This object can be contracted to a clustering matrix \mathbf{C} with elements $c_{j-i, k-j}$ and a clustering vector \mathbf{c} with elements c_{k-i} . The former gives information about the node waiting times in closed triangles and the latter measures the total time for the traversal of closed triangles in the network.

Although accessibility is a fundamental building block for the understanding of temporal networks, the development of a macroscopic theory of temporal networks is still in its infancy. A promising approach would consist in mapping temporal network properties onto some static network image and analyze the latter instead. Besides the obvious temporal nature of most network measures in temporal networks, the difficulty in such an approach lies in conceptional problems, such as the degeneration of connected components. These problems are mostly attributed to the non-transitivity of paths in temporal networks, which we discussed in Section 4.1.3. Hence, finding the transitive part of an accessibility graph could prove to be useful. The author suggests to quantify *transitivity* as follows: the transitivity matrix $\mathbf{T} = \mathcal{P}_T \circ \mathcal{P}_T^2$ contains the transitive edges of the accessibility graph (\circ denotes the Hadamard product). This measure could help to identify transitive paths in temporal networks and facilitate the generalization of other concepts of static network analysis.

A Appendix

A.1 Network implementation

In order to efficiently implement networks and their analysis on a computer, it is necessary to use appropriate data structures. A short and transparent introduction to data structures and algorithms is in the book of Skiena (2008). In this section, we review some essential data structures appropriate for network analysis and give a brief description of fundamental algorithms. The purpose of this section is to sketch the basic ideas behind the data structures and algorithms rather than to list algorithms and source code. For source code of data structures and algorithms, the reader is encouraged to the lecture of Skiena (2008) and Merali (2010).

Matrix implementation. To begin with, we consider the implementation of adjacency matrices as introduced in section 2.2.1. Adjacency matrices are by definition square matrices. Their entries are either 0 or 1. In weighted networks, their entries can take any floating-point value. The number of nodes in most complex network datasets is relatively large. Starting with small networks (100 nodes, conference contacts (Isella et al., 2011)), complex networks can be gigantic ($\sim 10^9$ nodes in the case twitter tweeds (Yang and Leskovec, 2011) or the world-wide web (Albert et al., 1999; Broder et al., 2000)) Note that the sizes of adjacency matrices scales with the square of the networks size, hence adjacency matrices of these networks are intractable for straightforward computer-based matrix analyses.

Nevertheless, it is a common feature of many real-world networks that they are sparse, i.e. the vast majority of their entries are zeros¹. Since zeros do not contribute to matrix operations as products or additions, it is reasonable to use data structures ignoring zeros. These data structures are called **sparse matrices**. Their advantages is (1) they save much memory and (2) computations are faster, because operations with zeros involved are not executed. Sparse matrix data structures are available in most modern computer languages (e.g. Matlab, Python: `scipy` library, C/C++: `boost` library). They perform well for problems based on adjacency matrices as the computation of the degree or eigenvector centrality. However, matrix methods are not suitable for the computation of many other network measures, such as betweenness, closeness or network navigation.

¹Typically, the number of edges in the network is of the same order as the number of nodes.

Graph implementation. The drawback of matrix representations of networks is that it is rather complicated to *traverse* a network using matrices. A traversal is a procedure of the following form: start at a node, visit all of its neighbors, from each neighbor visit its neighbor and so forth, until there are no more new nodes to traverse. This is a searching process. Network traversal is used in many implementations of graph theoretic methods.

As an alternative implementation of the adjacency matrix the **adjacency list** is a well suited data structure for network traversal. It stores the neighbors of every node and can be implemented as linked lists. Adjacency lists can be considered as a node centric view on the network, since they allow for a fast access to the neighborhood of each node. Considering the example network on the left panel of Figure A.1, the corresponding adjacency list is as follows:

$$\begin{aligned} 1 &\rightarrow 2, 3 \\ 2 &\rightarrow 4 \\ 3 &\rightarrow 2 \\ 4 &\rightarrow 2, 3. \end{aligned}$$

In order to traverse the graph starting at node 1, we choose one of the neighbors of 1 and repeat the process until we have traversed all nodes. One possible traversal starting at 1 would be $1 \rightarrow 3 \rightarrow 2 \rightarrow 4$.

During a traversal process, one can decide to either exploit the whole neighborhood of a node first and then traverse the next generation or choose a neighbor of every traversed node at every step. These two essential searching processes are called breadth-first-search (BFS) and depth-first-search (DFS), respectively. The difference between the two lies in the order of traversed nodes. Figure A.1 shows resulting search trees of the two methods. Starting at node 1, the traversal $1 \rightarrow 3 \rightarrow 2 \rightarrow 4$ would be found using a DFS-search, while a BFS-search would yield $1 \rightarrow 2 \rightarrow 3 \rightarrow 4$. It should be noted that in general there exist multiple BFS and DFS trees for each starting node.

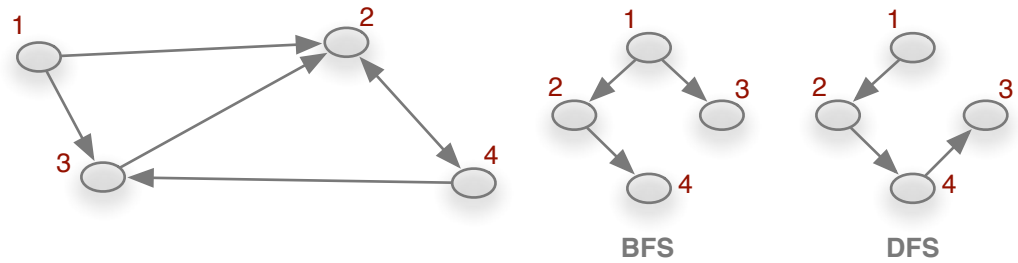


Figure A.1. Breadth-first-search and depth-first-search trees in a directed network. Search processes are started at node 1.

Both search algorithms are used in a large number of algorithmic applications. BFS is efficient to compute shortest paths in unweighted networks. With every generation in a BFS tree, the distance from the starting node is incremented by 1, and thus the set of nodes with a certain distance from the starting node can be directly read from the BFS tree (see Figure A.1). Shortest paths in weighted networks can be identified using a the algorithm of Dijkstra (Dijkstra, 1959). Connected components in directed graphs can be efficiently identified using closed DFS paths (Skiena, 2008).

Due to the sparsity of typical adjacency matrices, networks can also be efficiently stored as **edge lists**. An edge list is a list of tuples, where each tuple (u, v) is an edge connecting nodes u and v . The edge list of the network shows in Figure A.1 is

$$\begin{aligned} & (1, 2) \\ & (1, 3) \\ & (2, 4) \\ & (3, 2) \\ & (4, 2) \\ & (4, 3). \end{aligned}$$

Due to their human readable structure, edge lists are a convenient format to store networks as column wise text files. Edge lists can also be efficiently used for edge randomization and random graph generation.

Implementations of the graph structures discussed above are for example available in the libraries **networkx** (Python), **igraph** (C, Python, R), **Lemon** and **Boost** (C++).

Hard problems. The tools introduced above provide a huge and efficient toolbox for network analysis. Nevertheless, there are still network problems, where no efficient algorithm is known for their exact solution. In the language of complexity theory, the time to solve these problems scales with the problem size in non-polynomial time. There are two important complexity classes of problems in computational complexity theory. First, the class of NP-complete (NP stands for Non-deterministic Polynomial-time) problems, and second, the class of NP-hard problems. All problems mentioned in this thesis have been proven to be NP-complete in our context. For most practical questions, a distinction between the two classes is irrelevant, however. It is rather important to recognize intractable graph theoretical problems. NP complete problems can typically be solved exactly only for small system sizes.

Probably the most popular example is the *traveling salesman problem*: a salesman has to traverse a set of cities and thereby choose the order of those cities that minimizes the total distance. For small problem sizes, it is possible simply to try out all possible combinations and find the minimal total distance (brute-force search). The number of possible combinations, however, grows factorial with the system size, i.e. finding a

A Appendix

solution takes $t \propto n!$ for n cities. In other words, if the problem could be solved for 20 cities in 1 second, it would take 21 seconds to solve it for 21 cities, 7 minutes for 22 cities and 3 million years for 30 cities!

A more exhaustive overview about hard problems is in (Skiena, 2008) and the references therein. Generally, heuristic methods have to be used in order to get an approximate solution. It should be noted that the *maximum clique* problem (see section 4.3) and *graph partitioning* (see section 3.1, Equation (3.1)) belong to the class of hard problems (Brandes et al., 2007).

A.2 Degree vs. other centrality measures

In this section, we compute the centrality measures introduced in Section 2.2.2 and compare them with the degree. In particular, we compare the degree with betweenness, closeness and eigenvector centrality. Since the eigenvector centrality is defined only on connected networks, the analysis is restricted to the LSCC of the network. Figure A.2

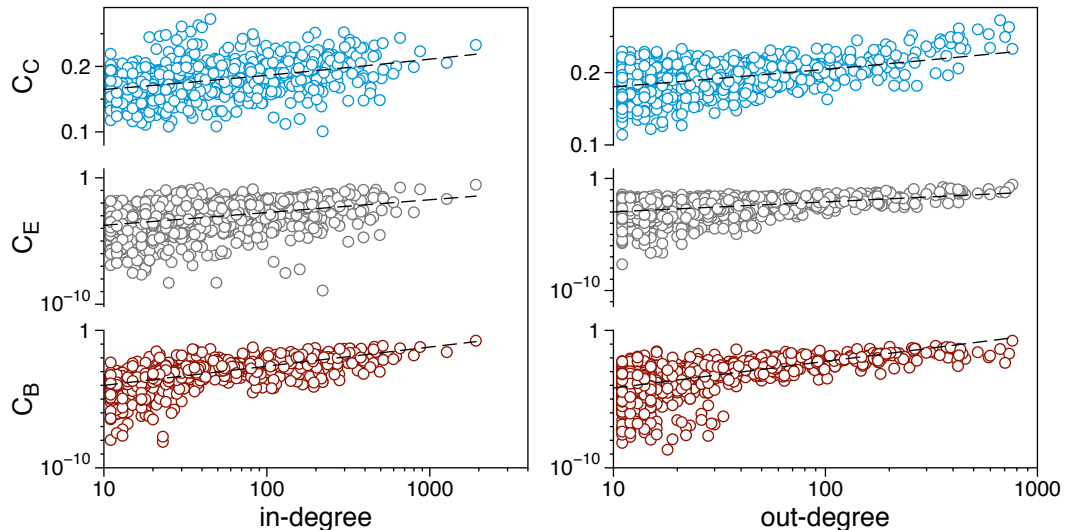


Figure A.2. Correlation between the degree and other centrality measures for the livestock trade network. The left panel shows the closeness centrality C_C , eigenvector centrality C_E and betweenness centrality C_B vs. the in-degree. The respective picture for the out-degree is shown on the right. Dashed lines show power-law fits of the data. Only nodes with in/out-degree greater than 10 are shown.

shows different centrality measures for the network being compared with the degree. Each point represents one node, and the dashed lines show power-law fits of the scatter

plots, respectively. The figure demonstrates that all considered centrality measures show a correlation with the degree.

A.3 Subgraphs and maximum modularity

Although computer generated modular networks are used in many applications, the author is not aware of any systematic analysis of the maximum value of modularity depending on the number of modules. Therefore, we derive an estimation of the maximum modularity value depending on the number of modules in the network. The results are derived for a clique of modules, but remain unchanged for a ring of modules as this distinction is reasonable in finite systems. In addition, the estimation is also valid for directed networks.

The modularity of a network with given modular structure can be computed using the equation

$$Q = \sum_i (e_{ii} - a_i^2), \quad (\text{A.1})$$

where e_{ij} is the fraction of edges pointing from community i to community j . The last term corresponds to the fraction of all edges that are connected to community i , i.e.

$$a_i = \sum_j e_{ij}.$$

Since the sum over all edge fraction has to be 1, it is $\sum_{ij} e_{ij} = 1$. If a network consists of two modules x and y , the fraction of edges in y is

$$y = c - x, \quad (\text{A.2})$$

where the constant $c < 1$ is the fraction of all inner module edges. In general, this expression is $c = \text{Tr}(e)$.

A.3.1 Two modules

In the case of two communities, the fraction of inter-module-edges is uniquely determined by the fraction of inner-module-edges.

The matrix e_{ij} takes the form

$$e_{ij} = \begin{pmatrix} x & \frac{1}{2}(1-x-y) \\ \frac{1}{2}(1-x-y) & y \end{pmatrix},$$

where x, y are the edge fractions in communities 1 and 2 and $\frac{1}{2}(1-x-y)$ is the fraction

of edges *between* communities 1 and 2. The corresponding expression for Q is.

$$Q = x - \left(x + \frac{1-x-y}{2} \right)^2 + y - \left(y + \frac{1-x-y}{2} \right)^2.$$

This function does not possess a maximum over the total domain, but there is a maximum in the subdomain $0 < x < 1, 0 < y < 1$. Condition (A.2) yields

$$Q = \frac{1}{2} + 2cx - 2x^2 - \frac{1}{2}c^2 + c.$$

Using condition (A.2) restricts the function to tuples (x, y) , where $x + y = c$, which corresponds to a line $y = c - x$. Thus, we are looking for the maximum along this line using the condition

$$\frac{\partial Q}{\partial x} = 2c - 4x = 0.$$

It follows $x = c/2$ and the maximum condition $\partial^2 Q / \partial x^2 = -4 < 0$ is satisfied. Using (A.2) gives the solution

$$x = \frac{c}{2}, \quad y = \frac{c}{2}. \quad (\text{A.3})$$

The corresponding modularity is

$$\begin{aligned} Q &= \frac{c}{2} - \frac{1}{4} \left(1 + \frac{c}{2} - \frac{c}{2} \right)^2 + \frac{c}{2} - \frac{1}{4} \left(1 + \frac{c}{2} - \frac{c}{2} \right)^2 \\ &= c - \frac{1}{2}. \end{aligned}$$

The case where a maximum fraction of edges is in the modules and a minimum fraction is between modules is met, if $c \rightarrow 1$. In this case, the modularity takes its maximum value. The limit is

$$\lim_{c \rightarrow 1} x = 1/2, \quad \lim_{c \rightarrow 1} y = 1/2, \quad \lim_{c \rightarrow 1} Q = 1/2. \quad (\text{A.4})$$

For the case of two modules, the maximum modularity is found for two equally sized modules of approximate size $1/2$. The maximum modularity is then $Q = 0.5$. We consider the case of more modules below.

A.3.2 Arbitrary number of modules

In the case of more than two modules, all modules can have different sizes in the first place and can be connected among themselves arbitrarily. The general module-matrix

takes the form

$$e_{ij} = \begin{pmatrix} x_1 & & \dots & & d \\ & x_2 & & & \\ \vdots & & \ddots & & \vdots \\ & & & & x_n \\ d & & \dots & & \end{pmatrix}. \quad (\text{A.5})$$

All non-diagonal elements are

$$d = \frac{1 - \text{Tr}(e)}{n(n-1)} = \frac{1-c}{n(n-1)}$$

with $c \equiv \text{Tr}(e) = \text{const.} < 1$. Thus, the general expression for modularity is

$$Q = c - \sum_i \left(\sum_j e_{ij} \right)^2. \quad (\text{A.6})$$

We use the above expression for the non-diagonal elements d and compute the expression $\sum_j e_{ij}$ in Equation (A.6).

$$\sum_j e_{ij} = e_{ii} + \sum_{j \neq i} e_{ij} = x_i + (n-1) \frac{1-c}{n(n-1)} = x_i + \frac{1-c}{n}. \quad (\text{A.7})$$

Now we insert $\sum_j e_{ij} = x_i + \frac{1-c}{n}$ in Equation (A.6) and after some algebra we get a general expression for the modularity for networks of the form (A.5):

$$Q = c - \sum_i x_i^2 - \frac{1-c^2}{n} = \sum_i x_i - \sum_i x_i^2 - \frac{1 - (\sum_i x_i)^2}{n}. \quad (\text{A.8})$$

In order to find the relevant maximum of (A.8), its slope has to vanish along a hyperplane defined by

$$\sum_i x_i = c = \text{const.} < 1. \quad (\text{A.9})$$

Since c is constant, the relevant part of (A.8) for the maximum is

$$\begin{aligned} Q_{\text{relevant}} \equiv Q_r &= - \sum_{i=1}^n x_i^2 = - \sum_{i=1}^{n-1} x_i^2 - \underbrace{\left(c - \sum_{i=1}^{n-1} x_i \right)^2}_{x_n^2} \\ &= - \sum_{i=1}^{n-1} x_i^2 - c^2 + 2c \sum_{i=1}^{n-1} x_i - \left(\sum_{i=1}^{n-1} x_i \right)^2. \end{aligned} \quad (\text{A.10})$$

Note that the sum on the right-hand side is up to $n - 1$. This effectively eliminates the last variable. The derivative of Q is

$$\frac{\partial Q}{\partial x_i} = \frac{\partial Q_r}{\partial x_i} = -2 \sum_{i=1}^{n-1} x_i + 2c(n-1) - 2(n-1) \sum_{i=1}^{n-1} x_i. \quad (\text{A.11})$$

In order to find a maximum, the derivative has to vanish, i.e.

$$\begin{aligned} 0 &= -2 \sum_{i=1}^{n-1} x_i + 2c(n-1) - 2(n-1) \sum_{i=1}^{n-1} x_i \\ &= - \sum_{i=1}^{n-1} x_i + c(n-1) - (n-1) \sum_{i=1}^{n-1} x_i \\ &= cn - c - n \sum_{i=1}^{n-1} x_i + \sum_{i=1}^{n-1} x_i - \sum_{i=1}^{n-1} x_i \\ &= cn - c - n \sum_{i=1}^{n-1} x_i. \end{aligned}$$

It follows

$$\underbrace{c - \sum_{i=1}^{n-1} x_i}_{x_n} = \frac{c}{n}.$$

Thus,

$$x_n = \frac{c}{n}. \quad (\text{A.12})$$

Hence, the maximum of Q is obtained, if all modules have the same size, i.e. $x_i = \frac{c}{n} \forall i$.

In order to find the maximum value of Q , we insert the module size $x_i = c/n$ into Equation (A.8) and get

$$Q = c - \sum_{i=1}^n \left(\frac{c}{n} \right)^2 - \frac{1 - c^2}{n} = c - \frac{c^2}{n} - \frac{1}{n} + \frac{c^2}{n}.$$

Thus, it follows for dense modules

$$Q_{\max} = \lim_{c \rightarrow 1} Q = 1 - \frac{1}{n}. \quad (\text{A.13})$$

Consequently, the maximum value of Q_{\max} is determined by the number of modules. A similar result was found using probabilistic arguments in (Good et al., 2010).

Finite systems. In finite systems, the minimum fraction of inter-module edges is obtained, when modules are connected to each other on a ring, each module having two nearest neighbors. In this case we set $e_{ij} = \frac{1}{n}(1 - c)$ for $j = i + 1$ and $j = i - 1$ and all other elements are zero. This yields

$$e_{ij} = \begin{pmatrix} x_1 & \frac{1}{n}(1 - c) & & \dots & & 0 \\ \frac{1}{n}(1 - c) & x_2 & \frac{1}{n}(1 - c) & & & \\ & \frac{1}{n}(1 - c) & \ddots & \ddots & & \\ \vdots & & \ddots & \ddots & \ddots & \vdots \\ & & & \ddots & x_{n-1} & \frac{1}{n}(1 - c) \\ 0 & & & \dots & \frac{1}{n}(1 - c) & x_n \end{pmatrix}. \quad (\text{A.14})$$

It follows immediately that $\sum_j e_{ij} = x_i + \frac{2(1-c)}{n}$, which is equivalent to (A.7) up to a factor 2. Inserting this into Equation (A.6) gives a similar expression for modularity (A.8) as for the general case:

$$Q = c - \sum_i x_i^2 - \frac{4(1 - c)}{n}.$$

Since the relevant part for maximum finding is the quadratic term as in (A.10), the results remain unchanged for modules along a chain and the maximum value is as above

$$Q_{\max} = 1 - \frac{1}{n}. \quad (\text{A.15})$$

Figure A.3 shows a comparison between Equation (A.15) and a computer simulation of a ring of modules where new modules are added to the system successively and the maximum modularity is computed. The edge density of each module is given by the edge occupation probability $p_{\text{in}} = 0.5$. The figure demonstrates that Equation (A.13) gives a good approximation of the maximum value Q_{\max} even for small systems.

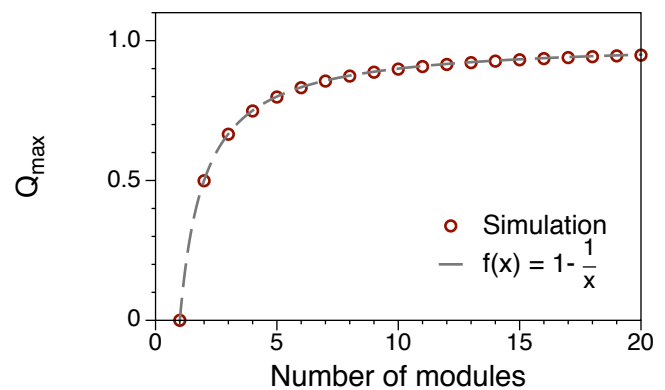
Directed networks. In analog to Equation (A.1) the modularity of directed networks can be written as (Kao et al., 2007)

$$Q = \sum_i e_{ii} - a_i^{\text{in}} a_i^{\text{out}}. \quad (\text{A.16})$$

where

$$a_j^{\text{in}} = \sum_i e_{ij} \quad \text{and} \quad a_i^{\text{out}} = \sum_j e_{ij}.$$

Figure A.3. Equation (A.15) (grey dashed line) reproduces the values found by numerical simulations (red circles). In the simulations, modules are dense, directed subgraphs ($p_{in} = 0.5$) with 32 nodes each. Modules are connected on a ring so that the resulting graph is connected.



The structure of the inter-module edges takes the form of the matrix (A.14) and thus results do not differ either for the directed case.

Acknowledgement

First of all, I would like to thank Thomas Selhorst for his endless support and for giving me the opportunity to work independently on an exciting topic. Furthermore, I thank Igor Sokolov for the many fruitful discussions and the development of new ideas, in particular our different approaches for the formulation of accessibility.

This thesis has been developed at two different locations: the Humboldt-University of Berlin and the Friedrich-Loeffler-Institute in Wusterhausen. Concerning the physical side of my work, I would like to thank Federico Camboni for discussions and calculations, particularly about matrices, and Vitaly Belik for sharing his ideas and knowledge about networks and epidemiology with me. I thank Mario Konschake for many fruitful discussions and for helping to increase my computer skills significantly.

I thank my colleagues from the Friedrich-Loeffler-Institute for guiding the focus of my research so that I could address some real-world problems. In particular, Jörn Gethmann, Christoph Staubach and Matthias Kramer provided a realistic picture of disease management. I would like to thank Hans Thulke for his great interest in my work and discussions about networks and automata.

I would also like to thank Tim Baldsiefen, Christian Schmeltzer for helping me with the manuscript. Finally, I thank my family for their support during the last years. I thank Sarah for bearing with me in phases of scientific frustration and hope that I'll have more time to spend with my daughters Laurena and Thalina in the future.

Bibliography

- Albert, R. and Barabási, A.-L. (2002). Statistical mechanics of complex networks. *Rev. Mod. Phys.*, 74:47–97.
- Albert, R., Jeong, H., and Barabási, A.-L. (1999). Diameter of the world-wide web. *Nature*, 401(6749):130–131.
- Albert, R., Jeong, H., and Barabási, A.-L. (2000). Error and attack tolerance of complex networks. *Nature*, 406(6794):378–382.
- Aldous, J. M. and Wilson, R. J. (2000). *Graphs And Applications: An Introductory Approach*. Springer Verlag.
- Amaral, L. A. N., Scala, A., Barthélémy, M., and Stanley, H. E. (2000). Classes of small-world networks. *Proc. Natl. Acad. Sci. U.S.A.*, 97(21):11149–11152.
- Anderson, R. M. and May, R. M. (1991). *Infectious diseases of humans: dynamics and control*. Oxford University Press.
- Bailey, N. T. J. (1957). *The mathematical theory of infectious diseases*. Charles Griffin & Company Ltd, 2nd edition.
- Bajardi, P., Barrat, A., Natale, F., Savini, L., and Colizza, V. (2011). Dynamical patterns of cattle trade movements. *PLOS ONE*, 6(5):e19869.
- Bak, P., Chen, K., and Tang, C. (1990). Forest-fire model and some thoughts on turbulence. *Phys. Lett. A*, 147:297–300.
- Balcan, D., Colizza, V., Gonçalves, B., Hu, H., Ramasco, J. J., and Vespignani, A. (2009). Multiscale mobility networks and the spatial spreading of infectious diseases. *Proc. Natl. Acad. Sci. U.S.A.*, 106(51):21484–21489.
- Balcan, D. and Vespignani, A. (2011). Phase transitions in contagion processes mediated by recurrent mobility patterns. *Nat. Phys.*, 7(7):581–586.
- Ball, F., Mollison, D., and Scalia-Tomba, G. (1997). Epidemics with two levels of mixing. *Ann. Appl. Probab.*, 7(1):46–89.
- Banerjee, A. and Jost, J. (2009). Graph spectra as a systematic tool in computational biology. *Discrete Applied Mathematics*, 157(10):2425–2431.

Bibliography

- Barabási, A.-L. and Albert, R. (1999). Emergence of Scaling in Random Networks. *Science*, 286:509.
- Barrat, A., Barthélémy, M., and Vespignani, A. (2008). *Dynamical processes on complex networks*. Cambridge University Press.
- Barrat, A., Fernandez, B., Lin, K. K., and Young, L.-S. (2013). Modeling Temporal Networks Using Random Itineraries. *Phys. Rev. Lett.*, 110(15):158702.
- Barrat, A. and Weigt, M. (2000). On the properties of small-world network models. *Eur. Phys. J. B*, 13(3):547–560.
- Bauch, C. T. and Earn, D. J. D. (2004). Vaccination and the theory of games. *Proc. Natl. Acad. Sci. U.S.A.*, 101(36):13391–13394.
- Belik, V., Geisel, T., and Brockmann, D. (2011). Natural Human Mobility Patterns and Spatial Spread of Infectious Diseases. *Phys. Rev. X*, 1(1).
- Bhadra, S. and Ferreira, A. (2003). Complexity of connected components in evolving graphs and the computation of multicast trees in dynamic networks. In *Ad-Hoc, Mobile, and Wireless Networks*, pages 259–270. Springer Verlag.
- Bianconi, G. and Barabási, A.-L. (2001). Competition and Multiscaling in evolving networks. *Europhys. Lett.*, 54:436–442.
- Bigras-Poulin, M., Barfod, K., Mortensen, S., and Greiner, M. (2007). Relationship of trade patterns of the Danish swine industry animal movements network to potential disease spread. *Prev. Vet. Med.*, 80(2-3):143–165.
- Bollobás, B. (1985). *Random Graphs*. London Academic Press.
- Bonacich, P. (1972). Factoring and weighting approaches to status scores and clique identification. *The Journal of Mathematical Sociology*, 2(1):113–120.
- Bonacich, P. (2007). Some unique properties of eigenvector centrality. *Soc. Networks*, 29(4):555–564.
- Brandes, U. (2001). A faster algorithm for betweenness centrality. *J. Math. Sociol.*
- Brandes, U., Delling, D., Gaertler, M., Görke, R., Hoefer, M., Nikoloski, Z., and Wagner, D. (2007). On finding graph clusterings with maximum modularity. In *Graph-Theoretic Concepts in Computer Science*, pages 121–132. Springer Verlag.
- Broder, A., Kumar, R., Maghoul, F., Raghavan, P., Rajagopalan, S., Stata, R., Tomkins, A. S., and Wiener, J. (2000). Graph structure in the web. *Comput. Netw.*, 33(1):309–320.

- Buchholz, U., Bernard, H., Werber, D., Böhmer, M. M., Remschmidt, C., Wilking, H., Deleré, Y., an der Heiden, M., Adlhoch, C., Dreesman, J., Ehlers, J., Ethelberg, S., Faber, M., Frank, C., Fricke, G., Greiner, M., Höhle, M., Ivarsson, S., Jark, U., Kirchner, M., Koch, J., Krause, G., Luber, P., Rosner, B., Stark, K., and Kühne, M. (2011). German Outbreak of Escherichia coli O104:H4 Associated with Sprouts. *N Engl J Med*, 365(19):1763–1770.
- Casteigts, A., Flocchini, P., Quattrociocchi, W., and Santoro, N. (2012). Time-varying graphs and dynamic networks. *Int. J. Parallel Emergent Distrib. Syst.*, 27(5):387–408.
- Chasnov, J. R. (2010). *Mathematical Biology: Lecture Notes*. The Hong Kong University of Science and Technology.
- Christley, R., Robinson, S. E., Lysons, R., and French, N. P. (2005). Network analysis of cattle movement in Great Britain. In *Proc. Soc. Vet. Epidemiol. Prev. Med.*, pages 234–244. Society for Veterinary Epidemiology and Preventive Medicine.
- Clauset, A. and Newman, M. E. J. (2009). Power-Law Distributions in Empirical Data. *SIAM Rev.*, 51(4):661.
- Clauset, A., Newman, M. E. J., and Moore, C. (2004). Finding community structure in very large networks. *Phys. Rev. E*, 70:066111.
- Cohen, R., Havlin, S., and ben Avraham, D. (2003). Efficient Immunization Strategies for Computer Networks and Populations. *Phys. Rev. Lett.*, 91(24):247901.
- Coleman, J. S. (1964). *An Introduction to Mathematical Sociology*. Collier-Macmillan, London, UK.
- Colizza, V., Barrat, A., Barthélémy, M., and Vespignani, A. (2006). The role of the airline transportation network in the prediction and predictability of global epidemics. *Proc. Natl. Acad. Sci. U.S.A.*, 103(7):2015–2020.
- Colizza, V., Pastor-Satorras, R., and Vespignani, A. (2007). Reaction-diffusion processes and metapopulation models in heterogeneous networks. *Nat. Phys.*, 3(4):276–282.
- Colizza, V. and Vespignani, A. (2007). Invasion threshold in heterogeneous metapopulation networks. *Phys. Rev. Lett.*
- Cross, P. C., Lloyd-Smith, J. O., Johnson, P. L. F., and Getz, W. M. (2005). Duelling timescales of host movement and disease recovery determine invasion of disease in structured populations. *Ecol. Lett.*, 8:587–595.
- de Solla Price, D. J. (1965). Networks of Scientific Papers. *Science*, 49(3683):510–515.

Bibliography

- de Solla Price, D. J. (1976). A general theory of bibliometric and other cumulative advantage processes. *J. Am. Soc. Inf. Sci. Technol.*, 27(5):292–306.
- Del Genio, C. I., Gross, T., and Bassler, K. E. (2011). All Scale-Free Networks Are Sparse. *Phys. Rev. Lett.*, 107(17):178701.
- Dijkstra, E. (1959). A note on two problems in connexion with graphs. *Numerische Mathematik*, 1:269–271.
- Dorogovtsev, S., Mendes, J., and Samukhin, A. (2001). Giant strongly connected component of directed networks. *Phys. Rev. E*, 64:025101(R).
- Dubé, C., Ribble, C., Kelton, D., and Mcnab, B. (2009). A Review of Network Analysis Terminology and its Application to Foot-and-Mouth Disease Modelling and Policy Development. *Transbound. Emerg. Dis.*, 56(3):73–85.
- Egghe, L. and Rousseau, R. (1990). *Introduction to informetrics: Quantitative methods in library, documentation and information science*. Elsevier, Amsterdam.
- Erdős, P. and Rényi, A. (1959). On random graphs. *Publ. Math., Debrecen*, 6:290–297.
- Erdős, P. and Rényi, A. (1960). On the evolution of random graphs. *Publ. Math. Inst. Hung. Acad. Sci., Ser. A*, 5:17–61.
- Erdős, P. and Rényi, A. (1961). On the evolution of random graphs II. *Bull. Inst. Int. Stat.*, 38(4):343–347.
- Euler, L. (1736). Solutio problematis ad geometrian situs pertinentis. *Comm. Acad. Sci. Imp. Petrop.*, 8:128–140.
- EUR-Lex (2000). Directive 2000/15/ec of the european parliament and the council of 10 april 2000 amending council directive 64/432/eec on health problems affecting intra-community trade in bovine animals and swine. EUR-Lex.
- Faloutsos, M., Faloutsos, P., and Faloutsos, C. (1999). On power-law relationships of the Internet topology. *SIGCOMM Comput. Commun. Rev.*, 29(4):251–262.
- Floyd, R. W. (1962). Algorithm-97 - Shortest Path. *Commun. ACM*, 5(6):345–345.
- Fortunato, S. (2010). Community detection in graphs. *Phys. Rep.*, 486:75–174.
- Fortunato, S. and Barthélemy, M. (2007). Resolution limit in community detection. *Proc. Natl. Acad. Sci. U.S.A.*, 104(1):36–41.
- Fortunato, S., Flammini, A., and Menczer, F. (2006). Scale-Free Network Growth by Ranking. *Phys. Rev. Lett.*, 96:218701.

- Fournié, G., Guitian, J., Desvaux, S., Cuong, V. C., Dung, D. H., Pfeiffer, D. U., Mangtani, P., and Ghani, A. C. (2013). Interventions for avian influenza A (H5N1) risk management in live bird market networks. *Proc. Natl. Acad. Sci. U.S.A.*
- Freeman, L. C. (1978). Centrality in social networks. *Soc. Networks*, 1:215–239.
- Fritzemeier, J. (2000). Epidemiology of classical swine fever in Germany in the 1990s. *Vet. Microbiol.*, 77(1-2):29–41.
- Garlaschelli, D. and Loffredo, M. (2004). Patterns of link reciprocity in directed networks. *Phys. Rev. Lett.*, 93:268701.
- Garrison, W. L. (1960). Connectivity of the interstate highway system. *Papers and proceedings of the regional science association*, 6:121–137.
- Girvan, M. and Newman, M. E. J. (2002). Community structure in social and biological networks. *Proc. Natl. Acad. Sci. U.S.A.*, 99(12):7821–7826.
- Good, B. H., de Montjoye, Y.-A., and Clauset, A. (2010). Performance of modularity maximization in practical contexts. *Phys. Rev. E*, 81:046106.
- Granovetter, M. S. (1973). The strength of weak ties. *Am. J. Sociol.*, pages 1360–1380.
- Grassberger, P. (1983). On the critical behavior of the general epidemic process and dynamical percolation. *Math. Biosci.*, 63(2):157–172.
- Green, D. M., Kiss, I. Z., and Kao, R. R. (2006). Modelling the initial spread of foot-and-mouth disease through animal movements. *Proc. R. Soc. B*, 273(1602):2729–2735.
- Grenfell, B. T. (1992). Chance and chaos in measles dynamics. *J. R. Stat. Soc. B*, 54:383–398.
- Grenfell, B. T. and Harwood, J. (1997). (Meta)population dynamics of infectious diseases. *Trends. Ecol. Evol.*, 12(10):395–399.
- Grindrod, P., Parsons, M., Higham, D., and Estrada, E. (2011). Communicability across evolving networks. *Phys. Rev. E*, 83(4):046120.
- Guimerà, R., Mossa, S., Turtschi, A., and Amaral, L. A. N. (2005). The worldwide air transportation network: Anomalous centrality, community structure, and cities' global roles. *Proc. Natl. Acad. Sci. U.S.A.*, 102(22):7794–7799.
- Guimerà, R., Sales-Pardo, M., and Amaral, L. A. N. (2004). Modularity from fluctuations in random graphs and complex networks. *Phys. Rev. E*, 70:025101.
- Hagberg, A. A. (2012). Networkx: High productivity software for complex networks. <http://networkx.lanl.gov>.

Bibliography

- Hagberg, A. A., Schult, D. A., and Swart, P. J. (2008). Exploring network structure, dynamics, and function using NetworkX. In *Proceedings of the 7th Python in Science Conference (SciPy2008)*, pages 11–15, Pasadena, CA USA. Pasadena, CA USA.
- Hamer, W. H. (1906). Epidemic disease in England. *Lancet*, 1:733–739.
- Hanski, I. (1998). Metapopulation dynamics. *Nature*, 396(6706):41–49.
- Harris, T. E. (1974). Contact interactions on a lattice. *Ann. Probab.*, 2:969–988.
- Haydon, D. T., Chase-Topping, M., Shaw, D. J., Matthews, L., Friar, J. K., Wilesmith, J., and Woolhouse, M. E. J. (2003). The construction and analysis of epidemic trees with reference to the 2001 UK foot-and-mouth outbreak. *Proc. R. Soc. B*, 270(1511):121–127.
- Hethcote, H. W. (2000). The mathematics of infectious diseases. *SIAM Rev.*, 42(4):599–653.
- Holland, P. W. and Leinhardt, S. (1971). Transitivity in Structural Models of Small Groups. *Small Group Research*, 2(2):107–124.
- Holme, P., Kim, B. J., Yoon, C. N., and Han, S. K. (2002). Attack vulnerability of complex networks. *Phys. Rev. E*, 65(5):056109.
- Holme, P. and Saramäki, J. (2012). Temporal networks. *Phys. Rep.*, 519(3):97–125.
- Horst, H. S. (1998). *Risk and economic consequences of contagious animal disease introduction*. PhD thesis, WAU, Wageningen.
- Hufnagel, L., Brockmann, D., and Geisel, T. (2004). Forecast and control of epidemics in a globalized world. *Proc. Natl. Acad. Sci. U.S.A.*, 101(42):15124.
- Isella, L., Stehlé, J., Barrat, A., Cattuto, C., Pinton, J.-F., and Van den Broeck, W. (2011). What's in a crowd? Analysis of face-to-face behavioral networks. *J. Theor. Biol.*, 271(1):166–180.
- Kao, R. R., Green, D. M., Johnson, J., and Kiss, I. Z. (2007). Disease dynamics over very different time-scales: foot-and-mouth disease and scrapie on the network of livestock movements in the UK. *J. R. Soc. Interface*, 4(16):907–916.
- Keeling, M. J., Danon, L., Vernon, M. C., and House, T. A. (2010). Individual identity and movement networks for disease metapopulations. *Proc. Natl. Acad. Sci. U.S.A.*, 107(19):8866–8870.
- Keeling, M. J. and Eames, K. T. D. (2005). Networks and epidemic models. *J. R. Soc. Interface*, 2(4):295–307.

Bibliography

- Kermack, W. O. and McKendrick, A. G. (1927). A contribution to the mathematical theory of epidemics. *Proc. R. Soc. A*, 115:700–721.
- Kim, Y., Son, S. W., and Jeong, H. (2010). Finding communities in directed networks. *Phys. Rev. E*, 81:016103.
- Kitching, R. P., Hutber, A. M., and Thrusfield, M. V. (2005). A review of foot-and-mouth disease with special consideration for the clinical and epidemiological factors relevant to predictive modelling of the disease. *Vet. J.*, 169(2):197–209.
- Kleinberg, J. M. (1999). Hubs, authorities, and communities. *ACM Comput. Surv.*, 31(4es).
- Kleinberg, J. M., Kumar, R., Raghavan, P., Rajagopalan, S., and Tomkins, A. S. (1999). The Web as a Graph: Measurements, Models, and Methods. In Asano, T., Imai, H., Lee, D. T., Nakano, S.-i., and Tokuyama, T., editors, *Lecture Notes in Computer Science*, pages 1–17. Springer Verlag.
- Konschake, M., Lentz, H. H. K., Conraths, F. J., Hövel, P., and Selhorst, T. (2013). On the Robustness of In- and Out-Components in a Temporal Network. *PLOS ONE*, 8(2):e55223.
- Krapivsky, P. and Redner, S. (2001). Organization of growing random networks. *Phys. Rev. E*, 63(6):066123.
- Leicht, E. and Newman, M. E. J. (2008). Community Structure in Directed Networks. *Phys. Rev. Lett.*, 100:118703.
- Lentz, H. H. K., Kasper, M., and Selhorst, T. (2009). Network analysis of the German cattle trade net - Preliminary results. *Berl. Munch. Tierarztl. Wochenschr.*, 122(5–6):193–198.
- Lentz, H. H. K., Konschake, M., Teske, K., Kasper, M., Rother, B., Carmanns, R., Petersen, B., Conraths, F. J., and Selhorst, T. (2011). Trade communities and their spatial patterns in the German pork production network. *Prev. Vet. Med.*, 98(2–3):176–181.
- Lentz, H. H. K., Selhorst, T., and Sokolov, I. M. (2012). Spread of infectious diseases in directed and modular metapopulation networks. *Phys. Rev. E*, 85:066111.
- Lentz, H. H. K., Selhorst, T., and Sokolov, I. M. (2013). Unfolding Accessibility Provides a Macroscopic Approach to Temporal Networks. *Phys. Rev. Lett.*, 110(11):118701.
- Liljeros, F., Edling, C., Amaral, L. A. N., and Stanley, H. E. (2001). The web of human sexual contacts. *Nature*, 411:907.

Bibliography

- Mackiewicz, A. and Ratajczak, W. (1996). Towards a new definition of topological accessibility. *Transpn. Res.-B*, 30(1):47–79.
- Martinez, N. D. (1991). Artifacts or attributes? Effects of resolution on the Little Rock Lake food web. *Ecol. Monogr.*, pages 367–392.
- Martínez-López, B., Ivorra, B., Ramos, A. M., and Sánchez-Vizcaíno, J. M. (2011). A novel spatial and stochastic model to evaluate the within- and between-farm transmission of classical swine fever virus. I. General concepts and description of the model. *Vet. Microbiol.*, 147(3-4):300–309.
- Martínez-López, B., Perez, A. M., and Sánchez-Vizcaíno, J. M. (2009). Social Network Analysis. Review of General Concepts and Use in Preventive Veterinary Medicine. *Transbound. Emerg. Dis.*, 56:109–120.
- Merali, Z. (2010). Computational science: Error. Why scientific computing does not compute. *Nature*, 467:775–777.
- Merton, R. K. (1968). The Matthew Effect in Science: The reward and communication systems of science are considered. *Science*, 159(3810):56–63.
- Milgram, S. (1967). The small world problem. *Psychology today*, 2(1):60–67.
- Mossong, J., Hens, N., Jit, M., Beutels, P., Auranen, K., Mikolajczyk, R., Massari, M., Salmaso, S., Tomba, G. S., and Wallinga, J. (2008). Social contacts and mixing patterns relevant to the spread of infectious diseases. *PLOS med.*, 5(3):e74.
- Newman, M. E. J. (2001). Scientific collaboration networks. I. Network construction and fundamental results. *Phys. Rev. E*, 64:016131.
- Newman, M. E. J. (2003). The Structure and Function of Complex Networks. *SIAM Rev.*, 45(2):167–256.
- Newman, M. E. J. (2004). Fast algorithm for detecting community structure in networks. *Phys. Rev. E*, 69:066133.
- Newman, M. E. J. (2006). Modularity and community structure in networks. *Proc. Natl. Acad. Sci. U.S.A.*, 103(23):8577–8582.
- Newman, M. E. J. (2010). *Networks: An Introduction*. Oxford University Press, New York, NY, USA.
- Newman, M. E. J. and Girvan, M. (2004). Finding and evaluating community structure in networks. *Phys. Rev. E*, 69:026113.

- Newman, M. E. J., Strogatz, S., and Watts, D. (2001). Random graphs with arbitrary degree distributions and their applications. *Phys. Rev. E*, 64:026118.
- Nicosia, V., Tang, J., Musolesi, M., Russo, G., Mascolo, C., and Latora, V. (2012). Components in time-varying graphs. *Chaos*, 22(2):023101.
- Noble, J. V. (1974). Geographic and temporal development of plagues. *Nature*, 250:726–729.
- Page, L. (1997). Method for node ranking in a linked database. *Patent US* 6285999.
- Pan, R. K. and Saramäki, J. (2011). Path lengths, correlations, and centrality in temporal networks. *Phys. Rev. E*, 84(1):016105.
- Pastor-Satorras, R. and Vespignani, A. (2001). Epidemic dynamics and endemic states in complex networks. *Phys. Rev. E*, 63:066117.
- Pastor-Satorras, R. and Vespignani, A. (2002a). Epidemic dynamics in finite size scale-free networks. *Phys. Rev. E*, 65:035108(R).
- Pastor-Satorras, R. and Vespignani, A. (2002b). Immunization of complex networks. *Phys. Rev. E*, 65(3):036104.
- Press, W. H., Teukolsky, S. A., Vetterling, W. T., and Flannery, B. P. (1992). *Numerical recipes in C (2nd ed.): the art of scientific computing*. Cambridge University Press, New York, NY, USA.
- Rocha, L. E. C., Liljeros, F., and Holme, P. (2010). Information dynamics shape the sexual networks of Internet-mediated prostitution. *Proc. Natl. Acad. Sci. U.S.A.*, 107(13):5706–5711.
- Rocha, L. E. C., Liljeros, F., and Holme, P. (2011). Simulated Epidemics in an Empirical Spatiotemporal Network of 50,185 Sexual Contacts. *PLoS Comput. Biol.*, 7(3):e1001109.
- Rolle, M. and Mayr, A. (2006). *Medizinische Mikrobiologie, Infektions- und Seuchenlehre*. Enke, Stuttgart, 8. edition.
- Ross, R. (1911). *The Prevention of Malaria*. Murray, London, 2nd edition.
- Salathé, M. and Jones, J. H. (2010). Dynamics and Control of Diseases in Networks with Community Structure. *PLoS Comput. Biol.*, 6(4):e1000736.
- Sander, L. M., Warren, C. P., and Sokolov, I. M. (2003). Epidemics, disorder, and percolation. *Physica A: Statistical Mechanics and its Applications*, 325:1–8.

Bibliography

- Sander, L. M., Warren, C. P., Sokolov, I. M., Simon, C., and Koopman, J. (2002). Percolation on heterogeneous networks as a model for epidemics. *Math. Biosci.*, 180:293–305.
- Schneider, C. M., Belik, V., Couronné, T., Smoreda, Z., and González, M. C. (2013). Unravelling daily human mobility motifs. *J. R. Soc. Interface*, 10(84):20130246.
- Sen, P., Dasgupta, S., Chatterjee, A., Sreeram, P. A., Mukherjee, G., and Manna, S. S. (2003). Small-world properties of the Indian railway network. *Phys. Rev. E*, 67:036106.
- Skiena, S. S. (2008). *The algorithm design manual*. Springer Verlag, 2nd edition.
- Sociopatterns (2012). Sociopatterns Collaboration. <http://www.sociopatterns.org>.
- StMELF, B. (2012). Herkunftssicherungs und Informationssystem für Tiere. <http://www.hi-tier.de>.
- Strauss, D. (1986). On a General Class of Models for Interaction. *SIAM Rev.*, 28(4):pp. 513–527.
- Sudarshan Iyengar, S. R., Veni Madhavan, C. E., Zweig, K. A., and Natarajan, A. (2012). Understanding Human Navigation Using Network Analysis. *Topics in Cognitive Science*, 4(1):121–134.
- Tang, J., Scellato, S., Musolesi, M., Mascolo, C., and Latora, V. (2010). Small-world behavior in time-varying graphs. *Phys. Rev. E*, 81(5).
- Vernon, M. C. and Keeling, M. J. (2009). Representing the UK’s cattle herd as static and dynamic networks. *Proc. R. Soc. B*, 276:469–476.
- Visser, R., Smith, A., Rissel, C., and Richters, J. (2003). Sex in Australia: Heterosexual experience and recent heterosexual encounters among a representative *Aust. N Z. J. Public Health*, 27(2):146–154.
- Vogel, P., Greiser, T., and Mattfeld, D. C. (2011). Understanding Bike-Sharing Systems using Data Mining: Exploring Activity Patterns. *Procedia Soc. Behav. Sci.*, 20:514–523.
- von Mises, R. and Pollaczek-Geiringer, H. (1929). Praktische Verfahren der Gleichungsauflösung. *ZAMM*, 9:152–164.
- Warshall, S. (1962). A theorem on boolean matrices. *J. ACM*, 9(1):11–12.
- Wasserman, S. and Faust, K. (1994). *Social Network Analysis*. Cambridge University Press.

Bibliography

- Watts, D. and Strogatz, S. (1998). Collective dynamics of small-world networks. *Nature*, 393:440–442.
- Yang, J. and Leskovec, J. (2011). Patterns of temporal variation in online media. In *Proceedings of the fourth ACM international conference on Web search and data mining*, pages 177–186, New York, NY, USA. ACM.
- Zachary, W. (1977). An information flow model for conflict and fission in small groups. *Journal Anthropol. Res.*, 33(4):452–473.

Selbständigkeitserklärung

Ich erkläre, dass ich die vorliegende Arbeit selbständig und nur unter Verwendung der angegebenen Literatur und Hilfsmittel angefertigt habe.

Berlin, den 12. November 2013

Hartmut Lentz

List of publications

1. **H. H. K. Lentz**, T. Selhorst and I. M. Sokolov
Unfolding Accessibility provides a Macroscopic Approach to Temporal Networks
Physical Review Letters 110: 118701 (2013).
2. M. Konschake, **H. H. K. Lentz**, F. J. Conraths, P. Hoevel and T. Selhorst
On the Robustness of In- and Out-Components in a Temporal Network
PLoS ONE 8(2): e55223 (2013).
3. **H. H. K. Lentz**, T. Selhorst and I. M. Sokolov
Spread of infectious diseases in directed and modular metapopulation networks
Physical Review E 85: 066111 (2012).
4. **H. H. K. Lentz**, M. Konschake, K. Teske, M. Kasper, B. Rother, R. Carmanns, B. Petersen, F. J. Conraths and T. Selhorst
Trade communities and their spatial patterns in the German pork production network
Preventive Veterinary Medicine 98: 176–181 (2011).
5. **H. Lentz**, M. Kasper and T. Selhorst
Beschreibung des Handels mit Rindern in Deutschland mittels Netzwerkanalyse – Ergebnisse von Voruntersuchungen
Berliner und Münchener Tierärztliche Wochenschrift 122: 193–198 (2009).